MODELING RADIATION EFFECTIVENESS FOR INACTIVATION OF

***BACILLUS* SPORES**

DISSERTATION

Emily A. Knight, Major, USAF

AFIT-ENC-DS-15-S-001

DEPARTMENT OF THE AIR FORCE
AIR UNIVERSITY

AIR FORCE INSTITUTE OF TECHNOLOGY

Wright-Patterson Air Force Base, Ohio

AFIT-ENC-DS-15-S-001

MODELING RADIATION EFFECTIVENESS FOR INACTIVATION OF *BACILLUS*

SPORES

DISSERTATION

Presented to the Faculty

Graduate School of Engineering and Management

Air Force Institute of Technology

Air University

Air Education and Training Command

in Partial Fulfillment of the Requirements for the

Degree of Doctoral of Philosophy in Applied Mathematics

Emily A. Knight, B.A., M.S.

Major, USAF

September 2015

AFIT-ENC-DS-15-S-001

MODELING RADIATION EFFECTIVENESS FOR INACTIVATION OF *BACILLUS*

SPORES

Emily A. Knight, B.A., M.S.
Major, USAF

Committee Membership:

Dr. William P. Baker
Chair

Dr. Larry W. Burggraf
Member

LTC Douglas R. Lewis
Member

Dr. Christine M. Schubert Kabban
Member

ADEDEJI B. BADIRU, Ph.D.
Dean, Graduate School of Engineering
and Management

AFIT-ENC-DS-15-S-001

Abstract

This research models and analyzes the inactivation of *Bacillus* spores following a radiation exposure and the process enacted by the *Bacillus* spore to repair the resulting damage. Irradiation of a spore and the medium surrounding the spore induces chemical reactions that produce reactive oxygen species (ROS). This research will consider the reaction-diffusion of these ROS throughout the spore. These ROS can react with the spore's DNA and enzymes to degrade them to such an extent that the DNA cannot be repaired or replicated, thus causing spore death. In order to survive a dose of radiation, a spore must repair its damaged DNA during germination. The DNA repair process is dependent on reactions catalyzed by enzymes that remain viable after the radiation treatment. Increased damage to the enzymes during radiation exposure effects the rate at which the spore's DNA is repaired. If the enzymes are damaged to such an extent that they cannot complete the DNA repair method, the spore will be unable to reproduce and achieve cellular outgrowth. A probability of survival model is created based on radiation damage due to the reaction of ROS with the spore's DNA and enzymes and the repair process.

This dissertation is dedicated to my husband who showed me how it's done. And to my family and friends who believed I could do this.

Acknowledgments

I would like to sincerely thank my advisor, Dr. Baker, for being a dedicated mentor and teacher. In addition, I would like to express my gratitude for my committee members, Dr. Burggraf, LTC Lewis, and Dr. Schubert Kabban. Their enthusiasm and patience while sharing their expertise is greatly appreciated.

Emily A. Knight

Table of Contents

List of Figures

x

List of Tables

List of Symbols

List of Acronyms

Acronym	Definition
B.a.	*Bacillus anthracis*
B.c.	*Bacillus cereus*
BER	Base Excision Repair
B.s.	*Bacillus subtilis*
B.t.	*Bacillus thuringiensis*
CDF	Cumulative Distribution Function
CPD	Cyclobutane Pyrimidine Dimer
DNA	Deoxyribonucleic Acid
DPA	Dipicolinic Acid
DSB	Double Strand Break
LET	Linear Energy Transfer
NER	Nucleotide Excision Repair
NHEJ	Non-Homologous End-Joining
PDF	Probability Density Function
RNA	Ribonucleic Acid
ROS	Reactive Oxygen Species
SASPs	Small Acid-soluble Spore Proteins
SP	Spore Photoproduct
SSB	Single Strand Break
UV	Ultraviolet

MODELING RADIATION EFFECTIVENESS FOR INACTIVATION OF *BACILLUS* SPORES

I. Introduction

The objective of this research is to model the inactivation of *Bacillus* spores following a dose of radiation. Irradiation of a spore and the medium surrounding the spore induces chemical reactions that produce reactive oxygen species (ROS). These ROS can react with the spore's deoxyribonucleic acid (DNA) and enzymes to degrade them to such an extent that the DNA cannot be repaired or replicated, thus causing spore death. The spore's DNA repair process is dependent on reactions catalyzed by enzymes that remain viable after the radiation treatment. If the enzymes are damaged to such an extent that they cannot complete the DNA repair method, the spore will be unable to reproduce and achieve cellular outgrowth. This research will model radiation damage to the *Bacillus* spore and its resulting repair mechanism in order to characterize a *Bacillus* population's probability of survival. This field of study has implications that range from food and water purification techniques to remediation of contamination from a bioweapon attack.

Multiple intentional and unintentional releases of *Bacillus anthracis* (*B.a.*) into the environment have caused widespread population panic. These cases culminated in 2001, following the terrorist attacks of 11 September, when *B.a.* spores were mailed through the U.S. Postal Service to members of the U.S. Senate and to national news agencies. These biological attacks resulted in 22 combined inhalational and cutaneous cases of infection. Of these 22 cases, five Americans died and "the nation was terrorized in what became the worst biological attacks in U.S. history" [5]. These attacks illustrated the prevalent need of the U.S. to consider the detection, recognition, environmental surveillance, and

decontamination of *B.a.* The Working Group on Civilian Biodefense identified *B.a.* as a biological agent that may be used as a weapon and "in worst case scenarios, could cause disease and deaths in sufficient numbers to gravely impact a city or region" [32]. The U.S. Department of Agriculture considers *B.a.* among the list of pathogens that could be used as a bioweapon [29]. In addition, the Center for Disease Control (CDC) has listed *B.a.* as a Select Agent which has "the potential to pose a severe threat to both human and animal health, to plant health, or to animal and plant products" [87]. And finally, the Department of Defense considers *B.a.* as a threat to military troops and describes it as "a disease that will kill, caused by a bacteria that already has been used as a weapon in America, and that terrorists openly discuss" [27]. Therefore, both political and military factions within the U.S. have stressed the need for counter terrorism weapons and biodefensive systems capable of destroying biological and chemical weapons [107].

Weaponized *B.a.* is not the only cause for concern with regards to the *Bacillus* genus. In August 2003, five members of the same family were admitted to a hospital with food poisoning symptoms and one child subsequently died due to a food-borne illness. *Bacillus cereus* (*B.c.*) was determined to be the causative agent [25]. The CDC estimates that one in six Americans contract a food-borne illness every year and 3000 of these annual cases are fatal. Furthermore, the most common causes of these cases are norovirus and bacteria [32]. Microbial growth of bacteria is thought to alter the character of food during handling, preparation, transportation, and storage. The presence of bacteria in food products can lead to food spoilage and food poisoning [2]. *B.c.* is a food-borne pathogenic bacterium that is linked to food poisoning and causes gastrointestinal diseases with symptoms ranging from mild nausea to frequent vomiting. However, as described above, contraction of the disease produced by *B.c.* can be fatal and the number of food poisoning cases caused by *B.c.* is thought to be underreported [92]. For both food safety and counter terrorism reasons, additional research must be completed on methods to inactivate *Bacillus* spores.

Further, recent events indicate that current laboratory processes to inactivate *Bacillus* spores are inadequate. The Pentagon claims that "insufficient technical information in the broader scientific community" was the cause of live *B.a.* spores being disseminated from a U.S. Army laboratory to 86 labs around the nation and seven foreign countries [74]. The spores were supposed to have been killed via gamma irradiation [102].

Specifically, this research will consider the inactivation of surface-adsorbed spores in a humid environment. This scenario can be applied to sterilization efforts of equipment that is contaminated with biological warfare agents. For example, researchers are examining military aircraft decontamination methods in order to prepare aircraft for use following a biological attack [3]. In addition, efforts are underway to investigate the microbial decontamination via UV radiation of spacecraft surfaces [56].

In summary, the proposed research couples radiation dose, damage, and repair in order to characterize a *Bacillus* population's probability of survival. This is done with the intent of modeling the inactivation of a population of *Bacillus* spores after it experiences radiation exposure. The specific proposed research objectives are listed below.

1.1 Research Objectives

- Analytically model the micro-level damage within a *B.a.* spore due to the reaction-diffusion of ROS throughout the spore following radiation exposure.

- Numerically model and analyze the nucleotide excision repair (NER) mechanism of a spore's damaged DNA.

- Relate the damage and repair models to determine a *B.a.* population's probability of survival based on the threshold killing mechanisms of *B.a.* spores.

1.2 Overview

The objectives previously defined will be presented in the following manner. The background material necessary to model biological processes is contained in Chapter 2.

Chapter 3 explains the radiation chemistry and production of ROS' that cause damage to a spore's DNA and enzymes. It describes the reaction-diffusion of these ROS throughout the spore and presents a mathematical model of the subsequent damage to the spore's DNA and enzymes. The development, numerical methods, and results of the DNA repair model will be presented in Chapter 4. Chapter 5 illustrates results of a probability of survival model for a *Bacillus* population based on the relationship between radiation dose, damage, and repair. Conclusions, as well as any suggested future work, are contained in Chapter 6.

II. Background

2.1   The *Bacillus* Spore

This research will discuss models that theorize the effects of radiation damage to different spore-forming *Bacillus* species such as *anthracis* and *cereus*. Other *Bacillus* spore formers that do not produce human disease (i.e. *Bacillus subtilis* (*B.s.*) and *Bacillus thuringiensis* (*B.t.*)) are often used as simulants for study of spore inactivation. Therefore it is necessary to discuss the the validity of using different species of the *Bacillus* genus to characterize spore radiation damage. All spores in the *Bacillus* genus share the same structural interior layers. *Bacillus* species differ with regards to the existence of the exosporium, which is the outermost layer of some *Bacillus* species. Specifically, the *Bacillus subtilis* (*B.s.*) species does not have an exosporium while its closely related species, *Bacillus anthracis* (*B.a.*), *Bacillus cereus* (*B.c.*), and *Bacillus thuringiensis* (*B.t.*), do [91]. Immediately inside the exosporium lays the spore coat and some *Bacillus* species are believed to have two spore coats instead of just one. Table 2.1 outlines the differences between the four *Bacillus* species mentioned above. The absence or presence of an exosporium is indicated by - or + respectively. Also included are size parameters for each species given in units of *microns* (μm) [16]. As discussed in the next section, these

Table 2.1: The *Bacillus* genus

Species	Exosporium	# of Coats	Diameter Range (μm)	Volume Range (μm^3)
B.a.	+	1	0.53-1.11	0.456-0.828
B.c.	+	1	0.76-1.14	0.543-0.771
B.s.	-	2	0.41-0.67	0.127-0.193
B.t.	+	1	0.59-0.96	0.424-0.574

structural differences do not contribute to the spore's radiation resistance. For these reasons it is assumed that radiation kill mechanisms are similar across the *Bacillus* genus.

2.1.1   *The Structure of Bacillus Spores.*

In order to adequately model damage to *Bacillus* spores there must be an understanding of the dormant spore's structure. From the outside of the spore to its center, the spore layers are the exosporium, the spore coat, the outer membrane, the cortex, the germ cell wall, the inner membrane, and the core. These are illustrated in Figure 2.1 (the layers are not drawn to scale) and each layer will be discussed in detail.
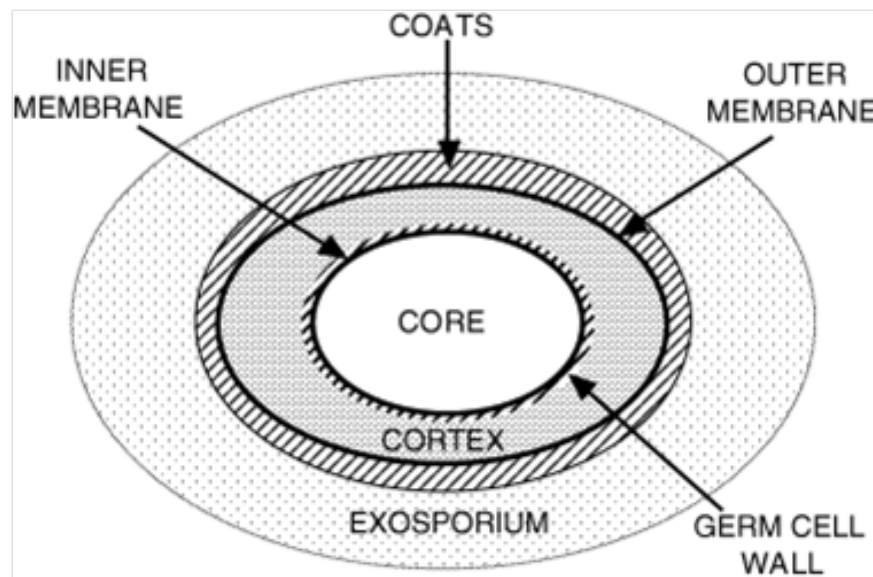
Figure 2.1: Structure of a *Bacillus* Spore. Figure reprinted with permission from [91]. Copyright 2006 John Wiley and Sons.

The outermost layer of the spore, the exosporium, is made up of proteins and the function of the exosporium is thought to be related to the types of cells that the *Bacillus* spore infects. The exosporium is readily permeable to small molecules and it does not contribute to the spore's resistance to radiation damage [2]. The spore coat is mainly composed of proteins but also contains small amounts of carbohydrates and lipids. The

coat acts as the spore's first line of defense against some chemical infiltration such as lytic enzymes that can harm the cortex layer. However, it is not considered to be a permeability barrier for other small molecules such as water molecules, and it does not provide the spore with any radiation resistance [2, 91].

The next layer, the outer membrane, is an essential structure for spore formation however it does not "constitute a significant permeability barrier against small molecules accessing the interior of the spore" [2]. In addition, it does not provide any spore resistance to radiation [91]. Multiple researchers have proved that the exosporium, spore coat, and outer membrane allow the passage of water molecules [28, 106]. Specifically, one of these experiments by Westphal and others found that an increase in relative humidity caused a spore to swell due to water intake.

Inside the outer membrane is the cortex which is a peptidoglycan layer. Peptidoglycan is a matrix of sugars and short polypeptides (a continuous chain of amino acids connected head-to-tail through peptide bonds) [99]. The cortex functions mainly as a retaining structure and reduces the water content of the spore core by allowing small molecules to pass through it [48]. The cortex is the most hydrated region of the spore as water makes up 48-57 percent of the cortex [2]. Immediately interior to the cortex is the germ cell wall which is also a peptidoglycan layer. The germ cell wall does not contribute to the spore's resistance to radiation damage [91].

The next layer of the spore is the inner membrane which is made up of lipids and proteins. The inner membrane is a strong permeability barrier which contributes to the spore's resistance to deoxyribonucleic acid (DNA)-damaging chemicals. "Even water may cross the spore's inner membrane very slowly" [91]. Yet experiments have demonstrated that approximately 97 percent of core water is transferable with its outside environment and while diffusion of water across the inner membrane is at least two orders of magnitude

slower than the membranes of vegetative cells, the movement of water through the inner membrane does occur [96].

The innermost spore layer is the core which contains most of the spore's enzymes and all of its DNA as well as other small molecules. Also found in the core are small acid-soluble spore proteins (SASPs) and dipicolinic acid (DPA). The SASPs are bound to the spore's DNA and both SASPs and DPA play a major role in the spore's resistance to ultraviolet radiation which will be discussed in Section 3.6.2. DPA may have a very minor influence on spore resistance to ionizing radiation by acting as a scavenger for radicals produced by water radiolysis (see Section 3.3) [2, 91]. Another contributing factor to a spore's resistance to radiation damage is its low core water content. The core water constitutes only 27 to 55 percent of the core wet weight and the extremely low amount of free water greatly restricts the macromolecular movement in the core. Specifically, the small water content may contribute to radiation resistance by reducing the amount of hydroxyl radicals that are formed but this fact has not yet been proven [68]. The effect of the water content in the spore will be discussed further in Chapter 3. The next section will concentrate on the structure of the spore's DNA.

2.1.2   The Structure of DNA [99, 105].

The spore's DNA is the genetic code of the spore and transfer of its information is possible due to its unique structure. The DNA is made up of bases and two sugar phosphate backbones composed of a deoxyribose sugar molecules linked to phosphate groups. The four bases are adenine, cytosine, guanine, and thymine and can be visualized in Figure 2.2. Note that thymine and cytosine, the pyrimidine bases, have single-ring structures while adenine and guanine, the purine bases, have double ring structures. In addition, Figure 2.2 shows the connection between complementary bases adenine and thymine via hydrogen bonds which are represented by dashed lines. The hydrogen-bonded adenine and thymine entity is called a base pair. Similarly, guanine and cytosine form a base pair. The bonding
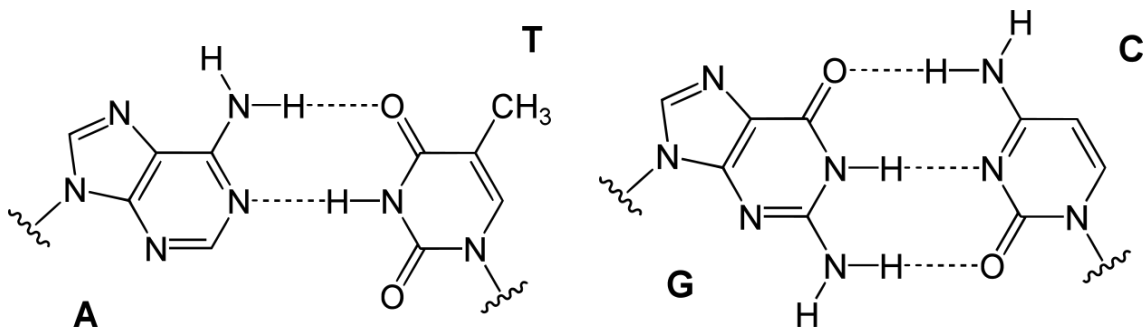
(a) Adenine (A) and Thymine (T) Base Pairs (b) Guanine (G) and Cytosine (C) Base Pairs

Figure 2.2: DNA Base Pairs. Figure reprinted with permission from [10]. Copyright Creative Commons.

of adenine, a double-ring structure, with thymine, a single ring structure, is very important to maintain the three dimensional structure of the DNA. The bonding of two single ring structures within a DNA strand would create a divot in its backbone. Similarly, if two double ring structures were paired together, there would be a bulge in the DNA's backbone. Any such conformational changes of the DNA structure must be repaired before the DNA can be accurately replicated. Repair processes will be described in Chapter 4. The straight lines in Figure 2.2 represent covalent bonds which are stronger than hydrogen bonds. The two long backbone strands of the DNA wrap around each other to form a double helix (see Figure 2.3).

The genetic information is encoded within the DNA by the sequence of the bases composing the DNA molecule. The spore uses its genetic information to synthesis proteins through a two stage process of transcription and translation. Transcription provides for the information from a segment of DNA (a gene) to be communicated to ribonucleic acid (RNA). Translation is the process by which information from the RNA is turned into proteins as shown in Figure 2.4. During translation, three bases encode for a letter in the genetic language, called a codon. A specific codon corresponds to a particular amino acid
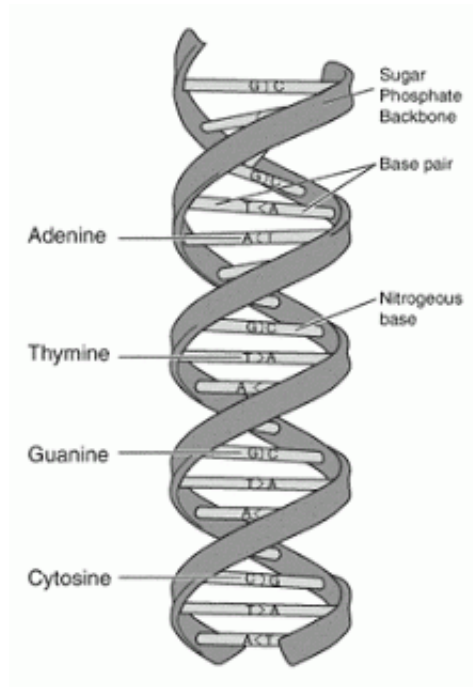
Figure 2.3: The DNA Double Helix. Figure reprinted with permission from [98]. Courtesy: National Human Genome Research Institute

(labeled A site in Figure 2.4) that is placed in a unique location of the protein polymer chain (labeled P site in Figure 2.4) during its synthesis.

Three bases of ordered information allow 64 possible encoding combinations. The capability of the three-base letter is more than sufficient to encode for 20 amino acids that make up the proteins, thus there exists redundancy in the code. As a result, removing or altering the third base pair in the sequence of three bases in a codon may or may not destroy the information content identifying its corresponding amino acid. However, it should be noted that removing the first base more frequently causes problems. One incorrect amino acid can dramatically alter the function of the protein. Hence, damage to a particular DNA base can have a range of effects depending on the information content of the codon or the information content of the base within the codon [48]. The process by which the dormant

10
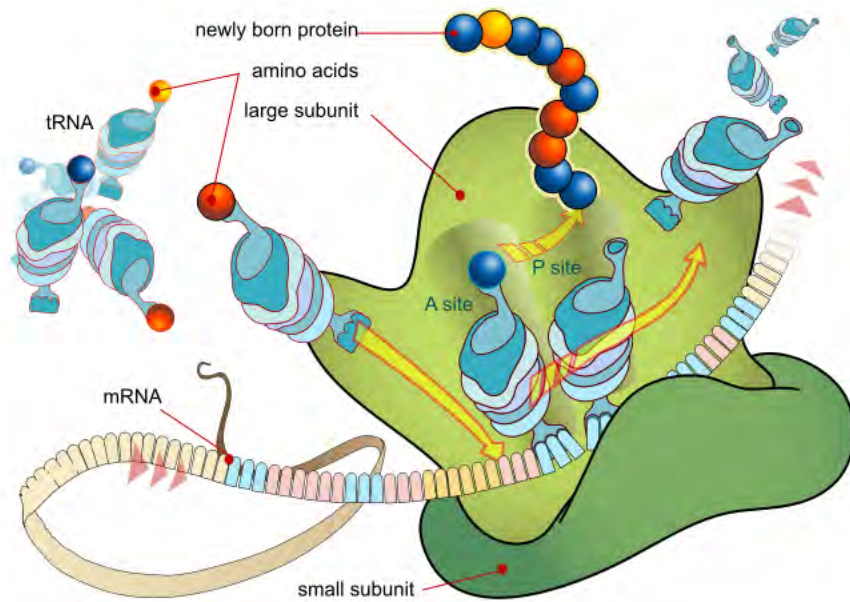
Figure 2.4: The Translation Process. Figure released into the public domain from [82].

spore is formed, how it becomes a vegetative cell, and the method by which it reproduces will be described in the next section.

2.2   Life Cycle of a Bacterial Spore

A dormant spore is formed via a multi-step process called sporulation (refer to Figure 2.5). The first step of sporulation is the replication of DNA within the core. DNA replication is an enzymatically controlled process that duplicates the base sequence of the DNA double helix. Replication begins with the separation of the two sugar phosphate backbones. In order to accomplish this separation, the hydrogen bonds between the complementary base pairs are severed while the backbones remain intact. A new DNA strand is synthesized from the base pairs with the cleaved hydrogen bonds. DNA replication is semiconservative as the two resulting double helices consist of one old sugar phosphate backbone and one new complementary strand [54].

11

After DNA replication, sporulation continues with the formation of the spore septum which is an ingrowth of the inner membrane. The spore septum separates the replicated DNA and a small portion of the core's cytoplasm to include enzymes. The structure enclosed by the spore septum is called the forespore. The next step of sporulation is the creation of a thick spore coat of proteins around the forespore. This new structure is called the endospore and once it matures, the endospore is freed from the vegetative cell by the rupturing of the spore cell wall [99].
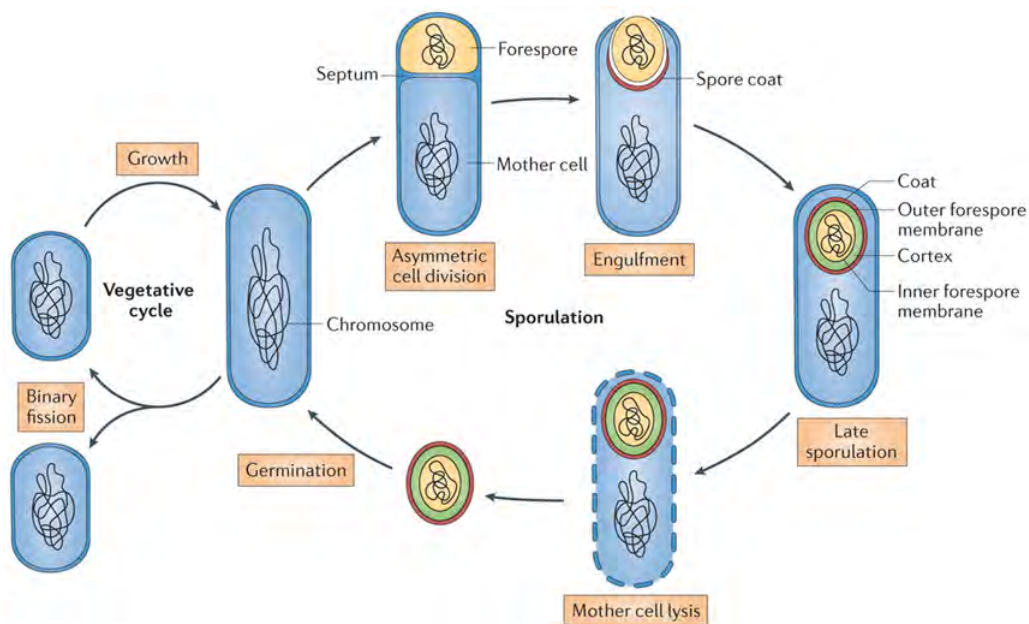
Figure 2.5: Sporulation. Figure reprinted by permission from Macmillan Publishers Ltd: Nature Reviews Microbiology [57], copyright 2012.

A dormant spore can survive for extremely long periods of time and in harsh environmental conditions. In a nutrient rich environment, the endospore will undergo germination which is the first step in the process by which bacteria transforms from a dormant spore into a vegetative cell [28]. The nutrient induced germination process allows changes to the permeability of the inner membrane. During the first few minutes of

germination, the spore core takes in water and releases DPA [20]. The water content of growing cells constitutes approximately 80 percent of its wet weight. In order to achieve this exchange of molecules during germination, the inner membrane expands (see Figure 2.5). This contributes to an increase in the spore's susceptibility to radiation damage during germination because of the increased molecular movement and amount of water molecules in the core. In addition, this process further demonstrates that the inner membrane is permeable. During germination the cortex and spore coat are degraded by enzymes which allows hydration of the spore core. Mutants lacking a single enzyme are still able to germinate, however dormant spores lacking both of the two cortex degrading enzymes are not able to initiate outgrowth [2]. Rehydration of the spore core allows protein mobility which, in turn, permits enzyme action. This triggers the transition from germination to vegetative metabolism and thus cellular outgrowth.

It is only during germination that the spore's enzymatic activity allows the spore to repair any damage incurred during dormancy [88]. DNA repair is conducted via spore enzymes and will be discussed further in Chapter 4. However, since dormant spores do not synthesis enzymes, the spore must contain enough viable enzymes to complete the repair process. If too much damage is accumulated, "this damage can overwhelm the capacity of repair systems and lead to the death of the germinated spore" [90].

Note that the sporulation process involves one vegetative cell creating one dormant spore thus sporulation is not a means of reproduction. Reproduction is the development of a vegetative cell instead of an endospore. Bacteria reproduce through binary fission which is the formation of two daughter cells from a single parent cell. Specifically, the DNA replicates itself and the germ cell wall and inner membrane elongate and begin to form around each of the two chromosomes. Eventually the cell wall and inner membrane fully encapsulate each DNA strand and the cells separate as shown by Figure 2.5 [99].

Outgrowth of a colony of bacteria occurs in four phases; the lag phase, the exponential phase, the stationary phase, and the decline or death phase. These phases are depicted in Figure 2.6. During the lag phase, the bacteria population experiences a large amount of metabolic activity in which it is repairing DNA and replicating both DNA and enzymes. There exists little to no binary fission during this phase. It is during the lag phase that the population is the most susceptible to radiation and chemical damage because adverse conditions will interfere with the growth process. The exponential phase is the phase in which the cells begin to divide and the population undergoes exponential growth. When the production of new cells is balanced with the number of cell deaths, the colony of bacteria has entered the stationary phase. During this period of equilibrium, the metabolic activity of individual cells is slowed. The death phase indicates that the number of cell deaths exceeds the number of vegetative cells being formed. The population size will decrease at a logarithmic rate until only a fraction of its cells remain or the population entirely dies out [99].
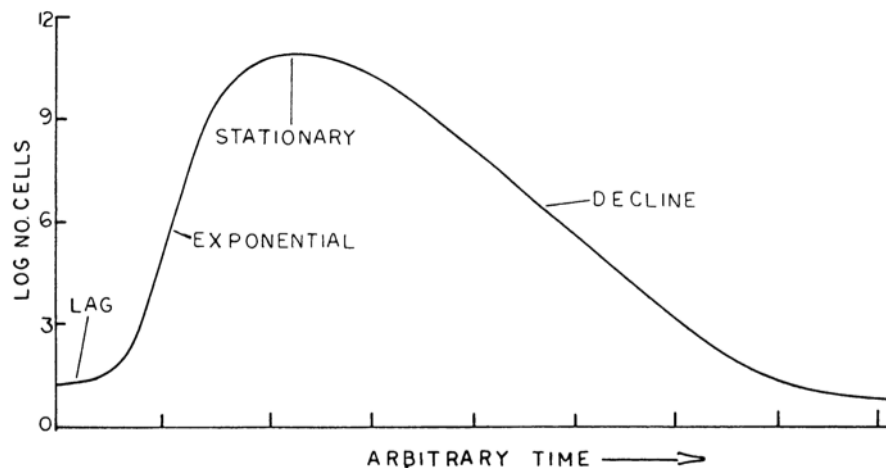
Figure 2.6: Phases of Outgrowth. Figure reprinted with permission from [84]. Copyright 1987, American Society for Microbiology.

14

2.3   Summary

This chapter has described the structure and life cycle of a *Bacillus* spore and the structure of its DNA. These characteristics will play an important role in the damage mechanisms and ultimately inactivation of *Bacillus* spores. This research will model damage to the *Bacillus* species by irradiation which is discussed in the next chapter.

III. Radiation Damage

Radiation damage to biological matter can be categorized into two broad groups; direct and indirect action. Direct action is the direct deposition of energy into a biological molecule of interest such as DNA. A single event of direct radiation action upon an important biological molecule will most likely result in a loss of biological activity of the molecule [4]. This research will focus on the inactivation of biological spores due to indirect action.

Indirect action is "the interaction of solute molecules and the reactive species of solvent molecules formed by the direct action of radiation on the solvent" [4]. Most indirect action in aqueous media will result from interactions of important biomolecules in the spore with reactive oxygen species (ROS) formed by the irradiation of adsorbed water molecules. Specific products formed by the irradiation of water molecules are discussed in Section 3.3. Prior to that, the two types of radiation (ultraviolet (UV) and ionizing radiation) will be examined along with the differences in their chemical reactions due to various levels of energy deposition.

3.1   Ionizing Radiation

Ionizing radiation produces highly energetic, ionizing rays and radiolysis is the absorption of a particle of ionizing radiation. When a quanta of ionizing radiation interacts with matter, a fast electron is produced which then proceeds to produce ionization along its track. When a material experiences radiolysis, one quantum or particle of ionizing radiation excites many molecules within the medium and the reactive species produced by ionizing radiation are not homogeneously distributed in the solution.

There are many forms of ionizing radiation such as β-, γ-, and X-rays and electrons, protons, and α-particles. Ionizing radiations are often categorized according to their linear

energy transfer (LET) [66]. LET for charged particles of ionizing radiation is the rate at which energy, E, is transferred to an absorbing material per unit length of track, x, which can be represented mathematically by

$$\text{LET} = -\frac{\mathrm{d}E}{\mathrm{d}x}.$$

At lower energies, the Bethe formula for stopping power, or energy loss suffered by a charged particle, is given by [64]

$$-\frac{\mathrm{d}E}{\mathrm{d}x} = \frac{4\pi z^2 e^4}{mv^2} NZ \ln \frac{2mv^2}{I}$$

where

ze = charge of the incident particle

e = electron

v = velocity of the incident particle

m = mass of the electron

N = molecules per volume

Z = number of electrons per molecule

I = average ionization potential.

As shown by this equation, LET of lower energy particles increases as kinetic energy $\left(\frac{1}{2}mv^2\right)$ decreases. In other words, as the ionizing particles are slowed down in the medium, their LET increases. Therefore, towards the end of a track, the LET will be much higher because the energy of the particle decreases significantly. This means that the region of ionization at the end of the track will be both bigger and denser. This region is referred to as a blob. In addition, spurs caused by ionization of secondary electrons may extend from the primary ionization track. Figure 3.1 depicts the extension of spurs from the main linear path of an ionizing particle. The specific nature of each track of ionization is dependent

17
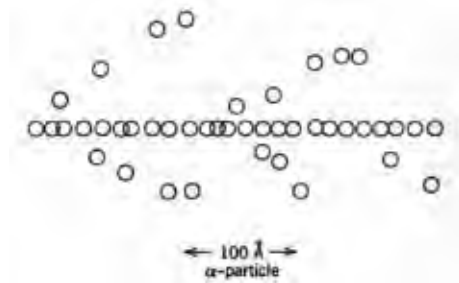
Figure 3.1: Track and Spur Depiction. Figure reprinted from [40] Copyright (1973), with permission from Elsevier.

upon the type of ionizing particle. For example, a 1 megaelectronvolt (1 *MeV*) electron,

a subatomic particle with a negative charge which belongs to the low-LET class, ionizes

approximately one molecule out of every 5000 along its track. In comparison, a 1 *MeV*

α-particle, a positively charged, high mass particle with high-LET, ionizes every molecule

along its track. This makes α-radiation the most destructive form of ionizing radiation [40].

Let A represent one molecule of matter. A typical chemical reaction resulting from

radiolysis is represented by

$$A + h\nu \rightarrow A^+ + e^- + h\nu'$$
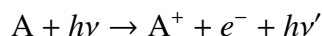
where $h\nu$ is the energy of the incoming photon and e is one electron. This reaction describes

the Compton effect in which a photon collides with an electron and drives the electron out

of its molecule. The photoelectric effect occurs when the photon collides with an electron

and is absorbed by that electron. In this case, the electron is known as the photoelectron

and is denoted by e^-. The reaction given by the photoelectric effect is characterized by [64]

$$A + h\nu \rightarrow A^+ + e^-.$$
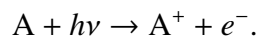
3.2   Ultraviolet Radiation

UV radiation emits quanta of energies (or photons) anywhere from one to ten

eV although it is more commonly categorized by its wavelength which ranges from

18

approximately 100 to 400 nanometers (nm). Table 3.1 distinguishes between the UV-A, UV-B, and UV-C ranges of the UV spectrum.

Table 3.1: UV Categories [2]

UV Type	Wavelength
UV-A	315-400 nm
UV-B	280-315 nm
UV-C	100-280 nm

UV radiation produces photolysis, otherwise known as photochemistry, in which chemical reactions are caused by absorption of light. In photochemistry, each quantum of radiation is absorbed by one molecule which produces one excited state therefore the excited states are homogeneously distributed in a homogeneous solution. The typical chemical reaction resulting from photolysis is

$$A + h\nu \rightarrow A^*$$
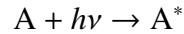
where A^* represents the excited state of the molecule of matter, A [40]. The specific interactive species produced by the radiolysis and photolysis of water are discussed in the next section.

3.3 Radiation of Water

The reactive species produced by the ionizing radiation of water are OH, H, H_2O_2, H_2, e_{aq}^-, H_3O^+, and OH^-. The chemical reactions that produce these interactive species will now be explored. According to Moore [64], regardless of the source of radiation, the first two chemical reactions due to radiation are

$$H_2O \rightarrow H_2O^+ + e_{aq}^- \qquad (3.1)$$

$$H_2O^+ + H_2O \rightarrow H_3O^+ + OH \tag{3.2}$$

which generates the hydrated electron, e_{aq}^-, and the hydroxyl radical, OH. Also according to Moore [64], radiolysis will produce many OH radicals close together and therefore they may combine to produce hydrogen peroxide:

$$2OH \rightarrow H_2O_2.$$
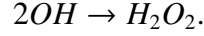
A subsequent chemical reaction is

$$OH + H_2O_2 \rightarrow HO_2 + H_2O$$
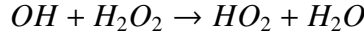
which produces the peroxy radical HO_2. The hydrated electron from Equation 3.1 reacts with water to create the hydrogen radical:

$$e_{aq}^- + H_2O \rightarrow H + OH^-.$$
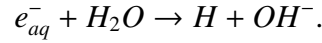
The hydrogen radicals can combine with each other in the following reaction:

$$2H \rightarrow H_2.$$
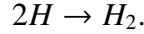
The previous reactions are just a few of the possible reactions that occur in pure water. If there exists a thin layer of adsorbed water on a surface, then the adsorbed water would be saturated with dissolved O_2. Thus the chemical reaction

$$H + O_2 \rightarrow HO_2 \tag{3.3}$$

could occur. Similarly, the presence of oxygen can produce the superoxide radical as shown by the following reaction:

$$e_{aq}^- + O_2 \rightarrow O_2^-.$$
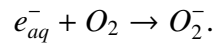
All of these reactions are governed by rates of reactions which will be discussed in the next section.

3.4 Reaction Kinetics

The study of rates of chemical processes is known as reaction kinetics. The main factors influencing the reaction rates are; the concentration and physical state of the reactants, the temporal behavior of the reactants and the presence of any catalyst in the reaction [67]. The rate at which HO_2 is produced from Equation 3.3 is given by

$$\frac{d\,[HO_2]}{dt} = k\,[H]\,[O_2]$$

where

$$[HO_2] = \text{concentration of } HO_2 \,(M)$$

$$t = \text{time (seconds (s))}$$

$$k = \text{reaction rate coefficient} \,(M^{-1}s^{-1})$$

$$[H] = \text{concentration of } H \,(M)$$

$$[O_2] = \text{concentration of } O_2 \,(M).$$

The units of $[HO_2]$, $[H]$, and $[O_2]$ are given by molarity, or molar concentration. Molarity is denoted by M and is defined as the number of moles of solute per litre of solvent (i.e. $M = mol/L$). The concept of reaction kinetics will be used throughout the development of mathematical models for damage, repair, and kill probability.

Table 3.2 contains the rate coefficients given in units of $M^{-1}s^{-1}$ for the chemical reactions described above and many more. When considering conflicting reaction rate coefficients found in the literature, the rate corresponding to a reaction in the most neutral pH environment was recorded. The reason for this is because most bacteria survive an environment with pH measurements between five and eight and "microbial cells require their internal pH to remain constant in order to maintain essential cell functions" [93]. It should also be noted that the chemical reactions that occur in highly alkaline solutions were not considered. And finally, the reaction $H + H_2O \rightarrow OH + H_2$ was not included because

Table 3.2: Reactants and Rate Coefficients for the Radiolysis of Aqueous Solutions [30, 40]

Reactant	Rate Coefficient ($M^{-1}s^{-1}$)
$H_2O^+ + H_2O \rightarrow H_3O^+ + OH$	1×10^{10}
$2OH \rightarrow H_2O_2$	5.3×10^9
$OH + H_2O_2 \rightarrow HO_2 + H_2O$	3.8×10^7
$e_{aq}^- + H_2O_2 \rightarrow OH + OH^-$	1.3×10^{10}
$e_{aq}^- + H_3O^+ \rightarrow H + H_2O$	2.06×10^{10}
$e_{aq}^- + H_2O \rightarrow H + OH^-$	1.6×10^{10}
$e_{aq}^- + H \rightarrow H_2 + OH^-$	3×10^{10}
$e_{aq}^- + e_{aq}^- \rightarrow H_2 + 2OH^-$	5×10^9
$e_{aq}^- + O_2 \rightarrow O_2^-$	1.9×10^{10}
$e_{aq}^- + OH \rightarrow OH^-$	3×10^{10}
$e_{aq}^- + HO_2 \rightarrow HO_2^-$	2×10^{10}
$OH + H \rightarrow H_2O$	3.2×10^{10}
$OH + H_2 \rightarrow H + H_2O$	6×10^7
$OH + HO_2 \rightarrow O_2 + H_2O$	7.1×10^9
$H + H \rightarrow H_2$	7.9×10^9
$H + HO_2 \rightarrow H_2O_2$	2×10^{10}
$H + O_2 \rightarrow HO_2$	2.6×10^{10}
$H + H_2O_2 \rightarrow OH + H_2O$	3.44×10^7
$OH + O_2^- \rightarrow O_2 + OH^-$	9.96×10^9
$OH + HO_2^- \rightarrow HO_2 + OH^-$	5×10^9
$HO_2 + O_2^- \rightarrow O_2 + HO_2^-$	9.5×10^7
$2HO_2 \rightarrow H_2O_2 + O_2$	8.1×10^5

this reaction only occurs in the absence of oxygen [4]. This table is not all inclusive as many other chemical reactions are possible; however, these are the predominant reactions.

The rate of reaction is limited by the encounter rate of reacting species and the rate of mutual diffusion. The diffusion controlled rate limits the frequency at which molecules can collide with each other in a solution. Diffusion controlled reactions occur so quickly that the rate of reaction becomes the rate of transport of the reactants through the solution. The diffusion controlled limit in water is on the order of 10^{10} $M^{-1}s^{-1}$ which means that in water the rate of reactions from Table 3.2 cannot be larger than 10^{10} $M^{-1}s^{-1}$ [105]. Molecular diffusion will be discussed in the next section.

3.5 Molecular Diffusion

Molecular diffusion is the movement of molecules from a region of higher concentration to that of a region with lower concentration. This transport of molecules is founded on random molecular movement. Diffusion is mathematically modeled via Fick's first law of diffusion which states that the flux of a species is proportional to its gradient of concentration [67]:

$$J = -D\nabla c \tag{3.4}$$

where

$$J = \text{flux} \left(\frac{M}{m^2\,s} \right)$$

$$D = \text{diffusion coefficient} \left(\frac{m^2}{s} \right)$$

$$c(x, t) = \text{concentration of a species (M)}$$

$$x = \text{position (meters (m))}$$

$$t = \text{time (s)}.$$

The diffusion coefficient measures "how efficiently the particles disperse from a high to a low density" [67]. The negative sign reflects the fact that molecular flow is from a

high concentration to a low concentration. Table 3.3 contains some of the molecular compounds produced by ionizing radiation and their diffusion coefficients in water. All diffusion constants are recorded in units of m^2s^{-1} and with water temperatures between 20 and 25 degrees Celsius (room temperature).

Table 3.3: Diffusion Coefficients [31, 40, 95, 105]

Reactant	Diffusion Coefficient (m^2s^{-1})
H_2O_2	1.4 x 10^{-9}
HO_2	2 x 10^{-9}
H_3O^+	3.62 x 10^{-7}
OH^-	1.97 x 10^{-7}
OH	2 x 10^{-9}
H	4.5 x 10^{-9}
O_2	2 x 10^{-9}
e_{aq}^-	4.25 x 10^{-7}

3.6   Radiation Damage to a Spore

Another difference between ionizing and UV radiation is the type of damage they inflict upon a dormant spore. The next two sections will describe the broad range of damage to the molecules within a spore caused by ionizing and UV radiation.

3.6.1   Ionizing Radiation Damage.

Some of the ROS' discussed in Section 3.3 cause indirect damage to the spore's DNA. They can produce radiation-induced base modifications within the DNA such as the severing of an amino group from a DNA's base pair. This type of base modification is called deamination. Another base modification example is depurination which is the loss of

24

a purine base. Base modifications will most likely induce a base pair mismatch which will create a bulge or divot in the DNA backbone. Without repair, this structural conformation of the backbone will prohibit the DNA from being read during the replication process which can be lethal to the spore. Table 3.4 gives the rate of reaction of the hydrated electron, e_{aq}^-, with the DNA bases. It has also been shown that base modifications can result from OH reacting with DNA bases and H reacting with the pyrimidine bases [14]. For example, the reaction of OH with thymine will result in an abstraction of an H-atom [26].

Table 3.4: Rates of Reaction of e_{aq}^- with DNA Bases [66]

DNA Base	Reaction Rate ($M^{-1}s^{-1}$)
Adenine	3×10^{10}
Cytosine	$7\text{-}10 \times 10^9$
Guanine	2.5×10^8
Thymine	1.7×10^{10}

In addition to base pair reactions, ROS can target the DNA backbone resulting in a broad range of radical-induced products. For example, the OH radical can react with the sugar-phosphate backbone of the DNA strand by abstracting an H-atom from a sugar molecule to form water. The H radical can also abstract H molecules from the sugars on the DNA strand to form H_2. Measured reaction rate constants of the OH and H radicals with the sugar moiety of the DNA strand are 8×10^8 M^{-1} s^{-1} and 7.8×10^8 M^{-1} s^{-1} respectively [4].

The reaction of OH and H radicals with the sugar-phosphate DNA backbone is one of the production mechanisms for single strand breaks (SSB), which are scissions of one of the DNA strands. Scissions of both strands simultaneously is called a double strand break (DSB). If two SSBs occur on opposite backbones and the SSBs lie within a close

proximity of each other, the two SSBs can lead to a DSB. While some researchers indicate that the maximum separation of two SSBs that can become a DSB is six to ten base pairs [4], others claim that multiple lesions within 20 base pairs of DNA can lead to a DSB [38]. Although SSBs are often easy to repair, DSBs are difficult to repair and can result in cell death, mutations, or carcinogenisis.

Indirect action has also been shown to damage the structure of spore layers. Oxidizing agents, to include H_2O_2, appear to kill spores by causing damage to the spore's inner membrane. Identical resistance to oxidizing agents was seen in "spores of strains with very different levels of unsaturated fatty acids" [19]. Therefore experimentalists believe oxidative damage to essential proteins in the inner membrane may be the cause of spore death. Researchers suggest that spore death occurs because the damaged inner membrane becomes non-functional or ruptures during germination [53]. Other researchers claim that H_2O_2 reacts with molecules in the spore cortex which protects the core from H_2O_2 damage. However, the exact method in which this would inactivate the spore is unknown [79].

Some researchers claim lethal doses of H_2O_2 inactivate spores by damaging its enzymes. Experiments have shown that enzymes necessary for germination and outgrowth have experienced lethal damage following a spore's treatment with H_2O_2 [73]. While there is no consensus on the precise target of H_2O_2 reactions, all researchers agree that H_2O_2 does not inactivate a spore by damaging its DNA. OH has been shown to cause damage to eukaryotic proteins following ionizing irradiation. And while this damage alone was not proven to be lethal, researchers believe that ionizing radiation-induced protein damage combined with DNA breakage may result in the inactivation of cellular activities necessary for DNA repair [51]. Repair of DNA damage will be detailed further in Chapter 4.

3.6.2 *UV Radiation Damage.*

The primary damage mechanism of UV radiation is direct action near the absorption site. UV radiation produces a wide range of DNA damage to include dimers and spore

26

photoproduct (SP), and in rare cases, SSBs and DSBs. "Cyclobutane pyrimidine dimers constitute the major DNA photoproducts upon exposure to UV-B light" while SP is the main damage mechanism experienced by the DNA after UV-C irradiation [61, 81]. However, both UV-B and UV-C irradiation of bacteria will cause dimers and SPs to form within the spore's DNA.

DNA bases, primarily the pyrimidine bases, directly absorb incident UV-B photons. A cyclobutane pyrimidine dimer (CPD) is the connection of two adjacent pyrimidine bases on the same DNA backbone strand. CPDs occur when absorbed photon breaks the hydrogen bonds of complementary base pairs and these pyrimidine bases bond with adjacent pyrimidine bases on the same DNA strand. The three types of CPDs are thymine-thymine, thymine-cytosine, and cytosine-thymine. Figure 3.2 demonstrates the formation of a thymine-thymine CPD. Dimers will create a kink in the DNA backbone which will prevent the DNA from being transcribed which is potentially lethal [105].
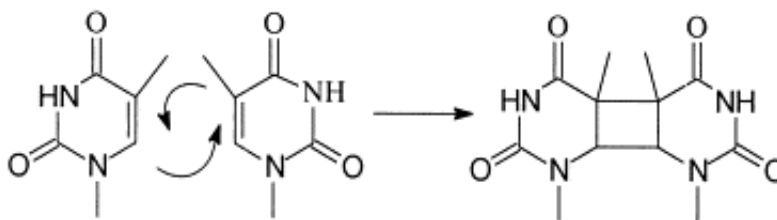
Figure 3.2: Formation of Thymine Cyclobutane Dimer. Figure reprinted with permission from [81]. Copyright 2001 Elsevier Science B.V.

Spore photoproduct is also created after a DNA base absorbs an incident photon. SP is formed between two adjacent thymine bases on the same DNA strand when the two bases bond to the same methyl group. See Figure 3.3 for a visual representation of the SP structure. Approximately 30 percent of UV irradiated DNA thymine is able to be converted

into SP. Similar to dimers, SP also causes helix-distorting lesions which if not repaired, can prevent the DNA from replicating [90].
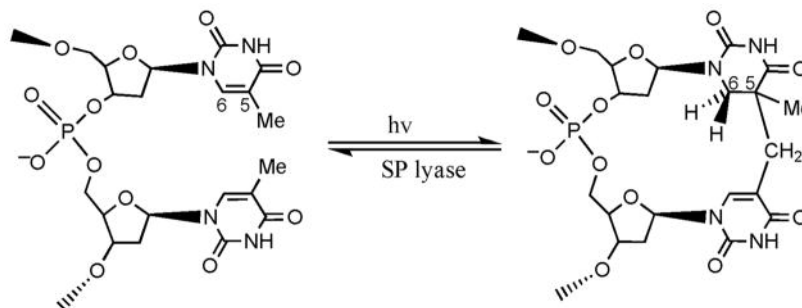
Figure 3.3: Spore Photoproduct. Figure reprinted with permission from [90]. Copyright 1996, American Society for Microbiology.

Small acid-soluble spore proteins (SASPs) of the α/β-type, so named after the two major proteins found in *Bacillus subtilis* , provide a significant contribution to the spore's UV radiation resistance. The α/β-type SASPs are double-stranded DNA binding proteins that each cover approximately five base pairs. There are enough SASPs in each spore to saturate the spore chromosome. By binding to the outside of the DNA helix, the α/β-type SASPs protect the backbone from enzyme and chemical attacks. Research has shown that mutant *Bacillus* spores lacking the α/β-type SASPs are much more UV sensitive than wild-type (existing in nature) spores. It is believed that due to their binding capability, α/β-type SASPs prevent the formation of dimers during UV irradiation, however, UV-B still produces enough thymine-thymine dimers to cause spore death [90]. The α/β-type SASPs are degraded during spore germination, and if not, "their continued presence interferes significantly with subsequent development...by blocking DNA transcription" [2]. Thus, the α/β-type SASPs are the reason that UV irradiated dormant spores form SPs while vegetative cells mainly experience CPD damage following UV irradiation. Now that radiation damage

mechanisms have been examined, the mathematical modeling of radiation damage in the literature will be explored.

3.7   Literature Review

Past research on mathematical modeling of ionizing radiation damage has focused on the effects of charged particles in their tracks. The charged particles create radiation-induced products and the species created diffuse and react with the matter in their track. Thus the majority of ionizing radiation modeling within a particle's track has utilized variations of the reaction-diffusion equation. The basic reaction-diffusion equation of a species with itself in the absence of scavengers, or reactants that react extremely quickly with other like species, is

$$\frac{\partial R}{\partial t} = D\Delta R - kR^2$$

where

R = concentration of the reactant species

t = time

D = diffusion coefficient

k = rate constant for a reaction of the species with itself.

Many one-radical models have been constructed in past research and some include the existence of a scavenger. However, models that only consider the reaction-diffusion of one radical are chemically unrealistic. The different rate and diffusion coefficients are each represented by one value and many models did not recognize the difference between radical recombinations and other chemical reactions which misrepresents chemical yields [66].

Kuppermann [66] constructed a multiradical diffusion model with a Gaussian initial distribution of radicals. The model contained seven reactive species and three scavengers. Kuppermann's model was solved numerically and compared to experimental data with

varying degrees of success. Schwartz [66] also constructed and numerically solved a multiradical model and allowed for five adjustable parameters related to initial radical yields and spur size. The adjustable parameters were fit to sets of experimental data.

In addition to the number of radicals and scavengers considered in a model, past ionizing radiation modeling research has also varied regarding the geometry of the track. Some researchers consider a cylindrical track while others claim a track is composed of widely spaced spherical spurs which can be thought of as a string of beads. The spherical spurs strung along a track are generated by low-LET irradiation. The effect of high LET, as with α-particles, is the merging of spurs to form a cylindrical track. A high LET cylindrical track allows for nearly complete radical recombination while a spherical spur only allows partial recombination [31].

Magee and Chatterjee [31] believe that the chemical product yield of particles should be modeled via reaction-diffusion equations but they claim that the track should be modeled as two separate entities. Magee and Chatterjee believe the track consists of the core and the penumbra which is the area immediately surrounding the core. Within the core, head-on collisions occur which have a high energy loss per event but only a few primary events account for this large energy loss. Glancing collisions occur within the penumbra and this type of collision has a low energy loss per event while the amount of events is relatively large.

Stochastic modeling of radiation chemistry has included Monte Carlo simulation, the master equation approach, and the independent reaction time model. Monte Carlo simulations model the reaction and diffusion of species via random flight simulations and average the probabilities of reaction, diffusion, and separation over a large number of trials. For example, if a particle is within the reaction radius of another particle, it is assumed the particles will react with a given probability. Stochastic approaches which allow for fluctuation in the number of reactant species have been suggested as a valid replacement of

the deterministic differential reaction-rate equations. Specifically Gillespie [36] provided a stochastic simulation algorithm which used a Monte Carlo procedure to model collision probability per unit time. The algorithm considered a number of molecules in a mixture of chemical species which can interact through specified chemical reaction channels present at an initial time. The model predicted what the molecular population levels would be at any later time. It was based on thermal activation energies and did not consider diffusion. Monte Carlo simulation is computationally intensive and has not yet successfully been compared to experimental data except in cases with very few reactants [66].

The master equation approach "considers the state of a spur at a given time to be composed of N_i particles of species i" where N_i is a random variable [66]. This method is mathematically similar to a variation of the diffusion equation and it can be easily generalized for multiradical spurs. However, it does not represent the various reactions of reactive products so it requires a relatively simple reaction scheme. The independent reaction time model treats the immediate reaction of a reactive species given an initial position differently than its intermediate reactions which are generated by the inversion of a first passage time problem. The model assumes that pairwise reaction times are independent of other reactions. Results of the independent reaction time model have compared positively to experimental data [66].

3.8   Mathematical Damage Model

This research will examine radiation damage to a spore's DNA and enzymes via an illustrative model to frame all of the important indirect radiation damage processes. The model described has relevance to sterilization of spores or eukaryotic cells adsorbed on surfaces in an ordinary humid environment. First, the mathematical model of damage to a spore's DNA via reaction-diffusion partial differential equations will be presented.

31

3.8.1 Reaction-Diffusion of ROS Within the Spore.

A demonstrative scenario will be explored in order to simulate the indirect effects of ionizing radiation in a spur on a spore. Consider a narrowly collimated source of radiation impinging on an inert solid plate having a thin layer of adsorbed water of thickness h and an adsorbed spore (refer to Figure 3.4). The distance between the radiation source and the spore is considered to be larger than the spore diameter of $2r$. The water layer is thick enough that $2r < h$ and yet thin enough that the layer can be assumed to be uniformly saturated with dissolved O_2 adsorbed from the air. This realizable scenario can be treated as an approximate two dimensional model of radiation induced damage to a spore by ROS.
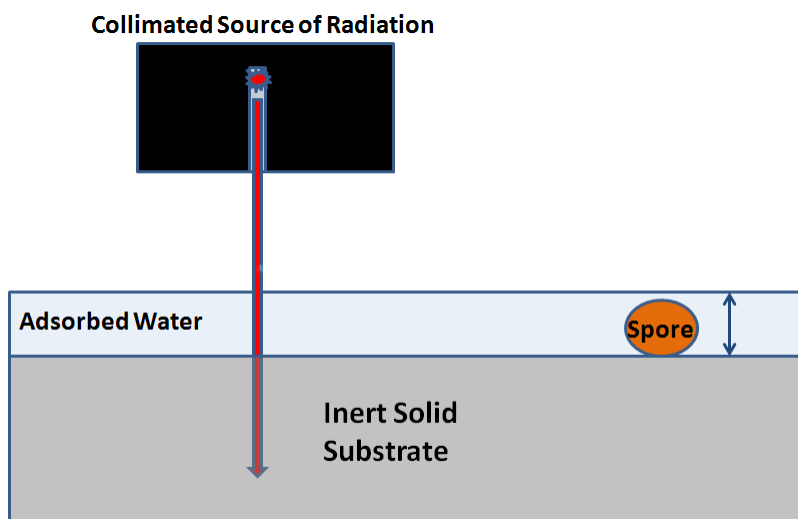
Figure 3.4: Illustration of Radiation, Medium, and Spore Scenario

As a result of the radiation source, several reactive species are generated in the neighborhood of the radiation path through the O_2 saturated water. These reactive species are loosely split into two classes. Class 1 will contain radicals which are highly reactive and diffuse rapidly in the water having molar concentration R_1. R_1 represents the class

that reacts quickly with the O_2 present in the adsorbed water and therefore instantaneously transforms into other species. The hydrated electron, e_{aq}^-, is an example of this class of reactants. Class 2 will contain radicals which are less reactive and diffuse slower having concentration R_2. R_2 represents the class that does not react as fast as the R_1 class and therefore does not get transformed as quickly. In other words, if k_i is the reaction rate constant for species R_i, then $k_2 \ll k_1$. This allows the class of R_2 reactants to diffuse to the outer boundary of the spore. HO_2 and O_2^- are examples of this class of reactants.

The concentration of class 2 reactants, R_2, can be determined as a function of the dose of the initial stream of radiation. Assume this concentration is uniformly impressed on the outer boundary of a spherical model for the spore as it would be if the spore is located far enough away from the radiation source that the reactants are dispersed uniformly throughout the substrate. This reactant class will react as it diffuses into the spore. The spore is assumed to have uniform material properties and there exist no permeability barriers within the spore that would interfere with the diffusion of reactants through the spore. Thus the spore is assumed to be spherically symmetric (no angular dependence) and the diffusivity, D_3, is assumed to remain constant across the radius, r, of the spore. Finally, it is assumed that initially there exist no radicals within the spore and there is no flux on the outer boundary of the spore. The process will be modeled as a partial differential equation with boundary and initial conditions and an analytical solution will be presented. In addition, an expression for the average reactant concentration within the spore's core will be discovered.

The partial differential equation which models the class 2 reactants as they diffuse into the spore is

$$\frac{\partial R_2}{\partial t} = \nabla \cdot D_3 \nabla R_2 - k_3 R_2 \tag{3.5}$$

where

$$D_3 = \text{diffusivity of } R_2 \text{ into the spore}$$

$$R_2(r, t) = \text{concentration of class 2 reactants}$$

$$r = \text{spherical distance}$$

$$t = \text{time}$$

$$k_3 = \text{reaction rate constant.}$$

Note that R_2 is a function of time, t, and the spherical distance, r. The term $k_3 R_2$ represents the rate of R_2 reactions within the spore. In other words, k_3 is rate at which class 2 reactants react with biological compounds within the spore as they diffuse throughout the spore. The constant diffusivity and lack of angular dependence allow the Laplacian to be evaluated in two dimensions and Equation 3.5 becomes

$$\frac{\partial R_2}{\partial t} = D_3 \left(\frac{\partial^2 R_2}{\partial r^2} + \frac{2}{r} \frac{\partial R_2}{\partial r} \right) - k_3 R_2 \tag{3.6}$$

Since the concentration of class 2 reactants is assumed to be uniformly impressed on the outer boundary of the spore, the initial concentration of R_2 outside the spore is a function of time is denoted as $f(t)$. The source term on the outer boundary gives the following boundary condition

$$R_2(r_o, t) = f(t) \text{ where } r_o \text{ represents the outer spore radius.} \tag{3.7}$$

Initially, there are no R_2 radicals in the spore, so

$$R_2(r, 0) = 0. \tag{3.8}$$

The solution must be finite (particularly at $r = 0$), that is,

$$|R_2(r, t)| < \infty. \tag{3.9}$$

The first step in solving Equation 3.6 is applying separation of variables. Letting $R_2(r, t) = X(r)T(t)$ gives

$$XT' = D_3 T X'' + \frac{2D_3 T}{r} X' - k_3 XT$$

$$\frac{T'}{T} = D_3 \frac{X''}{X} + \frac{2D_3}{r} \frac{X'}{X} - k_3 = -\mu \tag{3.10}$$

34

where μ is a separation parameter. The solution to $\frac{T'}{T} = -\mu$ is

$$T(t) = e^{-\mu t} \tag{3.11}$$

Upon multiplication of Equation 3.10 by $\frac{X}{D_3}$, it becomes

$$X'' + \frac{2}{r}X' + \frac{\mu - k_3}{D_3}X = 0$$

which written in self adjoint form is

$$\frac{1}{r^2}[r^2 X'(r)]' + \frac{\mu - k_3}{D_3}X(r) = 0. \tag{3.12}$$

Let $X(r) = \frac{J(r)}{r}$ for $r \neq 0$ so that $r^2 X(r) = rJ(r)$. In addition,

$$X'(r) = \frac{rJ'(r) - J(r)}{r^2}.$$

Substituting these definitions for $X(r)$ and $X'(r)$ into Equation 3.12 produces

$$\frac{1}{r^2}[rJ'(r) - J(r)]' + \frac{\mu - k_3}{D_3}\frac{J(r)}{r} = 0$$

which reduces to

$$J''(r) + \frac{\mu - k_3}{D_3}J(r) = 0.$$

Now let $\lambda^2(\mu) = \frac{\mu - k_3}{D_3}$ then $J''(r) + \lambda^2 J(r) = 0$ and $J(r) = E\cos(\lambda r) + F\sin(\lambda r)$ for $\frac{\mu - k_3}{D_3} > 0$. For $\frac{\mu - k_3}{D_3} \leq 0$, only the trivial solution exists. Therefore,

$$X(r) = \frac{E\cos(\lambda r) + F\sin(\lambda r)}{r}$$

and

$$X'(r) = \frac{-E\lambda r\sin(\lambda r) + F\lambda r\cos(\lambda r) - E\cos(\lambda r) - F\sin(\lambda r)}{r^2}. \tag{3.13}$$

It has been assumed that the spore is spherically symmetric therefore at the center of the spore, $\frac{\partial R_2}{\partial r}(0, t) = 0$, which means $X'(0)T(t) = 0$. Equivalently,

$$\lim_{r \to 0^+} X'(r) = 0.$$

35

This is applied to Equation 3.13 and leads to $E = 0$ so that

$$X(r) = \frac{F \sin(\lambda r)}{r}.$$

In order to satisfy the homogeneous boundary condition, $X(r_o) = 0$,

$$X(r_o) = \frac{F \sin(\lambda r_o)}{r_o} = 0. \tag{3.14}$$

To solve this equation, note that $F = 0$ will produce the trivial solution. Therefore, $\sin(\lambda r_o) = 0$ so

$$\lambda_n = \frac{n\pi}{r_o}, \quad n = 1, 2, ...$$

Thus the μ_n's are the eigenvalues (recall $\mu_n = D_3 \lambda_n^2 + k_3$) which give eigenfunctions, X_n's, defined as

$$X_n(r) = F_n \frac{\sin(\lambda_n r)}{r}, \quad n = 1, 2, ...$$

F_n is found by normalizing $X_n(r)$ which is done by choosing F_n such that

$$\begin{aligned}
1 &= \int_0^{r_o} \int_0^{2\pi} \int_0^{\pi} r^2 X_n^2 \sin(\phi) d\phi d\theta dr \\
&= 4\pi \int_0^{r_o} F_n^2 \sin^2(\lambda_n r) dr \\
&= 2\pi F_n^2 \int_0^{r_o} [1 - \cos(2\lambda_n r)] dr \\
&= 2\pi F_n^2 \left[r_o - \frac{\sin(2r_o\lambda_n)}{2\lambda_n} \right] \\
&= 2\pi F_n^2 \left[r_o - \frac{1}{\lambda_n} \sin(r_o\lambda_n) \cos(r_o\lambda_n) \right]
\end{aligned}$$

Equation 3.14 implies $\sin(r_o\lambda_n) = 0$ which means that $1 = 2\pi F_n^2 r_o$ so that

$$F_n = \frac{1}{\sqrt{2\pi r_o}},$$

and

$$X_n(r) = \frac{1}{\sqrt{2\pi r_o}} \frac{\sin\left(\frac{n\pi}{r_o} r\right)}{r}.$$

Lemma 3.8.1. *The eigenfunctions, $X_n(r)$, are orthonormal on the interval $(0, r_o)$ with respect to the inner product $<f, g> = 4\pi \int_0^{r_o} r^2 f(r)g(r)\mathrm{d}r$ (i.e. $<X_n, X_m> = \delta_{mn}$).*

Proof:

$$
\begin{aligned}
<X_n, X_m> &= 4\pi \int_0^{r_o} r^2 X_n(r)X_m(r)\mathrm{d}r \\
&= 4\pi \int_0^{r_o} r^2 \frac{1}{2\pi r_o r^2} \sin\left(\frac{n\pi}{r_o}r\right)\sin\left(\frac{m\pi}{r_o}r\right)\mathrm{d}r \\
&= \frac{2}{r_o} \int_0^{r_o} \sin\left(\frac{n\pi}{r_o}r\right)\sin\left(\frac{m\pi}{r_o}r\right)\mathrm{d}r
\end{aligned}
$$

if $n = m$ then

$$
\begin{aligned}
<X_n, X_m> &= \frac{2}{r_o} \int_0^{r_o} \sin^2\left(\frac{n\pi}{r_o}r\right)\mathrm{d}r \\
&= \frac{1}{r_o} \int_0^{r_o} \left[1 - \cos\left(\frac{2n\pi}{r_o}r\right)\right]\mathrm{d}r \\
&= \frac{1}{r_o}\left[r_o - \frac{r_o \sin(2n\pi)}{2n\pi}\right]
\end{aligned}
$$

and because $\sin(2n\pi) = 0$, this case gives $<X_n, X_m> = 1$. If $n \neq m$ then

$$
<X_n, X_m> = \frac{2}{r_o} \int_0^{r_o} \sin\left(\frac{n\pi}{r_o}r\right)\sin\left(\frac{m\pi}{r_o}r\right)\mathrm{d}r = 0
$$

therefore combining the two cases gives

$$
<X_n, X_m> = \delta_{mn}. \qquad \blacksquare
$$

Since $\mu_n = D_3\lambda_n^2 + k_3$, Equation 3.11 becomes

$$
T_n(t) = A_n e^{-\mu_n t}, \ n = 1, 2, ...
$$

where A_n is an arbitrary constant. Therefore, the solution to the homogeneous partial differential equation with homogeneous boundary conditions is of the form

$$
R_2(r, t) = \sum_{n=1}^{\infty} X_n(r)T_n(t) = \sum_{n=1}^{\infty} \frac{A_n}{\sqrt{2\pi r_o}} \frac{\sin\left(\frac{n\pi}{r_o}r\right)}{r} e^{-\left[D_3\left(\frac{n\pi}{r_o}\right)^2 + k_3\right]t}.
$$

Next, the forcing function at the boundary, $R_2(r_o, t) = f(t)$, should be considered. Let

$$R_2(r, t) = f(t) + W(r, t) \tag{3.15}$$

where $W(r, t) = \sum_{n=1}^{\infty} X_n(r) T_n(t)$. Note that $w(r_o, t) = 0$ and

$$\frac{\partial R_2}{\partial t} = f'(t, d) + W'(r, t) = f'(t) + \sum_{n=1}^{\infty} X_n(r) T_n'(t). \tag{3.16}$$

Recall that the original partial differential equation (Equation 3.5) was

$$\frac{\partial R_2}{\partial t} = \nabla \cdot D_3 \nabla R_2 - k_3 R_2$$

which can combine with Equation 3.16 to give

$$f'(t) + \sum_{n=1}^{\infty} X_n(r) T_n'(t) = -k_3 f(t) - k_3 \sum_{n=1}^{\infty} X_n(r) T_n(t) + \sum_{n=1}^{\infty} T_n(t) \frac{D_3}{r^2} \left[r^2 X_n'(r) \right]'. \tag{3.17}$$

Using Equation 3.12 for the last term in Equation 3.17 gives

$$f'(t) + \sum_{n=1}^{\infty} X_n(r) T_n'(t) = -k_3 f(t) - k_3 \sum_{n=1}^{\infty} X_n(r) T_n(t) + \sum_{n=1}^{\infty} T_n(t) \lambda_n^2 X_n(r)$$

or

$$\sum_{n=1}^{\infty} \left[T_n'(t) + k_3 T_n(t) + D_3 \lambda_n^2 T_n(t) \right] X_n(r) = -k_3 f(t) - f'(t).$$

After applying Lemma 3.8.1,

$$T_n'(t) + \mu_n T_n(t) = [-k_3 f(t) - f'(t)] < 1, X_n > \tag{3.18}$$

where, using integration by parts,

$$
\begin{aligned}
< 1, X_n > &= \frac{4\pi}{\sqrt{2\pi r_o}} \int_0^{r_o} r \sin\left(\frac{n\pi}{r_o} r\right) dr \\
&= \frac{4\pi}{\sqrt{2\pi r_o}} \left[\left(\frac{r_o}{n\pi}\right)^2 \sin\left(\frac{n\pi}{r_o} r\right) - \frac{r r_o}{n\pi} \cos\left(\frac{n\pi}{r_o} r\right) \right] \Big|_0^{r_o} \\
&= -\frac{4}{\sqrt{2\pi r_o}} \frac{r_o^2}{n} \cos(n\pi) \\
&= (-1)^{n+1} \frac{r_o^{3/2}}{n} \sqrt{\frac{8}{\pi}}.
\end{aligned}
$$

38

Multiply both sides of Equation 3.18 by the integrating factor $e^{\mu_n t}$ produces

$$e^{\mu_n t}\left[T'_n(t) + \mu_n T_n(t)\right] = \frac{d}{dt}\left[e^{\mu_n t} T_n(t)\right]$$

$$= e^{\mu_n t}[-k_3 f(t) - f'(t)] < 1, X_n >$$

Integrating both sides of the equation with respect to t gives

$$e^{\mu_n t} T_n(t) - T_n(0) = < 1, X_n > \int_0^t \left[-e^{\mu_n \tau} k_3 f(\tau) - e^{\mu_n \tau} f'(\tau)\right] d\tau$$

Integration by parts applied to the right hand side of the equation produces

$$e^{\mu_n t} T_n(t) - T_n(0) = < 1, X_n > \left\{ \int_0^t -e^{\mu_n \tau} k_3 f(\tau) d\tau - [e^{\mu_n \tau} f(\tau)]_0^t + \int_0^t \mu_n e^{\mu_n \tau} f(\tau) d\tau \right\}$$

$$= < 1, X_n > \left\{ \int_0^t \lambda_n^2 e^{\mu_n \tau} f(\tau) d\tau - e^{\mu_n t} f(t) + f(0) \right\}. \tag{3.19}$$

Initially (at time $t = 0$) there are no radicals in the spore, i.e. $R_2(r,0) = 0$. Therefore, Equation 3.15 becomes

$$R_2(r,0) = 0 = f(0) + \sum_{n=1}^{\infty} X_n(r) T_n(0)$$

$$-f(0) = \sum_{n=1}^{\infty} X_n(r) T_n(0).$$

Testing with X_n and applying Lemma 3.8.1 results in

$$T_n(0) = - < 1, X_n > f(0)$$

Using this initial condition, Equation 3.19 becomes

$$e^{\mu_n t} T_n(t) = < 1, X_n > \left\{ \int_0^t \lambda_n^2 e^{\mu_n \tau} f(\tau) d\tau - e^{\mu_n t} f(t) \right\}$$

or

$$T_n(t) = - < 1, X_n > f(t) + < 1, X_n > \int_0^t \lambda_n^2 e^{\mu_n(\tau - t)} f(\tau) d\tau.$$

Now

$$R_2(r, t) = f(t) + \sum_{n=1}^{\infty} X_n(r) T_n(t)$$

$$= f(t) + \sum_{n=1}^{\infty} X_n(r) \left\{ - <1, X_n> f(t) + <1, X_n> \int_0^t \lambda_n^2 e^{\mu_n(\tau-t)} f(\tau) d\tau \right\}$$

$$= \sum_{n=1}^{\infty} \lambda_n^2 X_n(r) <1, X_n> \int_0^t e^{-\mu_n(t-\tau)} f(\tau) d\tau \tag{3.20}$$

as

$$\sum_{n=1}^{\infty} X_n(r) <1, X_n> = 1.$$

The spore's DNA is located within its core. Therefore, to determine the amount of reactants that can damage the spore's DNA, the average concentration of class 2 reactants within the core must be calculated. Let $R_2^c(t)$ denote the average concentration of class 2 reactant within the core of the spore. In order to calculate the average concentration, the total R_2 concentration in the core is found first by integrating with respect to spherical coordinates over the core volume. Then the total concentration is divided by the core volume $\left(V_{\text{core}} = \frac{4}{3} \pi r_c^3 \right)$, where r_c denotes the radius of the spore's core.

$$R_2^c(t) = \frac{1}{V_{\text{core}}} \int_0^{r_c} \int_0^{2\pi} \int_0^{\pi} R_2(r, t) r^2 \sin(\phi) d\phi d\theta dr$$

$$= \frac{3}{4\pi r_c^3} \int_0^{r_c} R_2(r, t) r^2 \int_0^{2\pi} \int_0^{\pi} \sin(\phi) d\phi d\theta dr$$

$$= \frac{3}{r_c^3} \int_0^{r_c} R_2(r, t) r^2 dr. \tag{3.21}$$

Substituting Equation 3.20 into Equation 3.21 gives

$$R_2^c(t) = \frac{3}{r_c^3} \int_0^{r_c} \left\{ \sum_{n=1}^{\infty} \lambda_n^2 X_n(r) <1, X_n> \int_0^t e^{-\mu_n(t-\tau)} f(\tau) d\tau \right\} r^2 dr$$

$$= \frac{3}{r_c^3} \sum_{n=1}^{\infty} \left\{ \int_0^t e^{-\mu_n(t-\tau)} f(\tau) d\tau \right\} \left\{ \int_0^{r_c} \lambda_n^2 X_n(r) <1, X_n> r^2 dr \right\}$$

$$= \frac{3}{r_c^3} \sum_{n=1}^{\infty} [-2\cos(n\pi)] \int_0^t e^{-\mu_n(t-\tau)} f(\tau) d\tau \int_0^{r_c} \lambda_n r \sin(\lambda_n r) dr$$

$$= \frac{3}{r_c^3} \sum_{n=1}^{\infty} [-2\cos(n\pi)] \left\{ \frac{1}{\lambda_n} \sin(\lambda_n r_c) - r_c \cos(\lambda_n r_c) \right\} \int_0^t e^{-\mu_n(t-\tau)} f(\tau) d\tau \tag{3.22}$$

40

which reduces to

$$R_2^c(t) = \sum_{n=1}^{\infty} K_n \int_0^t e^{-\mu_n(t-\tau)} f(\tau) d\tau \tag{3.23}$$

where

$$K_n = \frac{3}{r_c^3} \lambda_n^2 < 1, X_n > \int_0^{r_c} X_n(r) r^2 dr \tag{3.24}$$

$$= (-1)^{n+1} \frac{6}{r_c^3} \left\{ \frac{1}{\lambda_n} \sin(\lambda_n r_c) - r_c \cos(\lambda_n r_c) \right\}. \tag{3.25}$$

The parameters utilized within the reaction-diffusion model are included in Table 3.5. The initial concentration of R_2 on the outer boundary of the spore, denoted by $f(t)$, is developed from experimental values and models of species' reaction-diffusion within an ionizing particle's spur. The collimated source is assumed to be low-LET radiation applied via a pulse (1 nanosecond (ns) pulse of 20 Mev electrons). Between 10^{-15} and 10^{-12} seconds after irradiation of an aqueous solution, ions and excited states are formed. Chemical reactions begin to take place around 10^{-12} seconds and radicals within a spur reach their initial yield, or highest concentration, at around 10^{-10} seconds as shown in Figure 3.5 [44, 66]. At this time, the chemical yields for OH, H, and H_2 are 5.9, 0.62, and 0.15 molecules per 100 eV respectively [31]. OH decays at a fast rate after it reaches its initial yield (i.e. the OH yield decreases by 30 percent within 3 ns where 1 ns is equivalent to 1 x 10^{-9} seconds) which is also depicted in Figure 3.5 [31, 44]. Note that the time scales for the horizontal axis in Figure 3.5 are different.

Table 3.5: Parameters of the Reaction-Diffusion Model

Parameter	Value	Source
r_o	.58 (μm)	[106]
r_c	.4 (μm)	[106]
k_3	.5 $\left(nM^{-1} s^{-1}\right)$	[4, 30]
D_3	2 x 10^3 $\left(\mu m^2 s^{-1}\right)$	[31]

(a) Production of Class 2 Radicals   (b) Decay of Class 2 Radicals
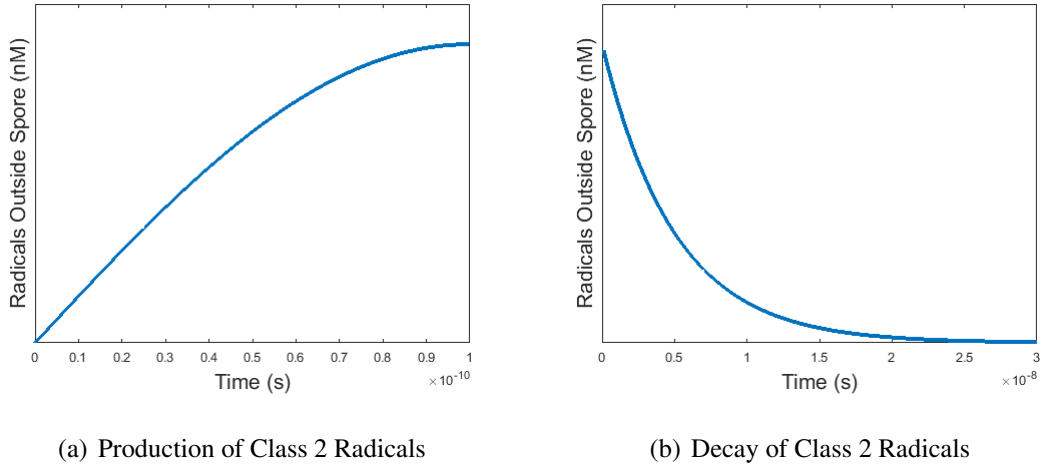
Figure 3.5: Concentration of R_2 on outer boundary of spore

The parameters in Table 3.5 and the initial concentration of R_2 on the outer boundary of the spore shown in Figure 3.5 are utilized to find the average concentration of class 2 reactants in the spore core given by Equation 3.23. Figure 3.6 demonstrates the evolution of R_2^c over time. Note that the core concentration of reactants reaches its maximum value at approximately 10 ns after the application of the low-LET radiation pulse and then decays rapidly due to the decrease of R_2 reactants on the spore boundary. Radicals in the core will damage the spore's DNA and enzymes which will be discussed in the next two sections.

3.8.2 DNA Damage.

The rate of DNA damage caused by ROS is modeled by

$$-\frac{\mathrm{d}[D]}{\mathrm{d}t} = k_d R_2^c(t)[D](t) \tag{3.26}$$

where

$[D](t)$ = concentration of DNA in the spore (nM)

t = time (s)

k_d = rate coefficient of ROS interaction with DNA $\left(\mathrm{nM}^{-1}\mathrm{s}^{-1}\right)$

42
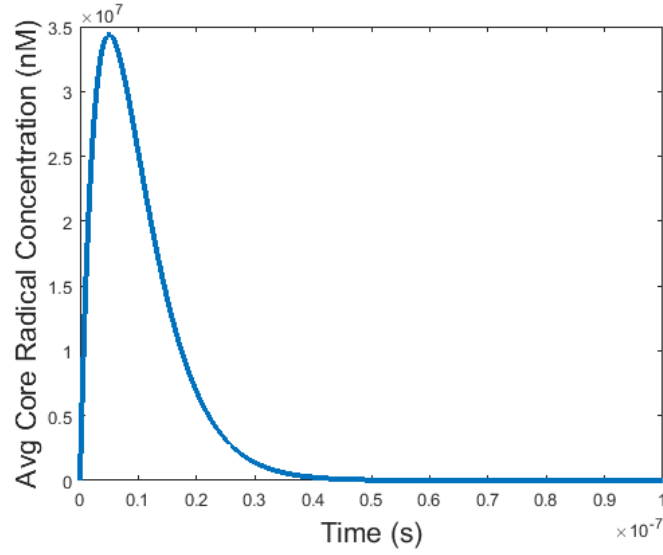
Figure 3.6: Average Concentration of R_2 Reactants in Spore Core

and $R_2^c(t)$ is the average concentration of class 2 reactants in the core defined by Equation 3.23. Equation 3.26 characterizes the rate of change in the DNA content of a spore. By integrating with respect to time, the solution to the rate equation is

$$[D](t) = [D]_T f_D(t) \tag{3.27}$$

with the fraction of DNA remaining after some radiation exposure time, t, defined as $f_D(t) = e^{-k_d R(t)}$ where

$$R(t) = \int_0^t R_2^c(\tau) d\tau. \tag{3.28}$$

At time $t = 0$, the initial concentration of DNA, $[D]_T$, is determined by a spore's total DNA concentration prior to radiolysis which is given by the value 2.87×10^7 nM [11]. The initial DNA concentration in the core is based on the concentration of DNA in the *E. coli* cell. It is utilized for the purpose of uniformity because while the concentration of DNA in the *B.a.* spore is known (3.23×10^7 nM [8]), repair rate parameters used in Chapter 4 are more readily available for the *E. coli* cell. The parameter, k_d, is given by the reaction rate of the hydroxyl radical with the sugar moiety of the DNA strand (i.e. 0.8 nM^{-1} s^{-1})

[4]. Figure 3.7 illustrates the fraction of undamaged DNA, f_D, remaining in the spore over time. As the radicals in the core react with and damage the spore's DNA, the percentage of viable DNA decreases. The irradiation via a low-LET pulse (1 ns pulse of 20 Mev electrons) damages approximately 10 percent (exactly 9.63 percent) of the DNA according to the model presented here.
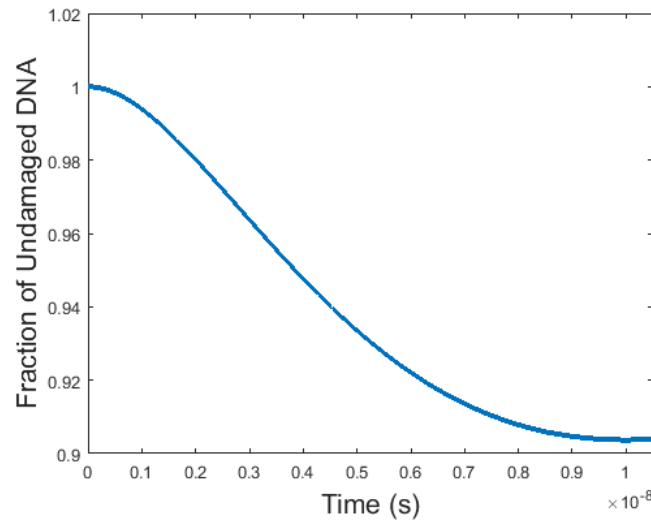
Figure 3.7: Fraction of Undamaged DNA in Spore After Irradiation

3.8.3 Enzyme Damage.

In addition to DNA damage, damage is inflicted on the spore's proteins during radiation exposure. As discussed in Section 3.6.1, ROS have been proven to damage the spore's enzymes which are proteins that catalyze chemical reactions. DNA repair proteins existing within the spore are necessary to repair damage accumulated within the dormant spore and thus are extremely important to spore outgrowth [42]. Since "accumulation of oxidative damage to proteins diminishes their catalytic activities and interactions" [22], some sources claim the death of a cell is more highly correlated to protein damage than to DNA damage [50]. Others go as far as to state that the spore's proteins are the "principal

44

target of the biological action" of ionizing radiation [23]. Therefore, DNA must be repaired before a viable cell is produced during germination and there must be a suitable amount of repair enzymes that survive the radiation exposure to accomplish this. Since ROS reacting with DNA and enzymes could decimate these molecules to such an extent that they can no longer be repaired, an enzyme damage model is presented.

There are six enzymes involved in nucleotide excision repair (NER) which is the primary mechanism of radiation repair. NER and the role each enzyme plays in the repair process will be described in Section 4.3. Let $e(t)$ be the vector of enzyme concentration for a given spore within the population at time t where $e(t) = [e_1(t), \ldots, e_6(t)]^T$. The rate of enzyme damage caused by reactions with ROS is represented by

$$-\frac{de}{dt} = K_e R_2^c(t) e(t) \tag{3.29}$$

where $R_2^c(t)$ is defined by Equation 3.23 and K_e is a diagonal matrix of rate coefficients for reactant interaction with each enzyme $\left(nM^{-1}s^{-1}\right)$ i.e. $K_e = \text{diag}\{k_{e_1}, \ldots, k_{e_6}\}$. This equation characterizes the rate of change in viable enzyme activity of a spore. By integrating with respect to time, Equation 3.29 becomes

$$e(t) = f_e(t) e_0 \tag{3.30}$$

where

$$f_e(t) = e^{-K_e R(t)}$$

is the diagonal matrix for the fraction of remaining enzymes after irradiation. The vector $e_0 = [e_{1_0}, \ldots, e_{6_0}]^T$ is the initial concentration and $R(t)$ is defined in Equation 3.28. For this work, the rate coefficients, k_{e_i}, are assumed to have the same value for each enzyme and are further assumed to be identical to k_d which is the reaction rate of the OH radical with DNA.

At time $t = 0$, prior to radiation exposure, the initial enzyme concentration, e_0 is determined by the spore chosen from a population with a certain enzyme content

density function based on various preparation parameters. "Spores prepared at different temperatures have a number of significant differences in properties" [35]. In addition, spore preparation temperature effects the core water content which in turn influences a spore's resistance to radiation damage [59]. Therefore, this research will consider that a population of radiation treated spores has a certain initial 'fitness' probability density function (PDF) based on viability of enzyme capacity to repair DNA, and by choosing one spore from the sample, we are provided a specific enzyme concentration. At time $t = 0$, e_0, is randomly drawn from this continuous PDF which has a mean of μ_{e_0} and a variance denoted by $\sigma_{e_0}^2$. Note that the initial enzyme 'fitness' is assumed to be independent of the fraction of remaining enzymes after irradiation.

The mean and variance of a continuous random variable can be defined in terms of expectations. Thus

$$\mu_{e_0} = E[e_0] \tag{3.31}$$

and

$$\sigma_{e_0}^2 = V[e_0] = E\left[(e_0 - \mu_{e_0})^2\right]. \tag{3.32}$$

Observe that within the variance expression, the square of $e_0 - \mu_{e_0}$ is done component wise. Expectation is a linear operator so given constants α and β, E[αX+β]=αE[X]+β for a random variable X [17]. Since e_0 is a random variable, $e(t)$ is also a random variable drawn from a PDF with mean, μ_e, and variance, σ_e^2. Using the linear operator properties and Equation 3.30, the mean of $e(t)$ is defined as

$$\mu_e = E[e(t)]$$

$$= E\left[f_e(t)e_0\right]$$

$$= f_e(t)E\left[e_0\right]$$

$$= f_e(t)\mu_{e_0}.$$

In addition, the variance of $e(t)$ is given by

$$
\begin{aligned}
\sigma_e^2 &= E\left[(e(t) - \mu_e)^2\right] \\
&= E\left[(f_e(t)e_0 - f_e(t)\mu_{e_0})^2\right] \\
&= (f_e(t))^2 E\left[(e_0 - \mu_{e_0})^2\right] \\
&= (f_e(t))^2 \sigma_{e_0}^2.
\end{aligned}
\tag{3.33}
$$

Note that the development of Equation 3.33 is possible because $f_e(t)$ is a diagonal matrix of constant values. So the variance of the $e(t)$ PDF, σ_e^2, is scaled by a matrix factor of $(f_e(t))^2$.

The six NER enzymes are UvrA, UvrB, UvrC, helicase II, polymerase I, and ligase. Values found in the literature for the number of UvrB molecules in an *E. coli* cell range from approximately 200 to 250 and approximately 20 to 25 copies of the UvrA enzyme are reported to be in each cell [100, 103]. Also, researchers have shown that approximately 2400 to 3000 molecules of the helicase II enzyme exist in each *E. coli* cell [7, 76]. Finally, 479 copies of polymerase I and 226 copies of ligase in the *E. coli* cell were counted during an experiment while other literature reports there are approximately 400 and 200 molecules per *E. coli* cell of polymerase I and ligase, respectively [101]. Therefore, the spore population's initial concentration for each of the six enzymes is modeled via the Uniform PDF with a range of 20 percent about their mean values (i.e. the range is plus/minus 10 percent from the mean). The state of each of the six enzymes is assumed to be independently distributed. The value used for the mean of each enzyme of the *E. coli* cell is outlined in Table 3.6. Note that both *E. coli* and the *Bacillus* genus utilize the same six NER enzymes however the number of copies for all of the enzymes in the *E. coli* cell is reported in the literature and for consistency, is used here.

The Uniform PDF is represented by

$$
\phi_X(x) = \begin{cases} \frac{1}{b-a}, & a \le x \le b \\ 0, & \text{otherwise} \end{cases}
\tag{3.34}
$$

Table 3.6: Enzyme Data for *E. coli*

Enzyme	Copies/Cell	Source	Concentration
A	23	[100, 103]	38.2 nM
B	225	[100, 103]	373.6 nM
C	10	[100, 103]	16.6 nM
H	2750	[7, 76]	4566.5 nM
P	440	[101]	730.6 nM
L	200	[101]	332.1 nM

where $b - a$ represents the range of X, the continuous random variable. The Uniform PDF has mean, $E[X] = \frac{b+a}{2}$ and variance, $V[X] = \frac{(b-a)^2}{12}$ [17]. Figure 3.8 is an illustration of the density function for the population's UvrB content prior to and after radiation exposure. The red line represents the PDF of the population's undamaged UvrB concentration which has a mean of 373.6 nM and a range of 336.2 to 411.0 nM. The black PDF depicts the distribution of the UvrB enzyme when it has been degraded to 90 percent of its original state (i.e. its mean is now 336.2 nM). The blue line illustrates the UvrB enzyme at 70 percent of its initial concentration (i.e. the PDF mean is 261.5 nM). Notice that the variance of each PDF decreases as the damage inflicted to the enzyme increases so that as the activity level decreases, the population begins to behave more like the population mean.

Assuming the six NER enzymes function independently, their joint density function of enzyme concentration values is given by

$$\phi\left(\boldsymbol{e}(t)\right) = \prod_{i=1}^{6} \phi_i(e_i(t)) = \begin{cases} \prod_{i=1}^{6} \frac{1}{b_i - a_i}, & a_i \le e_i \le b_i \\ 0, & \text{otherwise.} \end{cases} \tag{3.35}$$

where $\boldsymbol{e}$ represents the continuous random variables. Prior to any radiation damage (i.e.
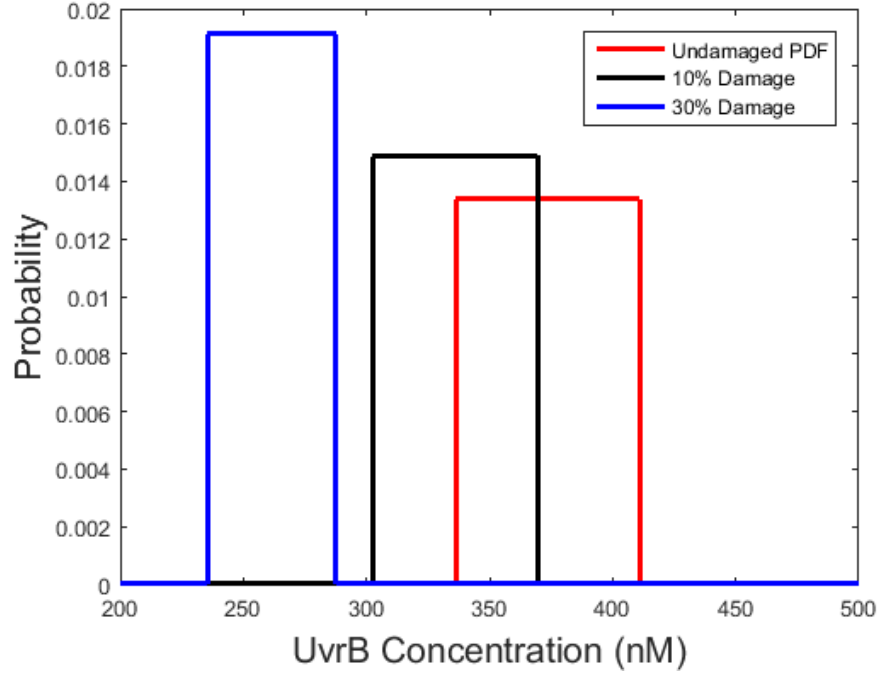
Figure 3.8: PDFs for Undamaged and Damaged UvrB Enzyme

when $t = 0$), the Uniform PDFs of the enzyme concentrations have a 20 percent span about

their mean, μ_{e_0}. Thus

$$a_i = f_e(t)\left(0.9\mu_{e_{i_0}}\right),$$

$$b_i = f_e(t)\left(1.1\mu_{e_{i_0}}\right),$$

and the range of the continuous random variable, e_i, is

$$b_i - a_i = 0.2 f_e(t)\mu_{e_{i_0}}.$$

Therefore the joint density function of enzyme concentration values given in Equation 3.35

becomes

$$\phi\left(e(t)\right) = \begin{cases} \dfrac{1}{[0.2f_e(t)]^6 \prod\limits_{i=1}^{6} \mu_{e_{i_0}}}, & 0.9 f_e(t)\mu_{e_{i_0}} \leq e_i \leq 1.1 f_e(t)\mu_{e_{i_0}} \\[2mm] 0, & \text{otherwise.} \end{cases} \tag{3.36}$$

49

The domain of the joint density function represents a 'hypercube' of possible enzyme combinations that are available to repair damaged DNA. This 'hypercube' will be explored further when building the population's probability of survival model in Chapter 5.

3.9 Summary

This chapter examined the indirect damage to a spore due to ionizing radiation. The primary insult mechanism considered was indirect damage from the production of reactive oxygen species (ROS). These reactants diffuse into the spore core and not only react with the DNA but also with the enzymes necessary for repair of the DNA. The evolution of the reactive oxygen species' within the core was determined based on a reaction-diffusion equation. Using the average core concentration of ROS, a damage model for both DNA and essential enzymes was considered. However, DNA repair mechanisms are extremely efficient thus the spore's repair of radiation damage must be taken into account before considering its probability of survival. DNA repair methods and a mathematical repair model will be outlined in the next chapter.

IV. Repair Model

A spore's damaged DNA is repaired via an intricate system involving interaction of multiple molecular processes. There are five outcomes from DNA repair, the first of which is that the damage is repaired correctly. The second occurs when DNA damage is repaired incorrectly but the damage did not take place in a critical location necessary for replication or transcription, so the spore may experience normal outgrowth. For example a mutation, which is a change in the DNA's base sequence, may occur to the third base which encodes a codon. However, due to redundancy in the genetic code, this may not effect the identification of its corresponding amino acid. The third result of DNA repair is that the damage is repaired incorrectly and it does lie in a critical location. In this case, the DNA may replicate a mutation which will then be passed onto future generations and only a fraction of cells survive this mutagenic process. Or the incorrectly repaired damage may prevent the spore from replicating and subsequent outgrowth which will lead to spore death. Finally, the DNA may not be repaired at all because sufficient proteins were not available within the spore for the repair or replication process. This scenario will be discussed further in Section 4.5.

As discussed in the previous chapter, damage to a spore's DNA includes, but is not limited to, base modifications, SSBs, and DSBs. As the range of radiation damage to DNA is very broad, so too are the DNA repair mechanisms. The four main DNA repair pathways, all of which incorporate a series of enzymatic processes, are base excision repair (BER), mismatch repair, nucleotide excision repair (NER), and DSB repair. This chapter will describe these four repair pathways as well mathematically model the NER process because it repairs the primary DNA damage mechanisms of ionizing radiation.

4.1 Base Excision Repair (BER)

The BER mechanism corrects base modifications such as depurination and deamination in which the DNA base is chemically altered, destroying its identity. The BER process is initiated by proteins which recognize a damaged base such as DNA glycosylase. Then the damaged base is removed and the DNA backbone is nicked on both sides of the cleaved base. These two steps are completed by one or more of the lyase enzymes. Next, the correct complementary base pair is filled in by DNA polymerase and finally, the DNA backbone is resealed via the ligase enzyme [39, 105].

4.2 Mismatch Repair

Mismatch repair corrects errors caused during DNA replication. Because mismatch repair occurs after replication, the damage detection enzymes must be able to identify which DNA strand contains the replication damage and which one is the original "correct" strand. It is possible for mismatch repair to misidentify the two strands and thus "fix" the wrong strand. This causes a mutation, or change, in the DNA which may be replicated in subsequent daughter chromosomes [105]. With the exception of occurring after replication, the mismatch repair process is very similar to NER.

4.3 Nucleotide Excision Repair (NER)

The NER process repairs a section of damaged DNA and it is responsible for the removal of a broad group of structurally unrelated DNA lesions to include SSBs and the interactions of damaged bases. Disruption of DNA base pairing, DNA bendability, and the presence of chemical modifications within the DNA are all fixed via NER [37]. In addition, bacterial spores use NER to repair dimers [105] and spore photoproduct (SP) and the repair process is "efficient and relatively error free" [68]. Recall from Section 3.6.2 that dimers and SP are the most likely types of damage produced by of UV radiation. The primary DNA damage mechanisms due to ionizing radiation are base modifications and

SSBs so this research will mathematically model the NER mechanism. As such, NER will be discussed in detail.

The NER process uses two broad stages to repair damage. The first involves recognition and incision of the location with the DNA strand containing the lesion and the second consists of restoring the original, undamaged DNA [6]. As the steps of NER are described, refer to Figure 4.1 for their pictorial representation.

The first step in the NER process is damage recognition which, in bacteria, is done by the proteins UvrA and UvrB. The UvrA protein is responsible for probing the DNA for damage and then signaling the location of possible damage to the UvrB protein. The presence of a lesion is then verified by the UvrB protein. The UvrA and UvrB proteins form a $UvrA_2B_2$ or a $UvrA_2B_1$ complex (see 'A_2B_1-DNA complex' in Figure 4.1). The $UvrA_2B$ complex is a member of the helicase super-family and therefore also unwinds and separates the DNA at the damage site and signals the location of the damage to the UvrC protein. UvrC nicks the DNA backbone on both sides of the damage (see '5' incision by UvrC' in Figure 4.1). The $UvrA_2B$ complex acting in coordination with the UvrC protein is often referred to as the UvrABC endonuclease [37, 43, 75].

The next step of NER is completed by the protein UvrD (also called helicase II) which displaces the damaged DNA strand. Then the enzyme, polymerase I (or Pol I) replaces the excised DNA by laying down the correct complementary base pairs. Finally, DNA ligase seals the nicks of the DNA backbone strand by connecting the newly corrected section of the backbone to the old backbone (see 'Repair synthesis and ligation' in Figure 4.1) [105].

4.4 Double Strand Break Repair (DSB)

DSBs are repaired by one of two methods; recombination repair or non-homologous end-joining. Bacteria can only initiate recombination repair after DNA replication because it requires two copies of the DNA. Recombination repair involves copying DNA sections of the daughter chromosome and using them to replace the sections of DNA containing the
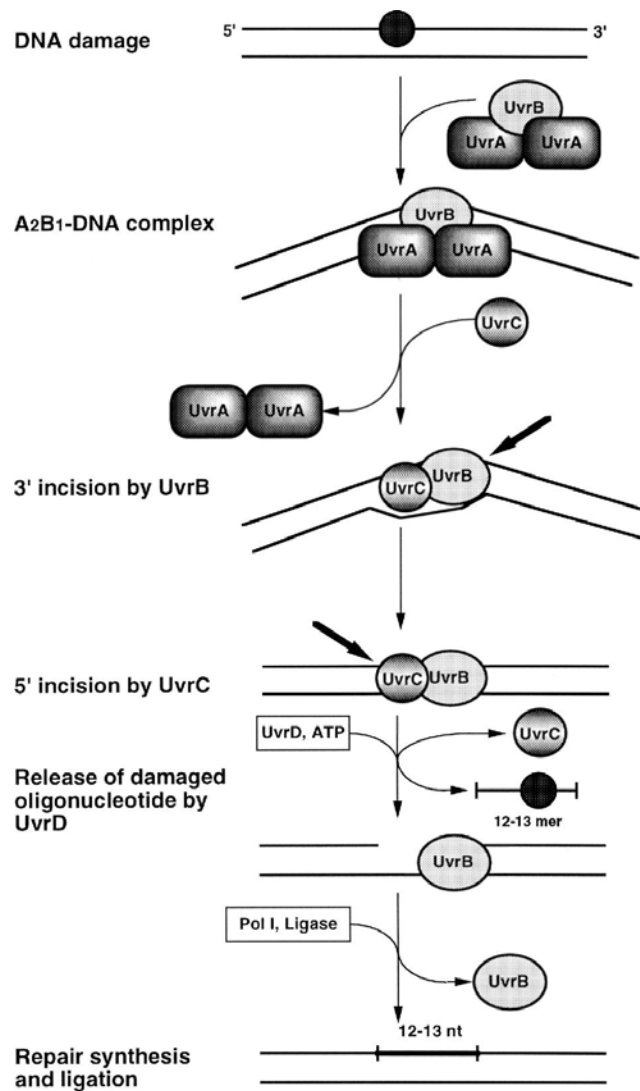
Figure 4.1: Nucleotide Excision Repair. Figure reprinted with permission. This image was published in [75]. Copyright Elsevier (1999).

DSB. While recombination repair is the preferred method of repair for DSBs, there exists significant complexity in identifying correct corresponding sequences and facilitating their cross over to the damaged strands. Non-homologous end-joining (NHEJ) directly rejoins the DNA chains. This process aligns the broken ends of the DSB, trims any frayed ends,

and ligates the strands. Recombination repair is the preferred mechanism for repairing DSBs because NHEJ is very error prone [105].

4.5 Literature Review

To date, mathematical modeling of DNA repair has almost solely focused on human cells. In addition, much of the research has concentrated on modeling the DNA repair processes as a whole by grouping together all the DNA repair mechanisms into one model and conducting some sort of data fitting. Foray et al. [33] proposed a stochastic and multicomponent model for repair of human cells based on "the existence of two subpopulations of DNA damage with a fast and a slow constant repair half-time" [34]. They showed that the Gamma distribution most accurately fit this hypotheses as compared to laboratory measurements. Gastaldo et al. [34] upheld this DNA repair rate interpretation and applied it to a combined DNA damage induction and repair model. Theoretical and experimental data was again analyzed however this theory also did not distinguish between the various repair mechanisms required to fix the multiple types of DNA damage such as base modifications, SSBs, and DSBs incurred after ionizing irradiation.

The first mathematical model that closely examined a single repair mechanism was proposed by Sokhansanj et al. [94]. They mathematically modeled the human BER pathway as a multi-step, sequential process using Michaelis-Menton kinetics and quantitative data on single proteins. In addition, the sensitivity of the pathway to altered enzyme kinetics was analyzed. Crooke et al. [21] also presented a model of the human BER process and incorporated the damage stage with the repair stage in the same model. Their model included a set of differential equations representing the sequence of enzymatic reactions in both the damage and repair pathways using Michaelis-Menton kinetics. This model assumed a certain initial amount of an oxidative estrogen compound that causes depurination of guanine when it reacts with DNA. So while the model included a damage stage, it did not relate a radiation dose to the amount of damage inflicted. Rahmanian et

al. [80] also modeled the human BER mechanism. They utilized differential equations to quantify the BER process in a step-by-step biochemical kinetic manner. In addition, these researchers assumed that the total concentration of the repair enzymes was conserved throughout the repair mechanism in order to normalize the differential equations.

This research will model the damage and repair of a spore's DNA following its exposure to a dose of ionizing radiation. The primary DNA damage mechanisms due to ionizing radiation are base modifications and SSBs which are both repaired via the NER process. Politi et al. [78] were among the first to mathematically model the human NER pathway. Their model considered damage via UV radiation and utilized a system of differential equations to sequentially model a six-step human NER pathway. The model takes into account the assembly of the necessary enzymes and gives association rates for each enzyme at each step. The model considers the assembly of each enzyme independently of the other enzymes in the system and regards the rate at which each binds to the lesion site to be the only important kinetic rate consideration.

Kesseler et al. [47] proposed a mathematical model which was also based on the association of the proteins to the damage sites. It incorporated kinetic "proofreading" into a human NER mathematical model and assumed that the kinetics in recruiting the correct enzymes to the lesion plays the most important role. The model integrated random order assembly of repair factors and assumed any binding of a repair enzyme to a damage site will increase cooperation among repair factors. As in the Politi et al. model, Kesseler et al. assumed each repair step takes the same amount of time.

Some researchers claim "repair mechanisms can be a double-edge sword" because simultaneous repair can cause DSBs to occur when two SSBs lie relatively close together on the DNA strand [46]. Karschau et al. [46] contend that there exists a critical threshold of the number of repair enzymes which if larger than this threshold, the survival of a bacterial cell is independent of the number of repair enzymes. They relate cell death to the rate of

56

DSB creation during repair instead of direct or indirect DNA damage. The DSB occurs when one SSB is in the process of being repaired via NER and repair begins on another relatively close SSB. Richard et al. [83] agree with this claim and argue there is an optimum level of repair enzymes in each cell which is "explained as the best trade-off between fast repair and a low probability of causing" DSBs [83]. Mathematical models based on this theory were presented however neither model accounted for the possibility of damage to both the cell's DNA and its repair enzymes.

The amount of proteins available for DNA repair is critical to the survival of the spore because a damaged spore will only be able to utilize the repair proteins that survived the damage mechanism. Specifically, Minton [60] showed that UvrA exposed to ionizing radiation resulted in degraded DNA repair. This author introduced the concept of initial protein 'fitness' applied to a population of bacteria and claimed that if the level of protein content was degraded below a critical threshold level, the spore would not have the ability to repair its DNA and thus would not survive [48]. Hurst [41] incorporated this idea of initial protein 'fitness' into the Sokhansanj et al. sequential BER model by assuming the enzymes experienced the same level of damage as DNA.

4.6   Mathematical Model

The repair model presented in this research will incorporate the DNA damage model described in Section 3.8 which predicts a level of damage based on a certain dose of radiation thus coupling dose, damage, and repair of the *Bacillus* spore. Since enzymes are necessary to repair DNA, a damaged spore will only be able to germinate with the enzymes that survived the radiation exposure. DNA must be repaired before a viable cell is produced during outgrowth and there must be a suitable amount of repair enzymes available to accomplish this. Thus, the model presented here will be based on the amount of enzymes available for repair given that the enzymes were also degraded by the ROS as described in Section 3.8.3. In addition, this model will include the concept of an initial enzyme 'fitness'

density function which was introduced by this author and incorporated within the Hurst model.

Recall from Section 4.3 that there are six enzymes involved in the NER process; UvrA, UvrB, UvrC, helicase II, polymerase I, and ligase. UvrA dimerizes prior to the initiation of the NER process. $UvrA_2$ and UvrB form the $UvrA_2B_1$ complex before binding to the DNA damage site. Then $UvrA_2$ conducts damage recognition and signals the damage to UvrB which conducts damage verification [24]. Some researchers believe the complex contains two UvrB proteins which allows scanning of both sides of the DNA to verify which backbone contains the site of the DNA damage [104]. This NER method requires $UvrA_2$ and two UvrB enzymes to form a $UvrA_2B_2$ complex prior to binding to the damaged DNA. In both cases, "once UvrB has detected the lesion the UvrA subunits are released from the complex" [37]. Next, UvrC attaches to the UvrB-DNA complex in order to nick the DNA strand on either side of the damage site. Then, helicase II associates with the damage site and removes the nicked portion of the DNA strand while also releasing the UvrC enzyme [75]. Polymerase I dissociates both UvrB and helicase II from the damage site and fills in the gapped DNA with a corrected strand [15, 69]. Finally, ligase releases the polymerase I enzyme and seals the DNA strand together.

This section will offer a mathematical model for both the $UvrA_2B_1$ and $UvrA_2B_2$ NER pathways since researchers do not agree as to which complex more accurately reflects the biological mechanism [71]. In addition, a model which incorporates simultaneous hydrolysis damage with the NER process will be presented. Finally, numerical solutions to these models will demonstrate the difference between the two NER pathways and the effect of continual hydrolysis damage.

4.6.1   NER with $UvrA_2B_1$ Complex.

The first mathematical model presented will consider the NER pathway which utilizes the $UvrA_2B_1$ complex. The process by which enzymes attach to and dissociate from the
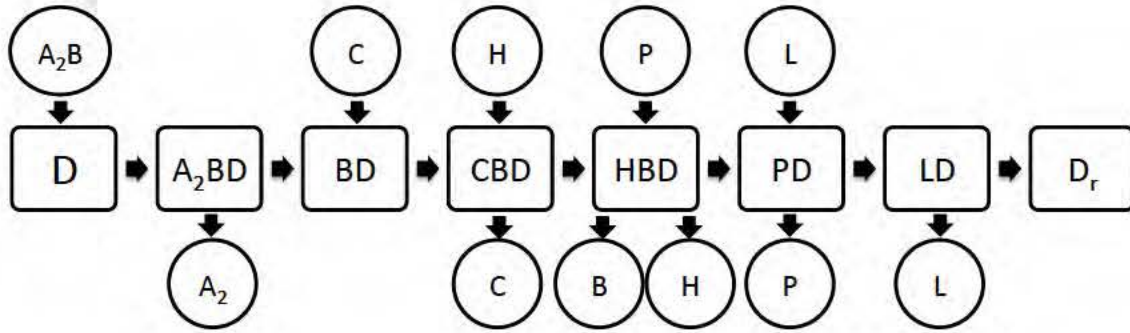
Figure 4.2: NER Enzymes and Products

where

A = UvrA H = helicase II

B = UvrB P = polymerase I

C = UvrC L = ligase

D = damaged DNA D_r = repaired DNA

and the $\mathrm{UvrA_2B_1}$ complex which is formed prior to its association with the DNA lesion is denoted by A_2B. Since UvrA dimerizes prior to the start of the NER process, this model assumes that UvrA is released from the DNA damage site as a dimer. This model also assumes that all helicase II, polymerase I, and ligase enzymes in the bacterial spore are available for the NER mechanism. In reality, some of these enzymes will participate in other cellular functions such as BER.

This process is described by the following chemical reactions:

$$A_2 + B \underset{k_{-1}}{\overset{k_1}{\rightleftharpoons}} A_2B \tag{4.1}$$

$$A_2B + D \overset{k_2}{\longrightarrow} A_2BD \tag{4.2}$$

59

$$A_2BD \xrightarrow{k_3} A_2 + BD \tag{4.3}$$

$$BD + C \xrightarrow{k_4} CBD \tag{4.4}$$

$$CBD + H \xrightarrow{k_5} HBD + C \tag{4.5}$$

$$HBD + P \xrightarrow{k_6} PD + B + H \tag{4.6}$$

$$PD + L \xrightarrow{k_7} LD + P \tag{4.7}$$

$$LD \xrightarrow{k_8} D_r + L \tag{4.8}$$

where k_i is the reaction rate constant for each reaction. The chemical reactions in Equations 4.1 through 4.8 and enzyme kinetics allow the NER mechanism to be modeled by the following differential equations:

$$\frac{d[A_2]}{dt} = k_3[A_2BD] + k_{-1}[A_2B] - k_1[A_2][B] \tag{4.9}$$

$$\frac{d[B]}{dt} = k_6[HBD][P] + k_{-1}[A_2B] - k_1[A_2][B] \tag{4.10}$$

$$\frac{d[C]}{dt} = k_5[CBD][H] - k_4[BD][C] \tag{4.11}$$

$$\frac{d[H]}{dt} = k_6[HBD][P] - k_5[CBD][H] \tag{4.12}$$

$$\frac{d[P]}{dt} = k_7[PD][L] - k_6[HBD][P] \tag{4.13}$$

$$\frac{d[L]}{dt} = k_8[LD] - k_7[PD][L] \tag{4.14}$$

$$\frac{d[D]}{dt} = -k_2[A_2B][D] \tag{4.15}$$

$$\frac{d[A_2B]}{dt} = k_1[A_2][B] - k_{-1}[A_2B] - k_2[A_2B][D] \tag{4.16}$$

$$\frac{d[A_2BD]}{dt} = k_2[A_2B][D] - k_3[A_2BD] \tag{4.17}$$

$$\frac{d[BD]}{dt} = k_3[A_2BD] - k_4[BD][C] \tag{4.18}$$

$$\frac{d[CBD]}{dt} = k_4[BD][C] - k_5[CBD][H] \tag{4.19}$$

$$\frac{d[HBD]}{dt} = k_5[CBD][H] - k_6[HBD][P] \tag{4.20}$$

$$\frac{d[PD]}{dt} = k_6[HBD][P] - k_7[PD][L] \tag{4.21}$$

$$\frac{d[LD]}{dt} = k_7[PD][L] - k_8[LD] \tag{4.22}$$

$$\frac{d[D_r]}{dt} = k_8[LD]. \tag{4.23}$$

These 15 differential equations characterize the process of repair. However, the system size can be reduced by recognizing some conserved quantities. For example, adding Equations 4.11 and 4.19 gives

$$\frac{d[C]}{dt} + \frac{d[CBD]}{dt} = 0$$

which implies $[C] + [CBD]$ is a constant. Therefore, assuming no further damage is done to the enzyme, the amount of the UvrC enzyme is always conserved whether the enzyme is a part of a complex or it exists as a free enzyme. Initially, at $t = 0$, the concentration of the complex CBD is zero. Therefore, let

$$[C] + [CBD] = [C]_0 \tag{4.24}$$

where $[C]_0$ represents the initial concentration of C. The same enzyme conservation principle applies to helicase II, polymerase I, and ligase since

$$\frac{d[H]}{dt} + \frac{d[HBD]}{dt} = 0$$

$$\frac{d[P]}{dt} + \frac{d[PD]}{dt} = 0$$

$$\frac{d[L]}{dt} + \frac{d[LD]}{dt} = 0$$

thus requiring

$$[H] + [HBD] = [H]_0 \tag{4.25}$$

$$[P] + [PD] = [P]_0 \tag{4.26}$$

$$[L] + [LD] = [L]_0 \tag{4.27}$$

where $[H]_0$, $[P]_0$, and $[L]_0$ represent the initial concentrations of helicase II, polymerase I, and ligase, respectively. Substituting Equation 4.24 into Equation 4.11 gives

$$\frac{d[C]}{dt} = k_5 \left([C]_0 - [C]\right)[H] - k_4[BD][C].$$

Substituting Equations 4.24 and 4.25 into Equation 4.12 yields

$$\frac{d[H]}{dt} = k_6 ([H]_0 - [H]) [P] - k_5 ([C]_0 - [C]) [H].$$

Substituting Equations 4.25 and 4.26 into Equation 4.13 produces

$$\frac{d[P]}{dt} = k_7 ([P]_0 - [P]) [L] - k_6 ([H]_0 - [H]) [P].$$

Substituting Equations 4.26 and 4.27 into Equation 4.14 results in

$$\frac{d[L]}{dt} = k_8 ([L]_0 - [L]) - k_7 ([P]_0 - [P]) [L].$$

Finally, substituting Equation 4.27 into Equation 4.23 and Equation 4.25 into Equation 4.10 gives

$$\frac{d[D_r]}{dt} = k_8 ([L]_0 - [L])$$

$$\frac{d[B]}{dt} = k_6 ([H]_0 - [H]) [P] + k_{-1}[A_2B] - k_1[A_2][B].$$

These substitutions have eliminated the CBD, HBD, PD, and LD terms. Thus Equations 4.9 through 4.23 are reduced to the following:

$$\frac{d[A_2]}{dt} = k_3[A_2BD] + k_{-1}[A_2B] - k_1[A_2][B] \tag{4.28}$$

$$\frac{d[B]}{dt} = k_6 ([H]_0 - [H]) [P] + k_{-1}[A_2B] - k_1[A_2][B] \tag{4.29}$$

$$\frac{d[C]}{dt} = k_5 ([C]_0 - [C]) [H] - k_4[BD][C] \tag{4.30}$$

$$\frac{d[H]}{dt} = k_6 ([H]_0 - [H]) [P] - k_5 ([C]_0 - [C]) [H] \tag{4.31}$$

$$\frac{d[P]}{dt} = k_7 ([P]_0 - [P]) [L] - k_6 ([H]_0 - [H]) [P] \tag{4.32}$$

$$\frac{d[L]}{dt} = k_8 ([L]_0 - [L]) - k_7 ([P]_0 - [P]) [L] \tag{4.33}$$

$$\frac{d[D]}{dt} = -k_2[A_2B][D] \tag{4.34}$$

$$\frac{d[A_2B]}{dt} = k_1[A_2][B] - k_{-1}[A_2B] - k_2[A_2B][D] \tag{4.35}$$

$$\frac{d[A_2BD]}{dt} = k_2[A_2B][D] - k_3[A_2BD \tag{4.36}$$

$$\frac{d[BD]}{dt} = k_3[A_2BD] - k_4[BD][C] \tag{4.37}$$

$$\frac{d[D_r]}{dt} = k_8 \left([L]_0 - [L]\right). \tag{4.38}$$

Note that the amount of the UvrA enzyme dimer is also conserved since adding Equations 4.28, 4.35, and 4.36 yields

$$\frac{d}{dt} \left([A_2] + [A_2B] + [A_2BD]\right) = 0.$$

Define $[A_2]_0$ to be the initial concentration of A_2, then

$$[A_2] + [A_2B] + [A_2BD] = [A_2]_0$$

implies that

$$[A_2BD] = [A_2]_0 - [A_2] - [A_2B]. \tag{4.39}$$

Similarly, let $[B]_0$ be the initial concentration of the UvrB enzyme. Adding Equations 4.10, 4.16, 4.17, 4.18, 4.19, and 4.20 gives

$$\frac{d}{dt} \left([B] + [A_2B] + [A_2BD] + [BD] + [CBD] + [HBD]\right) = 0$$

thus

$$[B] + [A_2B] + [A_2BD] + [BD] + [CBD] + [HBD] = [B]_0. \tag{4.40}$$

Substituting Equations 4.39, 4.24, and 4.25 into Equation 4.40 produces

$$[BD] = \left([B]_0 - [B]\right) - \left([A_2]_0 - [A_2]\right) - \left([C]_0 - [C]\right) - \left([H]_0 - [H]\right). \tag{4.41}$$

Equations 4.39 and 4.41 allow elimination of the A_2BD and BD terms. Therefore, Equations 4.28 through 4.38 are further reduced to the following equations,

$$\frac{d[A_2]}{dt} = k_3 \left([A_2]_0 - [A_2] - [A_2B]\right) + k_{-1}[A_2B] - k_1[A_2][B] \tag{4.42}$$

$$\frac{d[B]}{dt} = k_6 \left([H]_0 - [H]\right)[P] + k_{-1}[A_2B] - k_1[A_2][B] \tag{4.43}$$

$$\frac{\mathrm{d}[C]}{\mathrm{d}t} = k_5 \left([C]_0 - [C]\right)[H]$$

$$- k_4 \left\{\left([B]_0 - [B]\right) - \left([A_2]_0 - [A_2]\right) - \left([C]_0 - [C]\right) - \left([H]_0 - [H]\right)\right\}[C] \quad (4.44)$$

$$\frac{\mathrm{d}[H]}{\mathrm{d}t} = k_6 \left([H]_0 - [H]\right)[P] - k_5 \left([C]_0 - [C]\right)[H] \quad (4.45)$$

$$\frac{\mathrm{d}[P]}{\mathrm{d}t} = k_7 \left([P]_0 - [P]\right)[L] - k_6 \left([H]_0 - [H]\right)[P] \quad (4.46)$$

$$\frac{\mathrm{d}[L]}{\mathrm{d}t} = k_8 \left([L]_0 - [L]\right) - k_7 \left([P]_0 - [P]\right)[L] \quad (4.47)$$

$$\frac{\mathrm{d}[D]}{\mathrm{d}t} = - k_2 [A_2 B][D] \quad (4.48)$$

$$\frac{\mathrm{d}[A_2 B]}{\mathrm{d}t} = k_1 [A_2][B] - k_{-1}[A_2 B] - k_2 [A_2 B][D] \quad (4.49)$$

$$\frac{\mathrm{d}[D_r]}{\mathrm{d}t} = k_8 \left([L]_0 - [L]\right). \quad (4.50)$$

These equations are combined with the initial conditions, given by

$$[A_2](0) = [A_2]_0 \quad (4.51)$$

$$[B](0) = [B]_0 \quad (4.52)$$

$$[C](0) = [C]_0 \quad (4.53)$$

$$[H](0) = [H]_0 \quad (4.54)$$

$$[P](0) = [P]_0 \quad (4.55)$$

$$[L](0) = [L]_0 \quad (4.56)$$

$$[D](0) = [D]_0 \quad (4.57)$$

$$[D_r](0) = 0 \quad (4.58)$$

$$[A_2 B](0) = 0, \quad (4.59)$$

to characterize the evolution of the UvrA$_2$B$_1$ NER process.

The steady state solution of this system (located in Appendix A) demonstrates that without additional damage, all of the damaged DNA will eventually be repaired. Also in the long term, the concentrations of UvrC, helicase II, polymerase I, and ligase will approach their initial concentrations as they will no longer be needed for the repair process.

In addition, the concentrations of UvrA, UvrB, and the UvrA$_2$B$_1$ complex will exist in their equilibrium state given by the equation $k_{-1}[A_2B] = k_1[A_2][B]$ [85].

4.6.2 NER with UvrA$_2$B$_2$ Complex.

In some cases of NER, the UvrA dimer forms a complex with two UvrB molecules as shown by Figure 4.3 [37]. The UvrA$_2$B$_2$ complex allows UvrB to scan both DNA strands simultaneously in order to verify the damage detected by UvrA. UvrB does not form a dimer during this process. Instead, the two UvrB molecules attach to either side of the UvrA dimer [72]. Since UvrB does not form a dimer, the UvrB molecules are released as two monomers by the polymerase I enzyme.
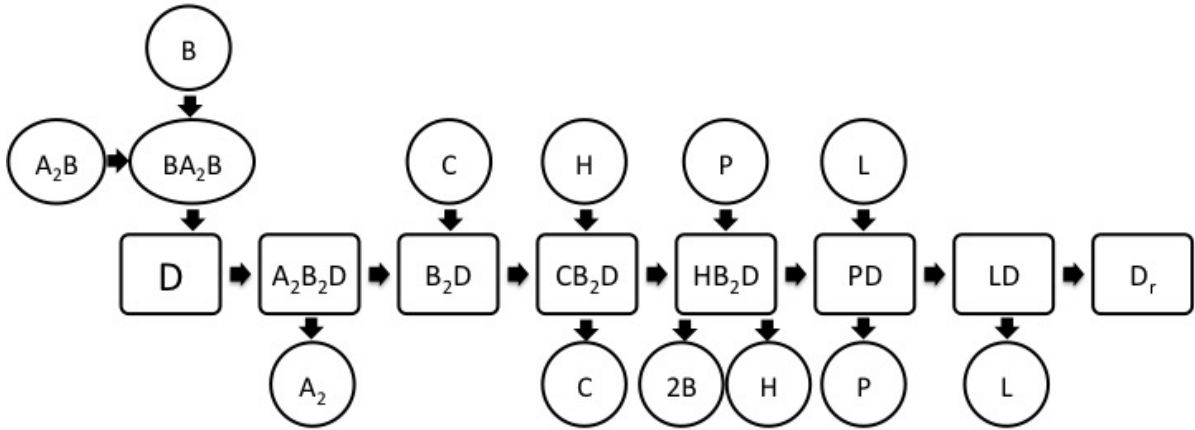
Figure 4.3: NER with UvrA$_2$B$_2$ Complex

This variation of the NER pathway is defined by the following chemical reactions:

$$A_2 + B \underset{k_{-1}}{\overset{k_1}{\rightleftharpoons}} A_2B \tag{4.60}$$

$$A_2B + B \underset{\tilde{k}_{-1}}{\overset{\tilde{k}_1}{\rightleftharpoons}} A_2B_2 \tag{4.61}$$

$$A_2B_2 + D \xrightarrow{k_2} A_2B_2D \tag{4.62}$$

$$A_2B_2D \xrightarrow{k_3} A_2 + B_2D \tag{4.63}$$

$$B_2D + C \xrightarrow{k_4} CB_2D \tag{4.64}$$

$$CB_2D + H \xrightarrow{k_5} HB_2D + C \tag{4.65}$$

$$HB_2D + P \xrightarrow{\tilde{k}_6} PD + 2B + H \tag{4.66}$$

$$PD + L \xrightarrow{k_7} LD + P \tag{4.67}$$

$$LD \xrightarrow{k_8} D_r + L. \tag{4.68}$$

These chemical reactions are also modeled by a system of differential equations.

$$\frac{d[A_2]}{dt} = k_3[A_2B_2D] + k_{-1}[A_2B] - k_1[A_2][B] \tag{4.69}$$

$$\frac{d[B]}{dt} = 2\tilde{k}_6[HB_2D][P] + k_{-1}[A_2B] + \tilde{k}_{-1}[A_2B_2] - k_1[A_2][B] - \tilde{k}_1[A_2B][B] \tag{4.70}$$

$$\frac{d[C]}{dt} = k_5[CB_2D][H] - k_4[B_2D][C] \tag{4.71}$$

$$\frac{d[H]}{dt} = \tilde{k}_6[HB_2D][P] - k_5[CB_2D][H] \tag{4.72}$$

$$\frac{d[P]}{dt} = k_7[PD][L] - \tilde{k}_6[HB_2D][P] \tag{4.73}$$

$$\frac{d[L]}{dt} = k_8[LD] - k_7[PD][L] \tag{4.74}$$

$$\frac{d[D]}{dt} = -k_2[A_2B_2][D] \tag{4.75}$$

$$\frac{d[A_2B]}{dt} = k_1[A_2][B] + \tilde{k}_{-1}[A_2B_2] - k_{-1}[A_2B] - \tilde{k}_1[A_2B][B] \tag{4.76}$$

$$\frac{d[A_2B_2]}{dt} = \tilde{k}_1[A_2B][B] - \tilde{k}_{-1}[A_2B_2] - k_2[A_2B_2][D] \tag{4.77}$$

$$\frac{d[A_2B_2D]}{dt} = k_2[A_2B_2][D] - k_3[A_2B_2D] \tag{4.78}$$

$$\frac{d[B_2D]}{dt} = k_3[A_2B_2D] - k_4[B_2D][C] \tag{4.79}$$

$$\frac{d[CB_2D]}{dt} = k_4[B_2D][C] - k_5[CB_2D][H] \tag{4.80}$$

$$\frac{d[HB_2D]}{dt} = k_5[CB_2D][H] - \tilde{k}_6[HB_2D][P] \tag{4.81}$$

$$\frac{d[PD]}{dt} = \tilde{k}_6[HB_2D][P] - k_7[PD][L] \tag{4.82}$$

$$\frac{d[LD]}{dt} = k_7[PD][L] - k_8[LD] \tag{4.83}$$

$$\frac{d[D_r]}{dt} = k_8[LD]. \tag{4.84}$$

The amount of each enzyme in the NER process that utilizes the $UvrA_2B_2$ complex is still conserved whether the enzyme is part of a compound or it exists as a free enzyme. Note that the stochiometry of the UvrB enzyme in this system leads to a different conservation principle for the UvrB molecule:

$$\frac{d}{dt}([B] + [A_2B] + 2[A_2B_2] + 2[A_2B_2D] + 2[B_2D] + 2[CB_2D] + 2[HB_2D]) = 0.$$

Therefore let

$$[B] + [A_2B] + 2[A_2B_2] + 2[A_2B_2D] + 2[B_2D] + 2[CB_2D] + 2[HB_2D] = [B]_0.$$

Using this conservation equation in addition to the conservation equations previously developed in Equations 4.24 through 4.27 and 4.39, Equations 4.69 through 4.84 are reduced to the following ten equations,

$$\frac{d[A_2]}{dt} = k_3 ([A_2]_0 - [A_2] - [A_2B] - [A_2B_2]) + k_{-1}[A_2B] - k_1[A_2][B] \tag{4.85}$$

$$\frac{d[B]}{dt} = 2\tilde{k}_6 ([H]_0 - [H]) [P] + k_{-1}[A_2B] + \tilde{k}_{-1}[A_2B_2] - k_1[A_2][B] - \tilde{k}_1[A_2B][B] \tag{4.86}$$

$$\frac{d[C]}{dt} = k_5 ([C]_0 - [C]) [H] - k_4 \left\{ \frac{1}{2} ([B]_0 - [B]) \right.$$

$$\left. - ([A_2]_0 - [A_2]) + \frac{1}{2}[A_2B] - ([C]_0 - [C]) - ([H]_0 - [H]) \right\} [C] \tag{4.87}$$

$$\frac{d[H]}{dt} = \tilde{k}_6 ([H]_0 - [H]) [P] - k_5 ([C]_0 - [C]) [H] \tag{4.88}$$

$$\frac{d[P]}{dt} = k_7 ([P]_0 - [P]) [L] - \tilde{k}_6 ([H]_0 - [H]) [P] \tag{4.89}$$

$$\frac{d[L]}{dt} = k_8 ([L]_0 - [L]) - k_7 ([P]_0 - [P]) [L] \tag{4.90}$$

$$\frac{d[D]}{dt} = -k_2[A_2B_2][D] \tag{4.91}$$

$$\frac{d[A_2B]}{dt} = k_1[A_2][B] + \tilde{k}_{-1}[A_2B_2] - k_{-1}[A_2B] - \tilde{k}_1[A_2B][B] \tag{4.92}$$

$$\frac{d[A_2B_2]}{dt} = \tilde{k}_1[A_2B][B] - \tilde{k}_{-1}[A_2B_2] - k_2[A_2B_2][D] \tag{4.93}$$

$$\frac{d[D_r]}{dt} = k_8 ([L]_0 - [L]) . \tag{4.94}$$

Again, we combine these equations with the initial conditions given in Equations 4.51 through 4.58 with the addition of the initial condition $[A_2B_2](0) = 0$, to characterize the evolution of the UvrA$_2$B$_2$ repair process.

4.6.3 Characteristic Scaling.

To convert the variables into dimensionless variables, certain characteristic scalings are introduced. This allows all calculations to be independent of particular units chosen. In order to non-dimensionalize enzyme concentration and time, let

$$[A_2](t) = [A_2]_0 \xi_1(\tau) \tag{4.95}$$

$$[B](t) = [B]_0 \xi_2(\tau) \tag{4.96}$$

$$[C](t) = [C]_0 \xi_3(\tau) \tag{4.97}$$

$$[H](t) = [H]_0 \xi_4(\tau) \tag{4.98}$$

$$[P](t) = [P]_0 \xi_5(\tau) \tag{4.99}$$

$$[L](t) = [L]_0 \xi_6(\tau) \tag{4.100}$$

$$[D](t) = [D_T] \xi_d(\tau) \tag{4.101}$$

$$[D_r](t) = [D_T] \xi_r(\tau) \tag{4.102}$$

where $\tau = k_3 t$ so τ is dimensionless time and D_T is the total concentration of DNA in the healthy, undamaged spore. These definitions were chosen because the initial concentrations of each enzyme are the maximum value each free enzyme concentration can be. Also, the maximum concentration that both damaged and repaired DNA can have is the concentration of the total DNA in the spore. The time scale, k_3, was chosen because this rate parameter has units of sec^{-1}. Finally, let

$$[A_2B](t) = [A_2]_0 \xi_7(\tau) \tag{4.103}$$

as the value of $[A_2]_0$ represents the maximum concentration that A_2B can be. Note that

$$\frac{\mathrm{d}}{\mathrm{d}t}[A_2](t) = \frac{\mathrm{d}}{\mathrm{d}t}\left([A_2]_0 \xi_1(\tau)\right) = [A_2]_0 \frac{\mathrm{d}\tau}{\mathrm{d}t}\frac{\mathrm{d}\xi_1}{\mathrm{d}\tau} = [A_2]_0 k_3 \frac{\mathrm{d}\xi_1}{\mathrm{d}\tau}.$$

In order to completely non-dimensionalize the system, define dimensionless parameters

$$\lambda_1 = \frac{k_6[H]_0}{k_3} \quad \lambda_2 = \frac{k_1[B]_0}{k_3}, \quad \lambda_3 = \frac{k_2[D]_T}{k_{-1}}, \quad \lambda_4 = \frac{k_5[C]_0}{k_3}, \quad \lambda_5 = \frac{k_7[L]_0}{k_3},$$

$$\alpha_1 = \frac{[P]_0}{[B]_0}, \quad \alpha_2 = \frac{[P]_0}{[H]_0}, \quad \alpha_3 = \frac{[A_2]_0}{[B]_0}, \quad \alpha_4 = \frac{[H]_0}{[C]_0}, \quad \alpha_5 = \frac{[P]_0}{[L]_0} \quad \alpha_6 = \frac{[A_2]_0}{[D_T]},$$

$$\beta_1 = \frac{k_8}{k_3}, \quad \beta_2 = \frac{k_{-1}}{k_3}, \quad \text{and} \quad \beta_3 = \frac{k_4}{k_1}. \tag{4.104}$$

4.6.3.1   *Non-dimesionalized NER UvrA$_2$B$_1$ Pathway.*

Utilizing Equations 4.95 through 4.103 and the dimensionless parameters, Equations 4.42 through 4.50 become:

$$\frac{d\xi_1}{d\tau} = 1 - \xi_1 + \xi_7 (\beta_2 - 1) - \lambda_2\xi_1\xi_2 \tag{4.105}$$

$$\frac{d\xi_2}{d\tau} = \lambda_1\alpha_1 (1 - \xi_4)\xi_5 + \alpha_3\xi_7\beta_2 - \lambda_2\alpha_3\xi_1\xi_2 \tag{4.106}$$

$$\frac{d\xi_3}{d\tau} = \lambda_4\alpha_4(1 - \xi_3)\xi_4$$

$$- \lambda_2\beta_3\xi_3 \left[1 - \xi_2 - \alpha_3 (1 - \xi_1) - \frac{\alpha_1}{\alpha_2\alpha_4} (1 - \xi_3) - \frac{\alpha_1}{\alpha_2} (1 - \xi_4) \right] \tag{4.107}$$

$$\frac{d\xi_4}{d\tau} = \lambda_1\alpha_2 (1 - \xi_4)\xi_5 - \lambda_4 (1 - \xi_3)\xi_4 \tag{4.108}$$

$$\frac{d\xi_5}{d\tau} = \lambda_5(1 - \xi_5)\xi_6 - \lambda_1 (1 - \xi_4)\xi_5 \tag{4.109}$$

$$\frac{d\xi_6}{d\tau} = \beta_1(1 - \xi_6) - \lambda_5\alpha_5(1 - \xi_5)\xi_6 \tag{4.110}$$

$$\frac{d\xi_d}{d\tau} = -\lambda_3\alpha_6\xi_7\xi_d\beta_2 \tag{4.111}$$

$$\frac{d\xi_7}{d\tau} = \lambda_2\xi_1\xi_2 - \xi_7\beta_2 (1 + \lambda_3\xi_d) \tag{4.112}$$

$$\frac{d\xi_r}{d\tau} = \frac{\beta_1\alpha_6\alpha_1}{\alpha_3\alpha_5}(1 - \xi_6). \tag{4.113}$$

This numerical solution to this system of non-dimensional differential equations will be presented in Section 4.6.5.

4.6.3.2 Non-dimesionalized NER UvrA₂B₂ Pathway.

In order to create a dimensionless system for the alternate NER pathway that utilizes the UvrA$_2$B$_2$ complex, additional dimensionless parameters must be defined. Let

$$\tilde{\lambda}_1 = \frac{\tilde{k}_6[H]_0}{k_3}, \quad \tilde{\lambda}_2 = \frac{\tilde{k}_1[B]_0}{k_3}, \quad \text{and} \quad \tilde{\beta}_2 = \frac{k_{-1}}{k_3}.$$

In addition, denote

$$[A_2B_2](t) = [A_2]_0\xi_8(\tau) \tag{4.114}$$

in order to non-dimensionalize concentration and time. With Equations 4.95 through 4.102, Equation 4.114, and the dimensionless parameters, Equations 4.85 through 4.94 become:

$$\frac{d\xi_1}{d\tau} = 1 - \xi_1(1 + \lambda_2\xi_2) - \xi_8 - \xi_7(1 - \beta_2) \tag{4.115}$$

$$\frac{d\xi_2}{d\tau} = 2\tilde{\lambda}_1\alpha_1(1 - \xi_4)\xi_5 + \alpha_3\left(\xi_7\beta_2 + \xi_8\tilde{\beta}_2\right) - \alpha_3\xi_2\left(\lambda_2\xi_1 + \tilde{\lambda}_2\xi_7\right) \tag{4.116}$$

$$\frac{d\xi_3}{d\tau} = \lambda_4\alpha_4(1 - \xi_3)\xi_4$$

$$\qquad - \lambda_2\beta_3\xi_3\left[\frac{1}{2}(1 - \xi_2) - \alpha_3\left(1 - \xi_1 - \frac{1}{2}\xi_7\right) - \frac{\alpha_1}{\alpha_2\alpha_4}(1 - \xi_3) - \frac{\alpha_1}{\alpha_2}(1 - \xi_4)\right] \tag{4.117}$$

$$\frac{d\xi_4}{d\tau} = \tilde{\lambda}_1\alpha_2(1 - \xi_4)\xi_5 - \lambda_4(1 - \xi_3)\xi_4 \tag{4.118}$$

$$\frac{d\xi_5}{d\tau} = \lambda_5(1 - \xi_5)\xi_6 - \tilde{\lambda}_1(1 - \xi_4)\xi_5 \tag{4.119}$$

$$\frac{d\xi_6}{d\tau} = \beta_1(1 - \xi_6) - \lambda_5\alpha_5(1 - \xi_5)\xi_6 \tag{4.120}$$

$$\frac{d\xi_d}{d\tau} = -\lambda_3\alpha_6\xi_8\xi_d\beta_2 \tag{4.121}$$

$$\frac{d\xi_7}{d\tau} = \lambda_2\xi_1\xi_2 + \xi_8\tilde{\beta}_2 - \xi_7\left(\beta_2 + \tilde{\lambda}_2\xi_2\right) \tag{4.122}$$

$$\frac{d\xi_8}{d\tau} = \tilde{\lambda}_2\xi_7\xi_2 - \xi_8\left(\tilde{\beta}_2 + \lambda_3\xi_d\beta_2\right) \tag{4.123}$$

$$\frac{d\xi_r}{d\tau} = \frac{\beta_1\alpha_6\alpha_1}{\alpha_3\alpha_5}(1 - \xi_6). \tag{4.124}$$

This system is also solved numerically and portrayed in Section 4.6.5.

4.6.4 Hydrolysis Damage.

This repair model assumes that all DNA damage is caused by radiation and occurs prior to germination. However, if a spore receives the nutrients it needs to germinate,

then the spore core will take in water which can produce hydrolysis damage. Hydrolysis is a reaction of a molecule with water. Water can react with polymers; such as DNA and enzymes, resulting in depolymerization (breaking a large strand of polymers into two smaller ones) or removal of a side group of the polymer [58].

In addition, water can react with DNA causing base modifications such as deamination and depurination as discussed in Section 3.6.1. These base modifications create a structural change in the DNA backbone which prevents the DNA from replicating properly thus causing spore death. This section will introduce a repair model which also includes hydrolysis damage to the DNA only.

Define the undamaged DNA in the cell or "good DNA" as D_g. Because damaged DNA is compounded with the repair enzymes during the NER process, the total DNA in the spore at any time, t, is not equal to the sum of the damaged DNA and the viable DNA. Rather, the total DNA is a combination of the undamaged DNA, damaged DNA that has not begun to be repaired, and DNA that is in the process of being repaired, i.e.

$$[D_T] = [D_g](t) + [D](t) + [D_c](t)$$

where $[D_c](t)$ represents damaged DNA that is compounded with repair enzymes. That is,

$$[D_c](t) = [A_2BD](t) + [HBD](t) + [CBD](t) + [BD](t) + [PD](t) + [LD](t).$$

Note that, $[D_g](0) = [D_T] - [D]_0$ because $[D_c](0) = 0$. With continual hydrolysis damage to the DNA, the NER model in Equations 4.42 through 4.50 require the addition of a differential equation for $[D_g]$,

$$\frac{d[D_g]}{dt} = k_8 ([L]_0 - [L]) - k^*[D_g], \qquad (4.125)$$

where k^* is the reaction rate constant that represents the averaged rate for all possible hydrolysis reactions in the spore. The only other change is the addition of one term to Equation 4.48 which becomes

$$\frac{d[D]}{dt} = -k_2[A_2B][D] + k^*[D_g]. \qquad (4.126)$$

These same two alterations apply to both the NER model with the $UvrA_2B_1$ complex and the model with the $UvrA_2B_2$ complex in Equations 4.85 through 4.94. The value k^* follows the Arrhenius equation which models the rate of chemical reactions [58]:

$$k^*(T) = Ae^{-\frac{E}{RT}}[H_2O]$$

where $[H_2O]$ is the concentration of water. Temperature, T, is assumed to be room temperature (i.e. 300 °K) and the gas constant, R, is 1.986×10^{-3} kcal/mol°K. The encounter frequency, A and the activation energy, E, are dependent upon the moisture content of the spore. Values of k^* for various levels of moisture content are displayed in Table 4.1.

Table 4.1: Parameters for k^* [108]

k^* (s^{-1})	Moisture Content (%)	E (kcal/mol)	$A^*[H_2O]$ (s^{-1})
3.77×10^{-9}	5	26.1	4.0×10^{10}
1.38×10^{-8}	9	24.5	1.0×10^{10}
1.95×10^{-5}	19	12.3	1.8×10^{4}
8.2×10^{-5}	30	10	1.6×10^{3}

Similarly, characteristic scaling is introduced in order to create a dimensionless system that represents the continual hydrolysis damage. With

$$[D_g](t) = [D_T]\xi_g(\tau) \quad \text{and} \quad \beta_4 = \frac{k^*}{k_3},$$

along with the dimensionless parameters and variables utilized in the original repair model (Equations 4.95 through 4.104), Equations 4.125 and 4.126 become

$$\frac{d\xi_d}{d\tau} = -\lambda_3\alpha_6\xi_7\xi_d\beta_2 + \beta_4\xi_g$$

$$\frac{d\xi_g}{d\tau} = \frac{\beta_1\alpha_6\alpha_1}{\alpha_3\alpha_5}(1-\xi_6) - \beta_4\xi_g.$$

The mathematical NER model that includes hydrolysis damage is also implemented and solved numerically. The results will be demonstrated in the next section.

4.6.5 Results.

The dimensionless repair models are numerically evaluated via a moderately stiff MATLAB solver using rate kinetics and enzyme concentrations found in the literature. A stiff solver is required for this system of differential equations because the time scales differ widely and "the solution being sought varies slowly, but there are nearby solutions that vary rapidly" [63]. The rate parameters are reported in Table 4.2. Recall from Section 3.8.2 that the *E. coli* cell's DNA concentration prior to radiolysis is 2.87×10^7 nM therefore this value is applied to $[D_T]$. The same section proved that 10 percent of the initial DNA is damaged therefore $[D]_0 = .1 * [D_T]$. Enzyme concentrations prior to radiation damage are found in Table 3.6. As the enzymes were also reduced to 90 percent of their initial activity level via radiation damage, the amount of each enzyme available for the repair process after a 10 percent reduction is listed in Table 4.3.

Table 4.2: Rate Parameters

Parameter	Value	Notes
k_1	1.1×10^{-7} nM^{-1}s^{-1}	*Geobacillus stearothermophilus* NER [72]
k_{-1}	8.5×10^{-5} s^{-1}	NER of *E. coli* [70]
k_2	6×10^{-5} nM^{-1}s^{-1}	UV-irradiated *E. coli* [69]
k_3	3×10^{-3} s^{-1}	UV-irradiated *E. coli* [100]
k_4	8.3×10^{-8} nM^{-1}s^{-1}	*E. coli* NER [109]
k_5	0.12 nM^{-1}s^{-1}	UvrD in *E. coli*; assumes UvrD dimer [55]
k_6	6.2×10^{-11} nM^{-1}s^{-1}	*E. coli* BER of DNA-methylation damage [101]
k_7	8.5×10^{-11} nM^{-1}s^{-1}	*E. coli* BER of DNA-methylation damage [101]
k_8	0.075 s^{-1}	UV-irradiated *E. coli* [52]

Table 4.3: Data for *E. coli* after Damage

Molecule	Concentration
$[A_2]_0$	17.2 nM
$[B]_0$	336.2 nM
$[C]_0$	14.9 nM
$[H]_0$	4109.9 nM
$[P]_0$	657.5 nM
$[L]_0$	298.9 nM
$[D]_0$	2.87 x 10^6 nM

Figure 4.4 displays the numerical results and differences of the NER process when utilizing the two UvrA$_2$B complexes. The horizontal axis represents real time in hours and the vertical axis corresponds to the fraction of DNA repaired so that 0.1 represents all damaged repaired. The blue line represents repair over time of a DNA strand via NER with the UvrA$_2$B$_1$ complex. This result is consistent with conclusions from researchers as Moeller et al. [61] found that 81 percent of SP and CPDs in a *B.s.* spore were repaired within one hour (recall that SP and CPDs are repaired via NER). The dotted red line represents the NER process that utilizes the UvrA$_2$B$_2$ complex and assumes that k_1 and $\tilde{k}_1$ are equal in value. Assuming the same amount of initial DNA damage, repair with the UvrA$_2$B$_2$ complex is slower than that with the UvrA$_2$B$_1$ complex because of the increased requirement for the UvrB enzyme. However, $\tilde{k}_1$ is most likely smaller in value than k_1 so results of the repair process with the UvrA$_2$B$_2$ complex and a $\tilde{k}_1$ value that is one order of magnitude smaller than that of k_1 are plotted via the black dashed line. The decrease in the $\tilde{k}_1$ rate causes NER with the UvrA$_2$B$_2$ complex to need an even longer period of time to complete its DNA repair process.
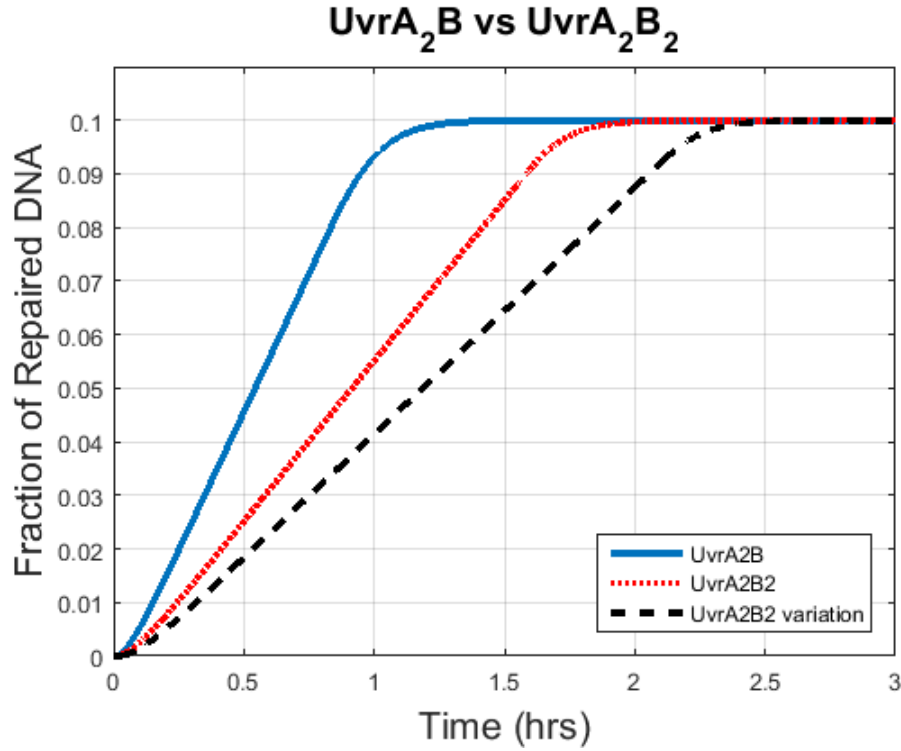
Figure 4.4: Repair Time Results for Variations of NER Model

Figure 4.5 depicts the behavior of UvrA, UvrB, and the $UvrA_2B_1$ complex during the NER mechanism. The horizontal axis corresponds to time in hours and it represents the same time scale as the horizontal axis in Figure 4.4. The vertical axis gives the fraction of enzyme concentration available during the NER process. The inset in Figure 4.5 represents the initial behavior of UvrA and UvrB in blue and red respectively. The behavior reflected in the inset graph occurs within the first second of the initiation of NER. Note, that both enzyme concentrations decrease initially as the $UvrA_2B_1$ complex is formed. In addition, UvrA decreases at a faster rate than UvrB as there is a lower concentration of UvrA in the spore than UvrB (see Table 4.3). However, UvrA is released from the damage site as soon as it passes the damage to UvrB for verification and then becomes available to form the $UvrA_2B_1$ complex again very quickly. UvrB is bound to the damaged DNA until it is

released by polymerase (refer back to Figure 4.2) and it is required to form the $UvrA_2B_1$ complex as soon as it is released. Therefore, UvrB is utilized almost at its maximum capacity during the NER process. The initial concentration of the $UvrA_2B_1$ complex is assumed to be zero. The complex attaches to the damage site almost immediately after it is formed. Note that when the majority of the damaged DNA is repaired, UvrA, UvrB, and the $UvrA_2B_1$ complex approach their equilibrium states given by the equation $k_{-1}[A_2B] = k_1[A_2][B]$ [85].

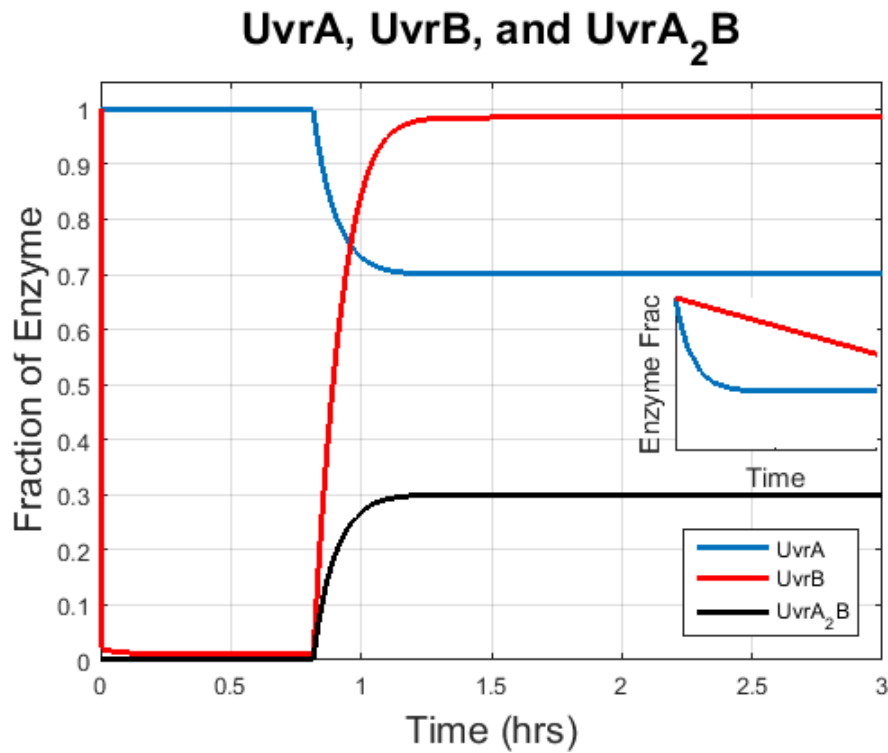Figure 4.5: UvrA, UvrB, and $UvrA_2B$ Behavior During NER

Helicase and polymerase behavior during the NER process is demonstrated in Figure 4.6. The range of time of the horizontal axis is the same as the previous two graphs. Notice that the vertical axis indicates almost 45 percent of polymerase is bound to the DNA damage site for repair while approximately 8 percent of helicase is utilized for repair. The

difference is due to the varying initial concentrations of each enzyme (see Table 4.3). The inset of Figure 4.6 represents the initial behavior of helicase and polymerase which occurs within two minutes after the start of NER. Recall that helicase is required for NER prior to polymerase. Interestingly, the maximum fraction of UvrB, helicase, and polymerase that is bound to the DNA damage site translates to an equivalent concentration for each of the three enzymes. This indicates that the concentration of UvrB dictates the concentrations of helicase and polymerase that are bound to the damage site.

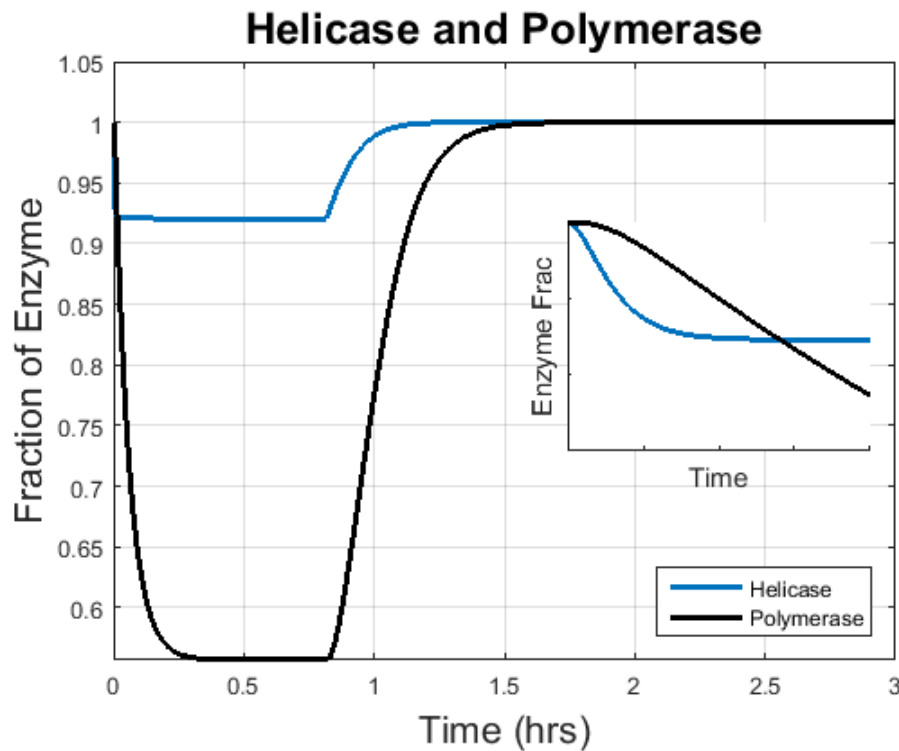Figure 4.6: Helicase and Polymerase Behavior During NER

The amount of ligase bound to the DNA damage site during NER is shown in Figure 4.7. The vertical axis corresponds to fraction of ligase used during the repair process. The behavior of ligase over time mimics the behavior of the helicase and polymerase enzymes. However, only 3.3×10^{-7} percent of the initial ligase concentration is bound to the DNA

damage site because ligase is only attached for one step of the NER mechanism and the rate parameter for this step is relatively fast compared to other rate constants (see Table 4.2). Rahmanian et al. [80] studied of the accumulation of enzymes to the DNA damage site during BER in human cells. Eukaryotic BER employs enzymes from both the polymerase and ligase families. The qualitative behavior of the polymerase and ligase enzymes as they accumulate to the damage site in this research is extremely similar to the laboratory results found by Rahmanian et al. Similar to ligase, only 2.5×10^{-8} percent of UvrC's initial concentration is bound to the damage site during NER. UvrC is also only attached to the DNA for one step of the repair process.
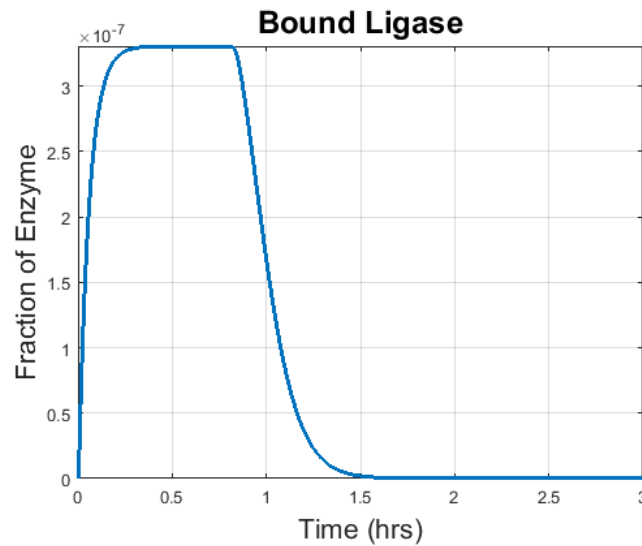
Figure 4.7: Ligase Behavior During NER

Figure 4.8 depicts the result of simultaneous hydrolysis damage on the repair model. The graph portrays the effects of differing values for k^* on the production of healthy DNA over time given that ten percent of the DNA is damaged prior to initiation of repair. Specifically, the vertical axis represents the percentage of undamaged DNA and the horizontal axis corresponds to time in hours. The solid black line demonstrates the

scenario with no hydrolysis damage (i.e. $k^*=0$). The red line represents the percentage of DNA repaired over time given a moisture content of 5 percent (refer to Table 4.1 for the corresponding k^* values). Since hydrolysis damage is continuously occurring, DNA is never 100 percent repaired. A 5 percent moisture content will permit repair of almost all of the damaged DNA (99.75 percent of the total DNA is viable). As shown by the dashed blue line, a moisture content of 9 percent requires an even longer period of time for 99 percent of the DNA to be healthy. These results from the hydrolysis model are also consistent with experiments. Uphoff et al. [101] found that oxidative DNA damage caused by the normal metabolism of *E. coli*, required approximately two hours to repair. If the rate of hydrolysis reactions overwhelms the repair capabilities of the spore, the concentration of
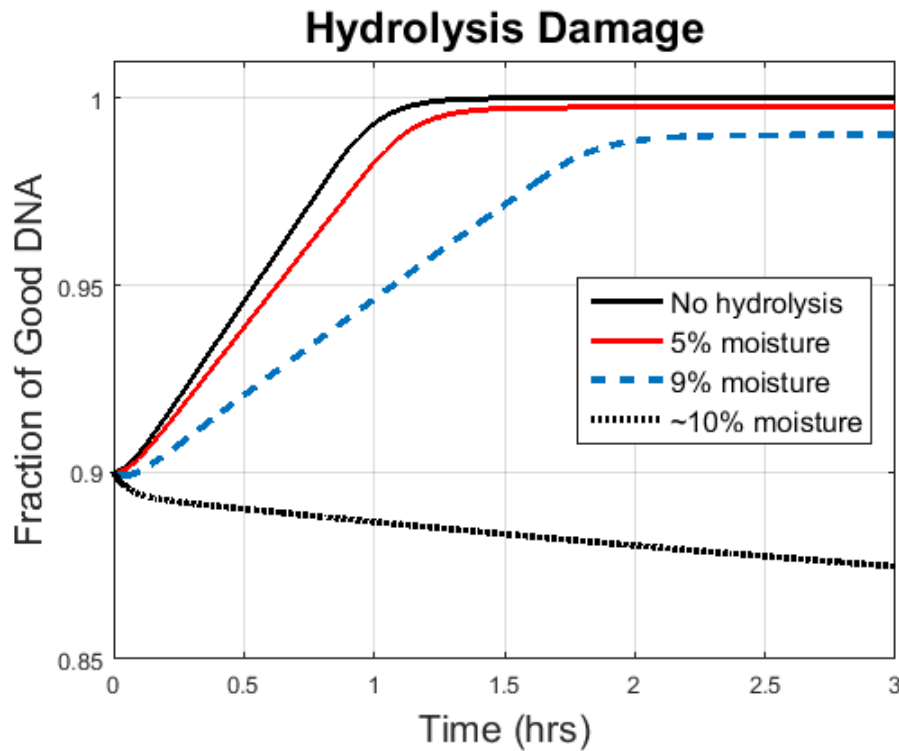

Figure 4.8: Numerical Results for Repair Model with Hydrolysis Damage

undamaged DNA will decrease over time. This scenario is illustrated by the dotted black

line in Figure 4.8 which represents repair with a k^* that corresponds to approximately a 10 percent moisture content. Therefore, as k^* increases, the rate at which DNA is repaired will decrease. In addition, the percentage of viable DNA that is repaired will decrease. This trend continues until the rate of hydrolysis damage overwhelms the spore's repair capacity and the amount of healthy DNA continuously decreases as shown by the dotted black line.

4.7   Summary

This chapter developed and examined repair processes for nucleotide damage to DNA. The mathematical model captures the relationship between six essential enzymes and the repair of damaged DNA. The chemical kinetics clearly show that the loss of any one enzyme stops the repair process. It follows that the reduction of them will slow repair.

Two distinct pathways to repair requiring either $UvrA_2B_1$ or $UvrA_2B_2$ complexes were examined. Results indicate that the $UvrA_2B_1$ pathway was faster than the $UvrA_2B_2$ pathway. This was likely due to the added step in formulating $UvrA_2B_2$ as well as the reduction in availability of the UvrB molecule.

The $UvrA_2B_1$ pathway was further extended to include the possibility of hydrolysis damage during the repair process. Because hydrolysis damage occurs simultaneously with repair, the viable DNA may never reach the necessary threshold for survival. The influence of moisture content is illustrated in Figure 4.8. The initial 'fitness' of each spore is reflected in the state of the essential enzyme population as well as the DNA. With the addition of hydrolysis damage, if this initial enzyme viability is not sufficient for DNA repair, the population will not survive. The probability of survival of a spore population is modeled in the next chapter.

V. Probability of Survival

The previous two chapters have focused on the damage and repair of a single spore. This chapter will consider the probability of survival for a population of spores assuming the population has a certain initial enzyme 'fitness' as described in Section 3.8.3. First, previous literature regarding biological survival curves will be reviewed. Then, the methodology for the probability of survival model developed for this research will be introduced, and finally, results will be presented.

5.1 Literature Review

Past mathematical modeling of biological survival curves has centered on data-fitting of probability of survival curves because there exists experimental data that can be used for comparison. For example, Brahmi et al. [12] modeled the UV inactivation of bacteria in wastewater as

$$\frac{N(t)}{N_0} = e^{-KIt}$$

where

$$N(t) = \text{number of bacteria at time, } t$$

$$N_0 = \text{number of initial bacteria}$$

$$K = \text{rate constant}$$

$$I = \text{UV intensity}$$

$$t = \text{time}$$

and instituted small deviations based on experimental results. This model is also known as the single stage exponential decay equation.

Prior to Brahmi et al.'s work, Kowalski et al. [49] used the same model to demonstrate the disinfection of air using UV irradiation. These researchers adapted the model to

consider two microbial populations; one that decays with initial exposure and one that is more resistant and will survive for longer periods of time. The model is

$$S(t) = (1 - f)e^{-k_1 It} + f e^{-k_2 It}$$

where $S(t)$ is the surviving fraction of the initial microbial population at time, t, f is the resistant fraction of the population, and k_1 and k_2 are rate constants. This equation is known as the two-stage model. Kowalski et al. also modified their models to account for what is known as the quasi-threshold. The quasi-threshold gives the shoulder of a biological survival curve that represents the period of time prior to which a bacterial population experiences exponential decay. In other words, there exists some accumulation of damage before the onset of exponential decay which is not demonstrated until the quasi-threshold time period is complete. This shouldered survival curve, as shown in Figure 5.1 is also known as the sigmoid survival curve.
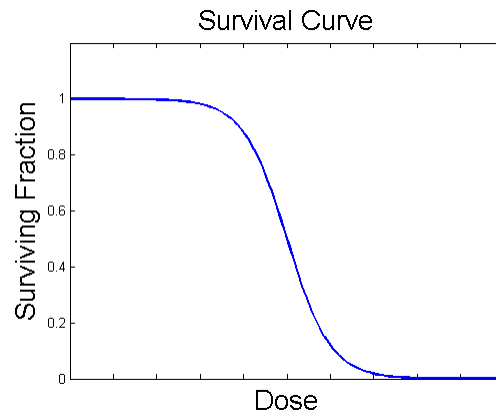

Figure 5.1: Sigmoid Survival Curve

The single stage and two stage models are extremely similar to the models developed within the target theory of cell survival. Target theory assumes that a cell contains a small volume of targets which can absorb energy to produce damage, otherwise known as a hit. In target theory, the shoulder portion of the survival curve represents the number of targets

that had to be inactivated before outgrowth of a bacterial colony can be deterred. The single-hit model assumes that the cell can only survive if it sustains no hits and it will die if it experiences one or more hits. The single-hit model is represented by

$$S(d) = e^{-\frac{d}{d_0}}$$

where S is the survival probability per cell, d is the dose, or hits per unit volume, and d_0 is the dose required to reduce the surviving fraction to $\frac{1}{e}$ of its initial value. This model does not account for the quasi-threshold, thus it was adapted to form a multitarget-single-hit model:

$$S(q, n, d) = 1 - \left(1 - e^{-qd}\right)^n$$

where each target is assumed to have the same probability of being hit (q) and there exists n targets in each cell. Note that for n greater than one, the multitarget-single-hit model requires a zero slope when the dose is equal to zero. Experimental data has not replicated this phenomenon, therefore a modified multitarget-single-hit model was developed to include the assumption that some fraction of cells irradiated are killed via direct action. This leads to

$$S(q, n, d) = e^{-q_1 d}\left[1 - \left(1 - e^{-q_n d}\right)^n\right]$$

where q_1 is the inactivation coefficient for the cell killing that arises from single hits and q_n is the inactivation coefficient for the previous multitarget-single-hit model [4]. Katz [9] claimed the modified multitarget-single-hit model demonstrated the cell's inactivation from a dose with two different modes such as low LET and high LET.

Target theory is a reasonable approach to modeling the survival of prokaryotic cells. If a dormant spore experiences radiation damage, it will not begin its repair processes until it germinates and has a vegetative metabolism. This negates the need to model the simultaneous repair of damage. However, modeling of eukaryotic cell survival requires consideration of these concurrent procedures. Therefore the linear-quadratic molecular

model was formulated by Chadwick and Leenhouts to account for simultaneous enzymatic repair [4]. Another benefit of the linear-quadratic model is that it accounts for the likelihood of two SSBs becoming a DSB when they occur at a similar time and in close proximity. This parameter is referred to as the biological effectiveness factor and is denoted by p in the linear-quadratic model given by

$$S(d) = e^{-p(\alpha d + \beta d^2)}$$

where α is a function of the number of sites that can sustain a DSB, the hit probability constant, the unrestored fraction of DSBs, and the fraction of the dose, d, that ruptures both strands in a single hit. The parameter β is a function of the unrestored fraction of DSBs, the effectiveness factor of two SSBs becoming a DSB, the number of critical molecular bonds on each DNA strand, the unrestored fraction of bonds in each strand, the hit probability constant, and the fraction of the dose that ruptures one of the strands in a single hit. In order to gain the benefit of the effectiveness factor and apply the linear-quadratic model to the survival of prokaryotic cells that do not allow simultaneous repair of damage, the unrestored fraction of breaks can be set to one [4].

Brynjolfsson [13] transformed the target theory models by assuming that a microbe in a cell that is essential for survival has a complement, such as double-stranded DNA. He further assumed this essential microbe is composed of subunits and if one subunit is destroyed, then its complement can be used to recreate it. While this model was validated by experimental data, it assumes that if both complementary subunits are hit, the cell cannot survive. Section 4.4 discussed the ability of spore to repair itself even if both strands of the DNA backbone are damaged.

Sutherland [97] proposed a stochastic model that considers the probability that a lethal damage can be repaired to predict a probability of survival curve. Lethal damage is defined as all lesions that can contribute to the inactivation of a cell despite their ability to be repaired or not. The probability of a lethal damage occurrence is assumed to be given by

84

the Poisson probability function and averaged repair probabilities and damage frequencies allow the calculation of an analytical solution in terms of Euler gamma functions. The model also assumes the cell has a limited repair capacity. The next section presents the methodology utilized in this research to develop a probability of survival curve for a population of spores.

5.2 Methodology

This research will demonstrate a stochastic model based on sampling from each of the spore population's enzyme 'fitness' distributions in order to determine the population's probability of survival. Recall from Section 3.8.3 that each of the six enzymes are assumed to be represented by a probability density function (PDF) that reflects the spore population's initial enzyme 'fitness' and that each enzyme's 'fitness' is mutually independent. That is, the 'fitness' associated with any one enzyme has not effect or bearing on the 'fitness' of any other enzyme. In addition, the initial 'fitness' of each enzyme is degraded due to oxidative damage caused by ROS within the spore core.

The first step of constructing the population's probability of survival is sampling from the cumulative distribution function (CDF) of each damaged enzyme. Sampling from the CDF allows the influence of occurrence of each enzyme to be reflected. The CDF, denoted by $\Phi_X(x)$, of the Uniform distribution is found by integrating Equation 3.34 with respect to x. $\Phi_X(x)$ is given by

$$\Phi_X(x) = \begin{cases} 0, & x < a \\ \frac{x-a}{b-a}, & a \leq x < b \\ 1, & x \geq b \end{cases}$$

where $\Phi_X(x)$ is bounded between a and b. Figure 5.2 illustrates the CDF of the damaged UvrB enzyme and demonstrates values of two samples from the CDF. It assumes a single dose of radiation produced 10 percent damage to the enzymes. The PDF of the UvrB enzyme's functional concentration after radiation exposure has a mean of 336.2 nM which
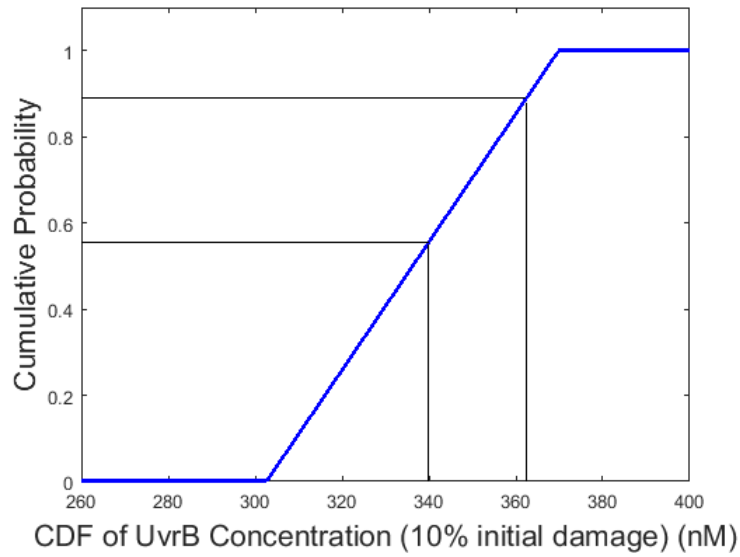
Figure 5.2: CDF and Sampling for UvrB

is 90 percent of the average UvrB concentration prior to irradiation. *a* and *b* are equal to 302.6 nM and 369.9 nM respectively. A total of ten evenly spaced samples are taken from the CDFs of each of the six repair enzymes. The samples from the damaged enzymes' CDFs are used as the initial enzyme concentrations for the repair model presented in Chapter 4. Ten samples from each of the six enzyme distributions result in a total of one million combinations of initial enzyme concentrations that are considered to determine the concentration of viable DNA, $[D_g]\left(t, e\left(\frac{d}{r}\right), [D_g]_0\left(\frac{d}{r}\right)\right)$, for a given repair time, t. The initial concentration of viable DNA, $[D_g]_0\left(\frac{d}{r}\right)$, and the state of the enzyme population, $e\left(\frac{d}{r}\right)$, is a function of dose, d. Dose, d, is equal to rt_e where r is the radiation rate and t_e is the radiation exposure time. Figure 5.3 portrays the estimated percentage of viable DNA (i.e. the vertical axis) as a function of time given that ten percent of the initial DNA concentration was damaged. The horizontal axis represents time in hours. The dashed red line demonstrates the DNA repair utilizing the mean values of the enzyme CDFs as the initial enzyme concentrations and the NER process with the $UvrA_2B_1$ complex. This

output corresponds to the results of the NER mechanism found in Section 4.6.5 and Figure 4.4. The black line represents repair over time with the maximum concentration values sampled from each of the enzyme CDFs while the blue line gives repaired DNA over time with the minimum enzyme concentration values.
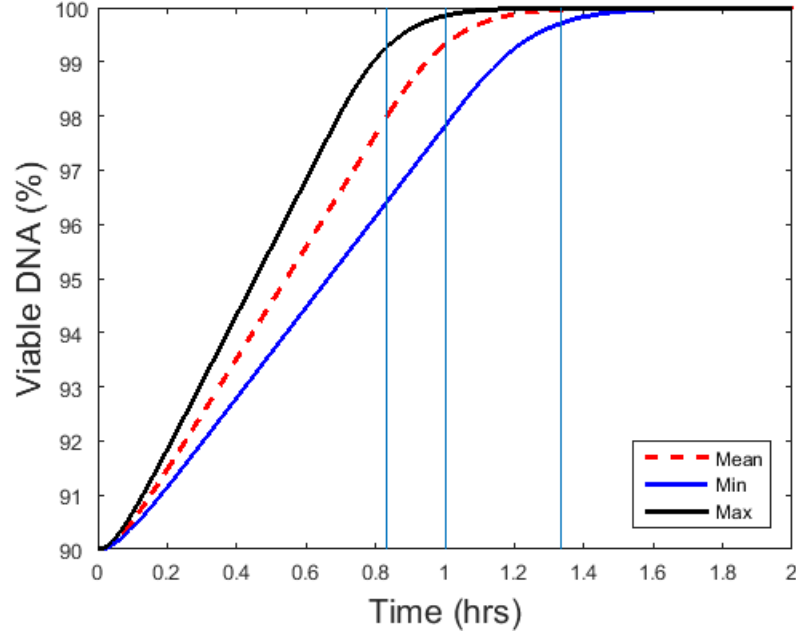

Figure 5.3: Estimated Minimum, Mean, Maximum Representations of Repaired DNA (10% initial damage)

A probability of kill, P_K, curve for the spore's population will be constructed at three different times during the repair process. Note that probability of survival, P_S is equivalent to $1 - P_K$. The three separate times demonstrate the difference between a population's chance of survival when only a short time period (i.e. 50 min) is permitted for repair versus when the repair process is allowed to proceed uninterrupted for a longer period of time (i.e. 80 min). In addition, the probability of survival given one hour of repair time will also be calculated to exhibit the evolution of a population's probability of survival between the

87

short and long repair times. In order to develop the kill curve, the concentration of viable DNA, $[D_g]\left(t_j, e\left(\frac{d}{r}\right), [D_g]_0\left(\frac{d}{r}\right)\right)$, is captured for all of the sample runs where t_j represents the different repair times ($j = 1, 2, 3$). The three vertical lines in Figure 5.3 depict the three times at which a probability of kill curve will be calculated. Recall that at each specified time, one million data points for $[D_g]\left(t_j, e\left(\frac{d}{r}\right), [D_g]_0\left(\frac{d}{r}\right)\right)$ are captured.

Histograms are constructed at each of the three specified times by dividing the horizontal axis, percentage of viable DNA, into equal length bins and drawing a rectangle with an area proportional to the number of observations in that bin. The bins are labeled with the minimum viable DNA percentage from that bin. Observe from Figure 5.3 that after 50 minutes of repair time, the amount of viable DNA is roughly symmetric about the mean. This is further demonstrated in the corresponding histogram (see Figure 5.4(a)). Histograms for the concentrations of viable DNA after one hour and 80 minutes of repair are also displayed in Figure 5.4. Note the range of the horizontal axis of each histogram is not the same. Figures 5.4(b) and 5.4(c) show that with additional repair time, the distribution of viable DNA becomes more skewed towards 100 percent repair of the DNA.

An estimate of the probabililty of kill is determined from the distribution of $[D_g]\left(t_j, e\left(\frac{d}{r}\right), [D_g]_0\left(\frac{d}{r}\right)\right)$ at each t_j by calculating its empirical distribution function, $F_n(x)$, defined by

$$F_n(x) = \frac{1}{n}\left(\#X_i \leq x\right).$$

Here, n is the number of samples such that $1 \leq i \leq n$ and $\#X_i$ is the count of observations of the random variable, X, less than the value, x. For this model, the ith observation of the random variable, X_i, is given by $[D_g]\left(t, e\left(\frac{d}{r}\right), [D_g]_0\left(\frac{d}{r}\right)\right)_i$ and n is one million. For ease of notation, the brackets are dropped. The estimated cumulative probability of kill, P_K, for a spore population is approximated by its empirical CDF for n sufficiently large,

$$P_K\left\{D_g\left(t, e\left(\frac{d}{r}\right), D_{g_0}\left(\frac{d}{r}\right)\right) \leq x\right\} \simeq F_n(x).$$
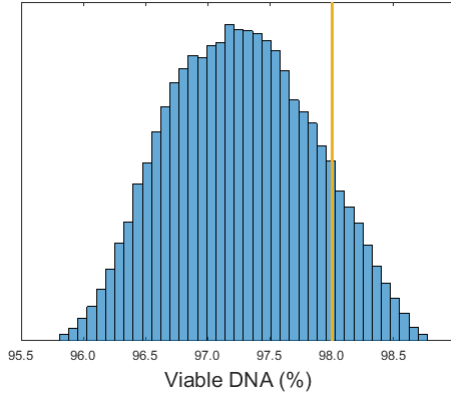
(a) Histogram at 50 Min
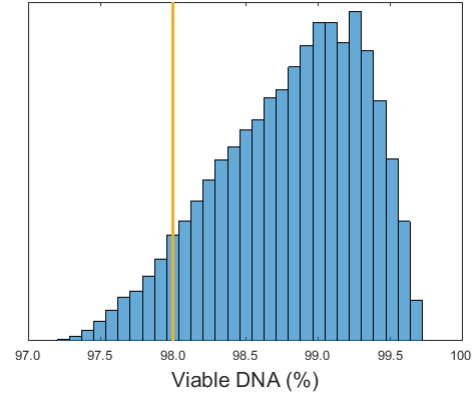
(b) Histogram at 1 Hr

(c) Histogram at 80 Min

Figure 5.4: Histograms of Viable DNA (%) at 50 Min, 1 Hr, and 80 Min (10% initial damage)

"While there can be repair of DNA damage ... if too much damage has been accumulated during spore dormancy, this damage can overwhelm the capacity of repair systems and lead" to spore death [91]. Let D_c denote the critical threshold such that if $D_g > D_c$ then the spore's DNA has been repaired to a viable level at which it can produce a cell during germination. Thus if $D_g > D_c$, the spore population will survive and if $D_g \leq D_c$
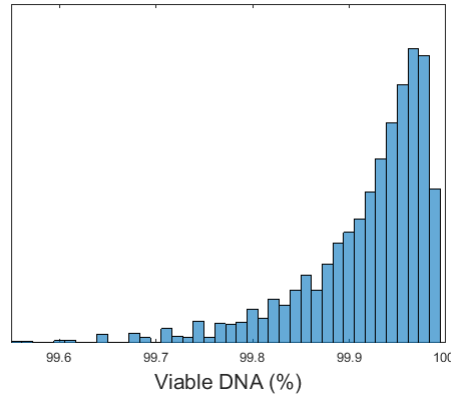
89

the population will be die, i.e.

$$P_K \left\{ D_g \left(t, e \left(\frac{d}{r} \right), D_{g_0} \left(\frac{d}{r} \right) \right) \le D_c \right\} \simeq F_n (D_c) = \frac{1}{n} \left[\# D_g \left(t, e \left(\frac{d}{r} \right), D_{g_0} \left(\frac{d}{r} \right) \right)_i \le D_c \right].$$

Survival models found in the literature, such as the linear-quadratic model, relate radiation dose to survival. To determine the explicit relationship between survival and dose, $S_t(d)$, note that the probability of survival, P_S, is equivalent to $1 - P_K$, therefore

$$S_t(d) = P_S \left\{ D_g \left(t, e \left(\frac{d}{r} \right), D_{g_0} \left(\frac{d}{r} \right) \right) > D_c \right\}. \tag{5.1}$$

Define $\Gamma(d)$ to be the support of $\phi \left(e \left(\frac{d}{r} \right) \right)$, the joint density function given by Equation 3.36, i.e.

$$\Gamma(d) = \left\{ e : e_i \in \left[0.9 f_e(t) \mu_{e_{i_0}}, 1.1 f_e(t) \mu_{e_{i_0}} \right], i = 1, \ldots, 6 \right\}. \tag{5.2}$$

Let $\Omega_t(d)$ be the region given by the viable DNA which has reached the critical DNA threshold after repair time, t, or

$$\Omega_t(d) = \left\{ e : D_g \left(t, e, D_{g_0} \left(\frac{d}{r} \right) \right) > D_c \right\}. \tag{5.3}$$

Survival of the spore population, $S_t(d)$, is represented by the intersection of $\Gamma(d)$ and $\Omega_t(d)$:

$$S_t(d) = \int_{\Gamma(d) \cap \Omega_t(d)} \phi(e) D_g \left(t, e, D_{g_0} \left(\frac{d}{r} \right) \right) de.$$

For this research, the joint density function is uniform for e therefore,

$$S_t(d) = \frac{1}{[0.2 f_e]^6 \prod\limits_{i=1}^{6} \mu_{e_{i_0}}} \int_{\Gamma(d) \cap \Omega_t(d)} D_g \left(t, e, D_{g_0} \left(\frac{d}{r} \right) \right) de.$$

The results from the probability of kill model are portrayed in the next section.

5.3 Results

The probability of kill of a spore population is first examined for the case of ten percent damage to its DNA and repair enzymes and utilizes NER repair with the $UvrA_2B_1$ complex. Assume the critical threshold, D_c, is 98 percent. Therefore, DNA must be repaired to 98

percent of its original capacity for the spore to accomplish necessary biological functions. This critical threshold is indicated by the vertical yellow lines in the histograms of Figure 5.4. Notice that after 50 minutes of repair time, the majority of the population has not met this critical threshold (see Figure 5.4(a)). The corresponding estimated probability of kill curve for this spore population is given by the blue line in Figure 5.5. Again, the vertical yellow line represents D_c and the horizontal axis is percentage of viable DNA. The probability of kill is given by the vertical axis. Therefore, given a repair time of 50 minutes, about 89 percent of the spore population will fail to meet the critical threshold of 98 percent DNA viability i.e.

$$P_K \left\{ D_g \left(50 \text{ min}, e \left(\frac{d}{r} \right), 90\% \right) \le 98\% \right\} = 89\%.$$

However, as shown by the red line in Figure 5.5, after one hour of repair, approximately eight percent of the spore population has failed to meet the critical DNA threshold. This is also demonstrated by the histogram in Figure 5.4(b). Also note that 80 minutes of repair time allows the estimated probability of kill for a spore population to be zero for the critical threshold of 98 percent viable DNA. Thus the population has an estimated 100 percent probability of survival (demonstrated by the black kill curve in Figure 5.5).

Next, the effect of simultaneous hydrolysis damage on the population's probability of kill is explored. Figure 5.6 depicts the estimated kill curves for the same repair times as the previous graphs (Figure 5.5) but includes the possibility of continual hydrolysis damage to the DNA given the spores in the population have a 5 percent moisture content. Observe that a 50 minute repair time results in an estimated 100 percent probability of kill for the population if the critical threshold of viable DNA is 98 percent. Even with an hour of repair time, about 65 percent of the population will fail to meet the critical threshold for viable DNA. However, 80 minutes of repair time gives an estimated 100 percent probability of population survival.

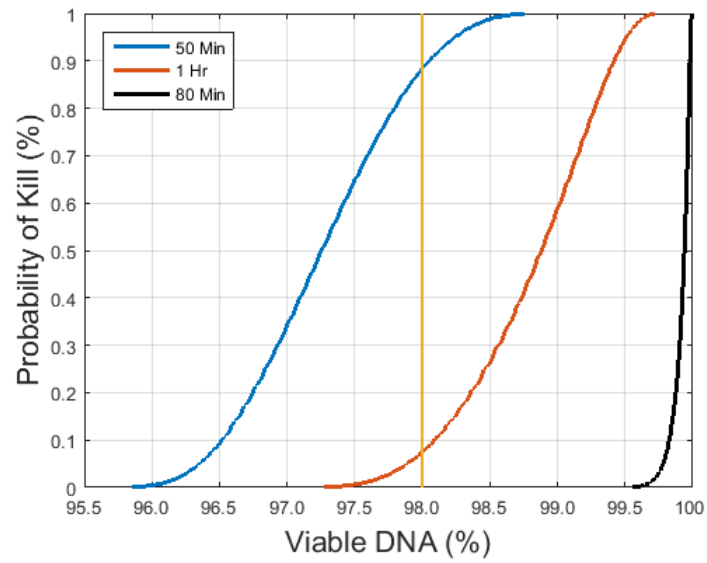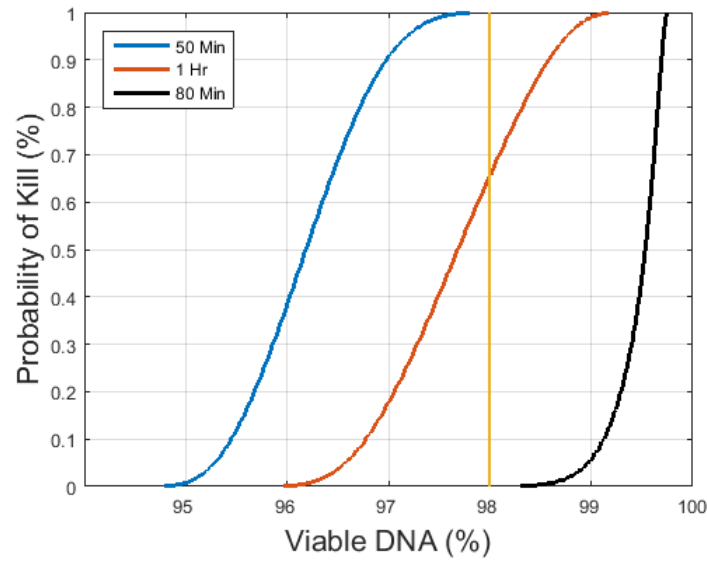Figure 5.5: Estimated Probability of Kill Assuming Repair with UvrA$_2$B$_1$ (10% initial damage)

Figure 5.6: Estimated Probability of Kill Assuming Repair with UvrA$_2$B$_1$ Including Hydrolysis Damage with 5% Moisture Content (10% initial damage)

Figure 5.7 represents the probability of kill of a spore population that experiences continual hydrolysis damage with a nine percent initial moisture content. These results indicate that the estimated probability of kill of a population that experienced 10 percent damage to its DNA and repair enzymes, is 100 percent for repair times less than or equal to an hour. Again, this is assuming a critical DNA threshold of 98 percent. Even with 80 minutes of allowed repair time, there is an estimated 98 percent probability that the population will fail to meet the critical DNA threshold.
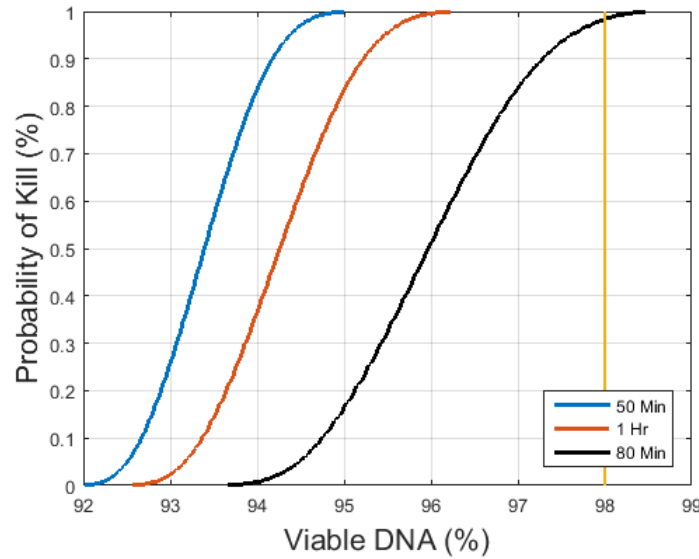
Figure 5.7: Estimated Probability of Kill Assuming Repair with UvrA$_2$B$_1$ Including Hydrolysis Damage with 9% Moisture Content (10% initial damage)

In order to examine the population's survival dependence on radiation exposure, recall from Section 3.8.2, Equation 3.30, that the concentration of DNA, $[D](t)$, is a function of the initial concentration of DNA, $[D]_T$, and the fraction of DNA remaining after some radiation exposure time, $f_D(t)$, i.e.

$$[D](t) = [D]_T f_D(t). \tag{5.4}$$

The dose dependence of this model is represented by exposure time which is related to dose, d, by the expression $d = rt_e$ where r is the radiation rate. Thus Equation 5.4 becomes

$$[D]\left(\frac{d}{r}\right) = [D]_T f_D\left(\frac{d}{r}\right). \tag{5.5}$$

As dose increases, the fraction of viable DNA decreases. The enzyme activity level as a function of exposure time is modeled similarly to Equation 5.5 (see Section 3.8.3). Figure 5.8 depicts the dose dependence on repaired DNA assuming no simultaneous hydrolysis damage occurs. The vertical axis represents the percentage of viable DNA while the horizontal axis gives time in hours. If both enzymes and DNA receive a radiation dose that damages their initial concentrations by 20 percent, the necessary DNA repair time will be increased as shown the by the red line in Figure 5.8. Utilizing the mean value from each of the six enzyme 'fitness' CDFs that were damaged by 20 percent results in an estimated repair time of approximately 3 hours. This is more than twice as long as the repair of DNA
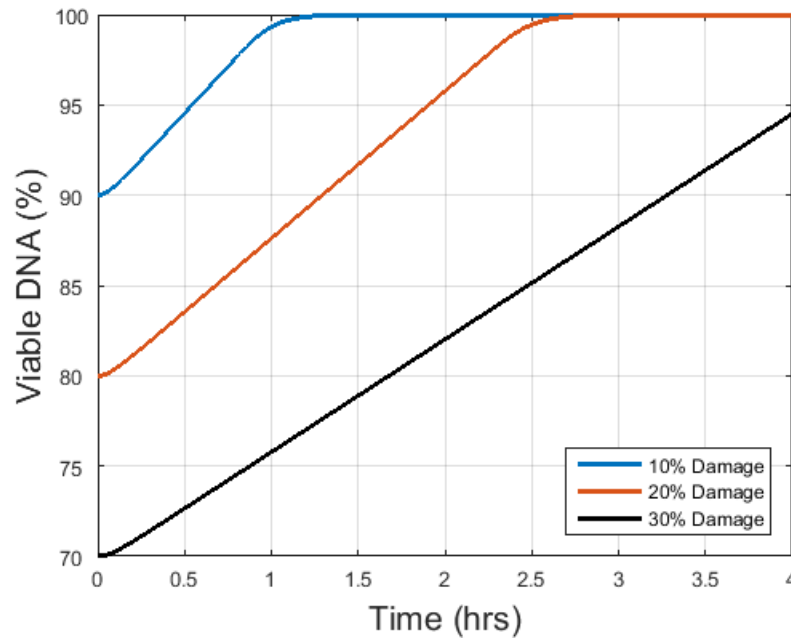
Figure 5.8: Dose Dependence of Viable DNA

which only experienced 10 percent initial damage to its DNA and the state of its enzymes (shown by the blue line). The black line in Figure 5.8 represents repair of DNA given that 30 percent of its initial DNA and repair enzymes were damaged. After four hours of repair, the DNA still has not been restored to 95 percent of its original state.

Next, the probability of kill for a population that experienced a radiation dose that damaged its DNA and the state of its enzymes by 20 percent will be determined. Figure 5.9 portrays the estimated percentage of repaired DNA (i.e. the vertical axis) as a function of time given that 20 percent of the initial DNA concentration was damaged and there exists no simultaneous hydrolysis damage. The horizontal axis represents time in hours. The dashed red line demonstrates the DNA repair utilizing the mean values of the enzyme CDFs as the initial enzyme concentrations and the NER process with the $UvrA_2B_1$ complex. The black line represents repair as a function of time using the maximum concentration values
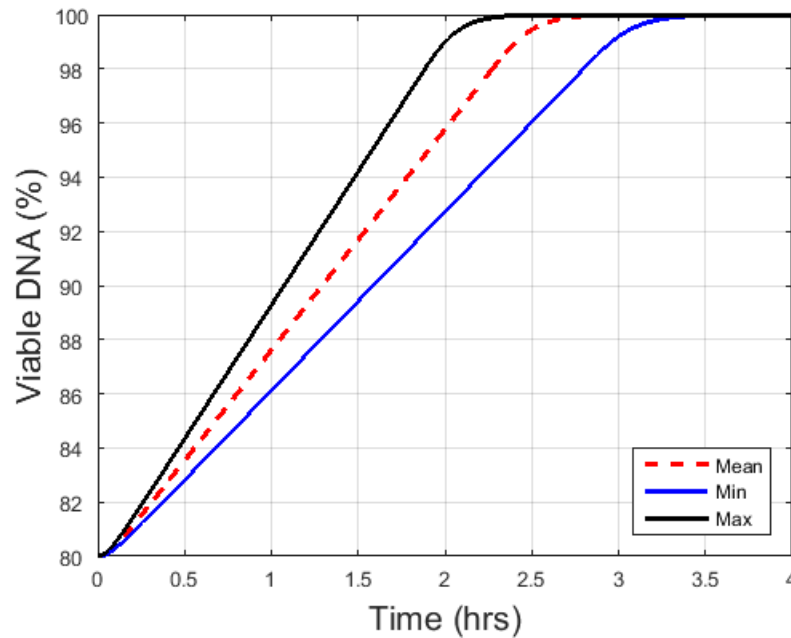
Figure 5.9: Estimated Minimum, Mean, Maximum Representations of Repaired DNA (20% initial damage)

sampled from each of the enzyme CDFs while the blue line gives repaired DNA over time with the minimum enzyme concentration values. For all three cases, the DNA repair time required is more than twice as long as the DNA repair time when only 10 percent of the DNA and enzymes were damaged.

Figure 5.10 illustrates the effect of an increased dose on the population's probability of kill. These kill curves are calculated for a population that experienced 20 percent damage to its DNA and repair enzymes but did not encounter any simultaneous hydrolysis damage. Note that these kill curves represent different repair times than the previous probability of kill curves (Figure 5.5). With the increased damage to DNA and enzymes, an estimated 100 percent of the population will fail to meet the critical threshold of 98 percent viable DNA after 80 minutes of repair time (refer to the blue line in Figure 5.10). A population's estimated probability of kill is still 99 percent after two hours of repair as shown by the red
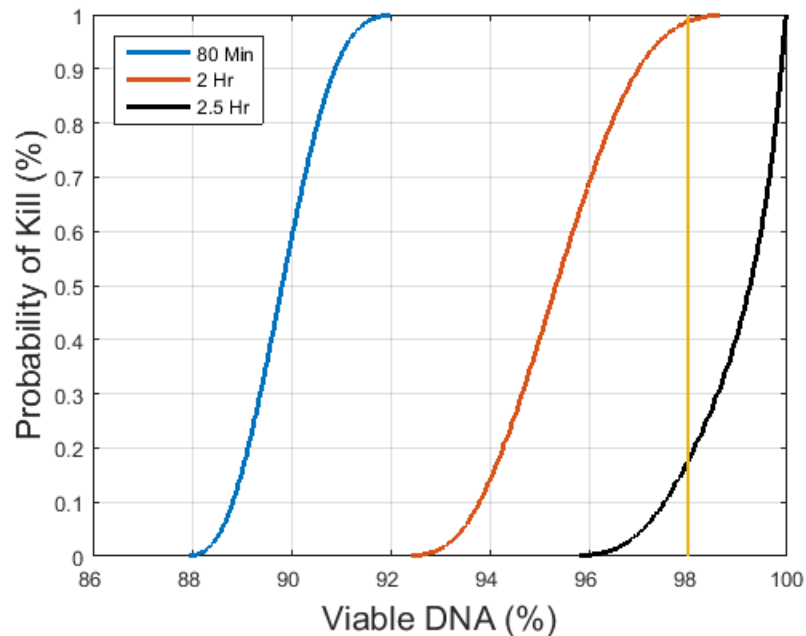
Figure 5.10: Repair with UvrA$_2$B$_1$ (20% initial damage)

line in Figure 5.10. The black line indicates that approximately 18 percent of the population will fail to meet the critical threshold of 98 percent viable DNA after two and a half hours of repair.

5.4 Summary

This chapter combined damage to a spore's DNA and enzymes with DNA repair to develop and explore a probability of kill model for a population of *Bacillus* spores. A critical threshold of DNA viability was assumed and the effect of repair time on a population's probability of survival was examined. An increase in allowable repair time decreases the population's kill probability. However, simultaneous hydrolysis damage increases the probability of kill and a spore population's chance of surviving decreases as the moisture content, and thus the hydrolysis damage, increases. In addition, a larger dose of radiation increases the damage to both DNA and repair enzymes which significantly decreases a spore population's survivability even with increased repair time. Finally, an expression for population survival as a function of radiation dose was found.

VI.   Conclusion

This research models the inactivation of a population of *Bacillus* spores after irradiation by coupling radiation dose, damage, and repair in order to characterize the population's probability of survival. Indirect damage to a *Bacillus* spore's DNA and essential enzymes was modeled via an ionizing radiation exposure. The irradiation of water produces radicals which react with biological material as they diffused into the spore. As a result, these reactive oxygen species (ROS) damaged the spore's DNA and repair enzymes within the core. The extent of this damage hampered the ability of the spore's DNA to be repaired and thus the spore's germination and outgrowth capability. All of these factors effect a population's probability of survival.

The production and diffusion of ROS and their subsequent reactions within the spore's core were shown to be dependent on the radiation exposure. This research considered a 20 Mev, 1 ns pulse of radiolysis impinging on an inert solid plate having a thin layer of adsorbed water and an adsorbed spore; simulating inactivation of spores adsorbed on surfaces in a humid environment. This produced a radical yield on the outer boundary of the spore which was in an ionizing particle's spur. The reaction-diffusion of these ROS into the spore core resulted in damage to the spore's DNA such as DNA base modifications and abstraction of molecules from the DNA strand. The average concentration of reactants in the core led to approximately 10 percent of the spore's DNA experiencing damage due to the irradiation considered in this research. The spore's repair enzymes were also degraded due to ROS reactions.

The repair mechanisms of *Bacillus* spores must be considered prior to examining a spore population's ability to survive. This research developed a model for nucleotide excision repair (NER) which is the primary mechanism by which indirect damage via ionizing radiation is repaired. The NER process repairs a section of damaged DNA and

it is responsible for the removal of a broad group of structurally unrelated DNA lesions to include SSBs and the interactions of damaged bases. Variations of the NER pathway were considered as well as an extension that included the possibility of simultaneous hydrolysis damage during the repair process. Because hydrolysis damage occurs simultaneously with repair, the level of viable DNA may never reach the necessary threshold for outgrowth. In addition, the length of required repair time and the rate of repair is dependent upon the moisture content of the spore.

The probability of kill for a spore population was examined under the assumption there exists some critical threshold of viability that the DNA must be repaired to in order for the population to conduct necessary biological processes for survival. In addition, a certain initial enzyme 'fitness' of the population was taken into account. As expected, the population's probability of kill decreases as allowed repair time increases. However, simultaneous hydrolysis damage has a significant effect on a population's probability of kill and increasing moisture content of the population further increases its kill probability. Also, increasing the radiation dose increases the damage via ROS to both the spore's DNA and enzymes. Subsequently, the population's probability of kill is increased when radiation dose increases. This research provides a characterization of a spore's probability of kill depending on radiation exposure, chemical reactions within the spore, and repair time.

6.1 Contributions

Contributions to the field of work provided by this research include a prokarytic NER model. To date, only the prokaryotic base excision repair (BER) and non-homologous end-joining processes have been mathematically modeled and even these models utilized eukaryotic enzyme rate kinetics. In addition, this research provided the first description of radiation damage in a humid environment in which hydrolysis contributes to the inactivation of the spore. Finally, a process by which dose is directly related to probability of survival was presented. This was done by coupling radiation dose, damage to DNA

and enzymes, and DNA repair while assuming a certain population initial enzyme 'fitness' probability density function.

6.2   Future Work

During development of the damage, repair, and probability of kill models contained in this research, the following areas were identified as requiring further analysis. The damage model assumed that there exist no significant permeability barriers within the spore that would prevent the movement of reactants from the outer boundary to the core. As discussed in Section 2.1.1 the exosporium, the spore coat, the outer membrane, the cortex, and the germ cell wall are not considered to be permeability barriers against small molecules. However, the inner membrane of the dormant spore might prevent a portion of the reactants from reaching the core and thus the spore's DNA. Therefore the diffusion of reactants through this membrane could be incorporated into the damage model.

The radiation damage model considered two classes of reactants. R_1 represents the class that reacts quickly with the O_2 present in the adsorbed water and therefore instantaneously transforms into other species. e^- is an example of this class of reactants. R_2 represents the class that does not react as fast as the R_1 class and therefore does not get transformed as quickly. This allows the class of R_2 reactants to diffuse to the outer boundary of the spore. OH belongs to this class of reactants. However, this model may be oversimplified. After examining the rate coefficients in Table 3.2 of OH with other species, a third class of reactants should be considered. Specifically, the reaction of OH with O_2^- has a reaction rate which is almost equivalent to the diffusion controlled rate. However, the reaction of OH with H_2O_2 has a reaction rate which is much slower (3.8 x 10^7 $M^{-1}s^{-1}$). Therefore, a damage model that breaks up the current definition of class 2 reactants into two separate categories thereby defining three different classes of reactants could be considered. The current R_2 class would be divided into a category of reactants that will reach the outer boundary of the spore and a category of reactants that would react with other species as

it diffuses through the water layer between the source and the spore. Furthermore, there exists a possible need for four reactant classes in order to model the reaction-diffusion of the OH, H, e^-, and H_2O_2 species.

In addition, the concentration of reactants was assumed to be uniformly impressed on the outer boundary of the spore. However, if the substrate is irradiated at only one location as in Figure 3.4 and the spore is located relatively close to the radiation source, the reactants would not be uniformly distributed within the substrate. A greater concentration of reactants would be expected on one side of the spore compared to the other side of the spore. For the case considered in this research, the radiation events would be randomly distributed around the spore. Integrating over this distribution of event locations could be an approach to determine the distribution of reactants on the outer boundary of the spore.

Certain values given in Section 4.6.5 for reaction rate parameters of the NER are not well known. For example, the rate at which polymerase I lays down corrected bases found in the literature applies to BER. During BER, only one base is replaced while NER requires multiple bases to be replaced. Sensitivity analysis on all of the repair rate parameters should be completed. Also, the NER model and thus the probability of survival model presented in this research assumed that no repair molecules were produced after the initiation of germination. Future work should examine the possibility of new repair enzyme creation from undamaged or repaired DNA.

The initial enzyme 'fitness' presented in Section 3.8.3 was modeled via a Uniform PDF. This representation is conservative and the effects of various density functions should be examined. In addition, the utilization of a continuous PDF was necessary due to the modeling of the repair process via differential equations. However, the low concentrations of the UvrA and UvrC enzymes might be more accurately modeled with a discrete distribution or a mixture distribution. Such an approach would require the NER process to be modeled as a discrete state difference equation.

Further, the histograms given in Figure 5.4 which characterize the distribution of the repaired DNA over time indicate that it may be possible to model the repaired DNA with a PDF as a function of time. Recall that the distribution of repaired DNA is related to the initial enzyme 'fitness' PDFs. Modeling the repaired DNA as a PDF over time would eliminate the need to conduct million-run simulations which require extensive computing power and time. However, in order to determine the density function of the repaired DNA, additional samples from each of the CDFs of the six repair enzymes should be considered. This research took ten evenly spaced samples from each enzyme's CDF. In order to gain the fidelity needed to calculate the repaired DNA distribution, one hundred samples from each enzyme CDF should be taken into account.

Finally, further analysis is necessary to compare this research to real data. Experiments conducted with live spores would allow comparison with data used in the mathematical models presented in this research. This research demonstrated a method to compute probability of kill curves but many assumptions were made during their development such as the critical DNA threshold value. These assumptions should be examined further in order to incorporate uncertainty and replicate with experimental results. Initial results of this cursory look at the survival curves is promising. Functional data analysis to refine the enzyme distributions should be completed In addition, replication of the method with experimental results and comparison with other methods of probability of survival estimation could be examined.

Appendix: Steady State Solution to the Mathematical Repair Model

This appendix presents the steady state solution to the NER mathematical model presented in Sections 4.6.1 and 4.6.4. This steady state solution is obtained when the time evolution of the system vanishes. Therefore, the differential equations are set to zero producing the algebraic system:

$$0 = k_3 \left([A_2]_0 - [A_2] - [A_2B]\right) + k_{-1}[A_2B] - k_1[A_2][B] \tag{A.1}$$

$$0 = k_6 \left([H]_0 - [H]\right)[P] + k_{-1}[A_2B] - k_1[A_2][B] \tag{A.2}$$

$$0 = k_5 \left([C]_0 - [C]\right)[H]$$

$$- k_4 \left\{[B]_0 + [A_2] - [A_2]_0 - [B] - ([C]_0 - [C]) - ([H]_0 - [H])\right\}[C] \tag{A.3}$$

$$0 = k_6 \left([H]_0 - [H]\right)[P] - k_5 \left([C]_0 - [C]\right)[H] \tag{A.4}$$

$$0 = k_7 \left([P]_0 - [P]\right)[L] - k_6 \left([H]_0 - [H]\right)[P] \tag{A.5}$$

$$0 = k_8 \left([L]_0 - [L]\right) - k_7 \left([P]_0 - [P]\right)[L] \tag{A.6}$$

$$0 = - k_2[A_2B][D] + k^*[D_g] \tag{A.7}$$

$$0 = k_1[A_2][B] - k_{-1}[A_2B] - k_2[A_2B][D] \tag{A.8}$$

$$0 = k_8 \left([L]_0 - [L]\right) - k^*[D_g]. \tag{A.9}$$

For convenience we set

$$x = k^*D_g, \quad y = [A_2B], \quad \text{and} \quad z = [A_2], \tag{A.10}$$

adopt the notation $z_0 = [A_2]_0$, and drop the brackets. Upon substitution and some algebraic reduction, we obtain a new set of equations:

$$k_8(L_0 - L) - x = 0 \tag{A.11}$$

$$k_7(P_0 - P)L - x = 0 \tag{A.12}$$

$$k_6(H_0 - H)P - x = 0 \tag{A.13}$$

$$k_5(C_0 - C)H - x = 0 \tag{A.14}$$

$$k_3(z_0 - z) - k_3 y - x = 0 \tag{A.15}$$

$$k_1 zB - k_{-1}y - x = 0 \tag{A.16}$$

$$k_2 yD - x = 0 \tag{A.17}$$

$$k_4 C[(B_0 - B) - (z_0 - z) - (C_0 - C) - (H_0 - H)] - x = 0 \tag{A.18}$$

Equation A.11 is from A.9 and Equations A.12 through A.14 are obtained by sequential substitution of this result. Equations A.1, A.2, and A.7 are Equations A.15, A.16, and A.17 respectively. Finally, Equation A.18 is Equation A.3 with the replacement given from Equation A.14. The results from Equation A.8 are not included as they only reproduce Equation A.16. An additional equation is necessary to complete the algebraic system. It is attained from the DNA conservation requirement that

$$D_T = D_g + D + D_c$$

as described in Section 4.6.4 with

$$D_c = A_2 BD + HBD + CBD + BD + PD + LD.$$

Using the enzyme conservation equations of Section 4.6.1, we obtain

$$D_T = D_g + D + (B_0 - B) + (P_0 - P) + (L_0 - L) - [A_2 B].$$

Substituting the definitions of Equation A.10 results in

$$\frac{x}{k^*} + D + (B_0 - B) + (P_0 - P) + (L_0 - L) - D_T - y = 0 \tag{A.19}$$

Now Equations A.11 through A.19 form a complete set of algebraic equations to determine the steady state behavior of the NER process.

Begin by examining the case where no hydrolysis damage is occurring (i.e. $k^* = 0$) which implies $x = 0$. Then from Equations A.11 through A.14 it is clear that

$$L = L_0, \quad P = P_0, \quad H = H_0, \quad \text{and} \quad C = C_0. \tag{A.20}$$

104

Consequently, over time, the concentrations of UvrC, helicase II, polymerase I, and ligase will approach their initial concentrations. From Equation A.17, we find either $y = 0$ or $D = 0$. If $y = 0$ then Equation A.15 implies $z = z_0$. Substituting this along with Equation A.20 into Equation A.18 leads to $B = B_0$. Now Equation A.16 becomes $zB = z_0B_0 \neq 0$ which is a contradiction. Therefore $y \neq 0$ and

$$D = 0 \tag{A.21}$$

which implies complete DNA repair has taken place. Now Equation A.17 is satisfied. From Equation A.15 and subsequently from Equation A.18 we have

$$z = z_0 - y \quad \text{and} \quad B = B_0 - y. \tag{A.22}$$

Note that Equation A.16 is the equilibrium equation implying that the concentrations of UvrA, UvrB, and the UvrA$_2$B$_1$ complex will all exist in their equilibrium state given by the equation $k_{-1}[A_2B] = k_1[A_2][B]$ where $\frac{k_{-1}}{k_1}$ is the equilibrium constant [85]. Substituting Equation A.22 into the equilibrium equation produces

$$k_1(z_0 - y)(B_0 - y) - k_{-1}y = 0.$$

Solving this quadratic equation for y with $\lambda = \frac{k_{-1}}{k_1}$ admits two solutions,

$$y = \frac{1}{2}\left[(\lambda + z_0 + B_0) \pm \sqrt{(\lambda + z_0 + B_0)^2 - 4z_0B_0}\right].$$

Because as $B_0 \to 0$ requires $[A_2B] = y \to 0$, it follows the minus sign must be chosen. Therefore

$$[A_2B] = y = \frac{1}{2}\left[(\lambda + z_0 + B_0) - \sqrt{(\lambda + z_0 + B_0)^2 - 4z_0B_0}\right] \tag{A.23}$$

Thus the steady state solution with no hydrolysis damage included is given by Equations A.20 through A.23.

Next explore the case where $k^* \neq 0$. Using Equations A.11 through A.19 and solving for L, P, B, H, C, y, and z in terms of x and D gives

$$B = -\frac{xk_3(k_{-1} + Dk_2)}{k_1\,[x(k_3 + Dk_2) - Dk_2k_3z_0]} \tag{A.24}$$

$$C = C_0 - \frac{xk_6}{k_5}\,\frac{x(k_8 + P_0k_7) - L_0P_0k_7k_8}{-x^2k_7 + x(H_0k_6k_8 + L_0k_7k_8 + H_0P_0k_6k_7) - H_0L_0P_0k_6k_7k_8} \tag{A.25}$$

$$H = H_0 - \frac{xk_7}{k_6}\,\frac{x - L_0k_8}{x(k_8 + P_0k_7) - L_0P_0k_7k_8} \tag{A.26}$$

$$L = L_0 - \frac{x}{k_8} \tag{A.27}$$

$$P = P_0 + \frac{x}{k_7}\frac{k_8}{x - L_0k_8} \tag{A.28}$$

$$y = \frac{x}{Dk_2} \tag{A.29}$$

$$z = z_0 - x\left(\frac{1}{Dk_2} + \frac{1}{k_3}\right) \tag{A.30}$$

Notice that C, H, L and P depend only on x while B, y, and z depend on both x and D. These results are substituted into Equations A.18 and A.19 to obtain a system of equations for x and D.

$$k_4\left(C_0 - \frac{xk_6}{k_5}\,\frac{x(k_8 + P_0k_7) - L_0P_0k_7k_8}{-x^2k_7 + x(H_0k_6k_8 + L_0k_7k_8 + H_0P_0k_6k_7) - H_0L_0P_0k_6k_7k_8}\right)$$
$$\left[\left(B_0 + \frac{xk_3(k_{-1} + Dk_2)}{k_1\,[x(k_3 + Dk_2) - Dk_2k_3z_0]}\right) - x\left(\frac{1}{Dk_2} + \frac{1}{k_3}\right) - \left(\frac{xk_7}{k_6}\,\frac{x - L_0k_8}{x(k_8 + P_0k_7) - L_0P_0k_7k_8}\right)\right.$$
$$\left.\left. - \left(\frac{xk_6}{k_5}\,\frac{x(k_8 + P_0k_7) - L_0P_0k_7k_8}{-x^2k_7 + x(H_0k_6k_8 + L_0k_7k_8 + H_0P_0k_6k_7) - H_0L_0P_0k_6k_7k_8}\right)\right] - x = 0 \right. \tag{A.31}$$

$$\frac{x}{k^*} + D + \left(B_0 + \frac{xk_3\,(k_{-1} + Dk_2)}{k_1\,[x(k_3 + Dk_2) - Dk_2k_3z_0]}\right) - \left(\frac{x}{k_7}\frac{k_8}{x - L_0k_8}\right) + \left(\frac{x}{k_8}\right) - D_T - \frac{x}{Dk_2} = 0 \tag{A.32}$$

Further progress with these equations must be made numerically.

Bibliography

[1] Abramowitz, M., and Stegun, I.A. *Handbook of Mathematical Functions with Formulas, Graphs, and Mathematical Tables (10th Edition).* New York: Dover Publications, Inc., 1972.

[2] Abel-Santos, E. *Bacterial Spores: Current Research and Applications.* Norfolk, UK: Caister Academic Press, 2012.

[3] U.S. Army. "Army to study biological decontamination of aircraft interiors" ECBC Communications, May 31, 2013. 23 August 2015 http://www.army.mil/article/104266/Army to study biological decontamination of aircraft interiors/

[4] Alpen, E. *Radiation Biophysics (Second Edition).* San Diego: Academic Press, 1990.

[5] United States Department of Justice. "Amerithrax Investigation" Federal Bureau of Investigation, 2008. 12 January 2009 http://www.fbi.gov/anthrax/amerithraxlinks.htm.

[6] Araujo, S.J. and Wood, R.D. "Protein complexes in nucleotide excision repair," *Elsevier Mutation Research*, 435: 23-33 (1999).

[7] Arthur, H.M. and Eastlake, P.B. "Transcriptional control of the uvrD gene of *Escherichia coli*," *Gene*, 25(2-3): 309-316 (1983).

[8] National Center for Biotechnology Information. "Bacillus anthracis strain BA1015, complete genome," Nucleotide, 20 August 2015 http://www.ncbi.nlm.nih.gov/nuccore/CP009544.1.

[9] Ballarini, F. "From DNA Radiation Damage to Cell Death: Theoretical Approaches," *Journal of Nucleic Acids,* 2010 (2010).

[10] "Base Pair," Wikipedia, 24 May 2014. 20 June 2014 http://en.wikipedia.org/wiki/Base pair

[11] Blattner, F.R., Plunkett III, G., Bloch, C.A., Perna, N.T., Burland, V., Riley, M., Collado-Vides, J., Glasner, J.D., Rode, C.K., Mayhew, G.F., Gregor, J., Davis, N.W., Kirkpatrick, H.A., Goeden, M.A., Rose, D.J., Mau, B., and Shao, Y. "The Complete Genome Sequence of *Escherichia coli* K-12," *Science*, 277:1453-1462 (5 September 1997).

[12] Brahmi, M. and Hassen, A. "Disinfection of Wastewater by UV Irradiation: Influence of Hydrodynamics on the Performance of the Disinfection," *Environmental Engineering Research,* 16(4):243-252 (December 2011).

[13] Brynjofsson, A. "Mathematical Models for Microbial Kill by Radiation," *Proceedings Food Preservation by Irradiation,* 21-25 (1978).

[14] Cadet, J., Douki, T., Gasparutto, D., and Ravanat, J.-L. "Radiation-induced damage to cellular DNA: measurement and biological role," *Radiation Physics and Chemistry,* 72: 293-299 (2005).

[15] Caron, P.R., Kushner, S.R., and Grossman, L. "Involvement of helicase II (uvrD gene product) and DNA polymerase I in excision mediated by the uvrABC protein complex," *Proceedings of the National Academy of Sciences USA* 82: 4925-4929 (August 1985).

[16] Carrera, M., Zandomeni, R.O., Fitzgibbon, J., and Sagripant, J.-L. "Difference between the spore sizes of *Bacillus anthracis* and other *Bacillus* species," *Journal of Applied Microbiology*, 102: 303-312 (2007).

[17] Casella, G. and Berger, R.L. *Statistical Inference (Second Edition)*. Pacific Grove: Duxbury, 2002.

[18] Collins, A.R., Ai-guo, M., and Duthie, S.J. "The kinetics of repair of oxidative DNA damage (strand breaks and oxidized pyrimidines) in human cells," *Mutation Research*, 336: 69-77 (1995).

[19] Cortezzo, D.E., Koziol-Dube, K., Setlow, B., and Setlow, P. "Treatment with oxidizing agents damages the inner membrane of spores of *Bacillus subtilis* and sensitizes spores to subsequent stress," *Journal of Applied Microbiology*, 97: 838-852 (2004).

[20] Cowan, A.E., Koppel, D.E., Setlow, B., and Setlow, P. "A soluble protein is immobile in dormant spores of Bacillus subtilis but is mobile in germinated spores: Implications for spore dormancy," *Proceedings of the National Academy of Sciences USA* 100(7): 42094214 (April 2003).

[21] Crooke, P.S. and Parl, F.F. "A Mathematical Model for DNA Damage and Repair," *Journal of Nucleic Acids,* 2010: 352603 (2010).

[22] Daly, M.J. "Death by protein damage in irradiated cells," *DNA Repair,* 11: 12-21 (2012).

[23] Daly, M.J., Gaidamakova, E.K., Matrosova, V.Y., Vasilenko, A., Zhai, M., Leapman, R.D., Lai, B., Ravel, B., Li, S-M.W., Kemner, K.M., and Fredrickson, J.K. "Protein Oxidation Implicated as the Primary Determinant of Bacterial Radioresistance," *PLoS Biology* 5(4): 0769-0779 (April 2007).

[24] DellaVecchia, M.J., Croteau, D.L., Skorvaga, M., Dezhurov, S.V., Lavrik, O.I., and Van Houten, B. "Analyzing the Handoff of DNA from UvrA to UvrB Utilizing DNA-Protein Photoaffinity Labeling," *The Journal of Biological Chemistry,* 279(43): 45245-45256 (2004).

[25] Dierick, K., Coillied, E.V., Swiecicka, I., Meyfroidt, G., Devlieger, H., Meulemans, A., Hoedemaekers, G., Fourie, L., Heyndrickx, M., and Mahillon, J. "Fatal

Family Outbreak of Bacillus cereus-Associated Food Poisoning," *Journal of Clinical Microbiology,* 43(8): 4277-4279 (August 2005).

[26] Dizdaroglu, M., Jaruga, P., Birincioglu, M., and Rodriguez, H. "Free Radical-induced Damage to DNA: Mechanisms and Measurement," *Free Radical Biology and Medicine,* 32(11): 1102-1115 (2002).

[27] News Release. "DoD to Resume Anthrax Vaccinations" Department of Defense, 16 October 2006. 16 June 2014 http://www.defense.gov/releases/release.aspx?releaseid=10083.

[28] Driks, A. "The *Bacillus subtilis* spore coat," *Microbiology and Molecular Biology Reviews,* 63: 1-20 (March 1999).

[29] United States Department of Agriculture. *Epizootiology and Ecology of Anthrax*, Animal and Plant Health Inspection Service, 23 April 2014 http://www.aphis.usda.gov/animal-health/emergingissues/downloads/anthrax.pdf.

[30] Ershov, B.G. and Gordeev, A.V. "A model for radiolysis of water and aqueous solutions of H_2, H_2O_2, and O_2," *Radiation Physics and Chemistry*, 77: 928-935 (2007).

[31] Farhataziz and Rodgers, M.A.J. *Radiation Chemistry: Principles and Applications.* New York: VCH Publisher, Inc., 1987.

[32] Centers for Disease Control and Prevention. "Food Safety," Food Safety Homepage, 24 April 2014 http://www.cdc.gov/foodsafety/facts.html.

[33] Foray, N., Charvet A.-M., Duchemin D., Favaudon, V., and Lavalette, D. "The repair rate of radiation-induced DNA damage: A stochastic interpretation based on the Gamma function," *Journal of Theoretical Biology,* 236: 448-458 (June 2005).

[34] Gastaldo, J., Viau, M., Bouchot, M., Joubert, A., Charvet, A.-M., and Foray, N. "Induction and repair rate of DNA damage: A unified model for describing effects of external and internal irradiation and contamination with heavy metals," *Journal of Theoretical Biology,* 251: 68-81 (November 2007).

[35] Gerhardt, P.C. and Marquis, R.E. "Spore thermoresistance mechanisms," *Regulation of Prokaryotic Development*, Washington DC: American Society for Microbiology, (1989).

[36] Gillespie, D.T. "Exact Stochastic Simulation of Coupled Chemical Reactions," *The Journal of Physical Chemistry,* 81(25): 2340-2361 (1977).

[37] Goosen, N. "Scanning the DNA for damage by the nucleotide excision repair machinery," *DNA Repair*, 9: 593-596 (2010).

[38] Harrison, L., Brame, K.L., Geltz, L.E., and Landry, A.M. "Closely opposed apurinic/apyrimidinic sites are converted to double strand breaks in *Escherichia coli* even in the absence of exonuclease III, endonuclease IV, nucleotide excision repair and AP lyase cleavage," *DNA Repair*, 5:324-335 (2006).

[39] Huffman, J.L., Sundheim, O., and Tainer, J.A. "DNA base damage recognition and removal: New twists and grooves," *Mutation Research,* 577: 55-76 (June 2005).

[40] Hughes, G. *Radiation chemistry*. Oxford, Clarendon Press, 1973.

[41] Hurst, A.X. *Modeling of Bacillus Spores: Inactivation and Outgrowth*. MS thesis, AFIT/GAM/ENC/11-01. Graduate School of Engineering and Management, Air Force Institute of Technology (AU), Wright-Patterson AFB OH, March 2011.

[42] Ibarra, J.R., Orozco, A.D., Rojas, J.A., Lopez, K., Setlow, P., Yasbin, R.E., and Pedraza-Reyes, M. "Role of Nfo and ExoA Apurinic/Apyrimidinic Endonucleases in Repair of DNA Damage during Outgrowth of *Bacillus subtilis* Spores," *Journal of Bacteriology,* 190(6): 2031-2038 (March 2008).

[43] Jia, L., Kropachev, K., Ding, S., Van Houten, B., Geacintov, N.E., and Broyde, S. "Exploring Damage Recognition Models in Prokaryotic Nucleotide Excision Repair with a Benzo[a]pyrene-Derived Lesion in UvrB," *Biochemistry*, 48(38): 8948-8957 (2009).

[44] Jonah, C.D. and Miller, J.R. "Yield and Decay of the OH Radical from 200 ps to 3 ns," *The Journal of Physical Chemistry*, 81(21): 1974-1976 (1977).

[45] Jones, D.S. and Sleeman, B.D. *Differential Equations and Mathematical Biology*. Boca Raton: Chapman & Hall/CRC, 2003.

[46] Karschau, J., de Almeida, C., Richard, M.C., Miller, S., Booth, I.R., Grebogi, C., and de Moura, A.P.S. "A Matter of Life or Death: Modeling DNA Damage and Repair in Bacteria," *Biophysical Journal*, 100: 814-821 (February 2011).

[47] Kesseler, K.J., Kaugmann, W.K., Reardon, J.T., Elston, T., and Sancar, A. "A mathematical model for human nucleotide excision repair: damage recognition by random order assembly and kinetic proofreading," *Journal of Theoretical Biology,* 249(2): 361-375 (November 2007).

[48] Knight, E.A. *Modeling Thermal Inactivation of Bacillus Spores*. MS thesis, AFIT/GAM/ENC/09-01. Graduate School of Engineering and Management, Air Force Institute of Technology (AU), Wright-Patterson AFB OH, March 2009.

[49] Kowalski, W.J., Bahnfleth, W.P., Witham, D.L., Severin, B.F., and Whittam, T.S. "Mathematical Modeling of Ultraviolet Germicidal Irradiation for Air Disinfection," *Quantitative Microbiology,* 2: 249-270 (2000).

[50] Krisko, A. and Radman, M. "Biology of Extreme Radiation Resistance: The Way of *Deinococcus radiodurans*," *Cold Springs Harbor Perspectives in Biology,* 5: 1-11 (2013).

[51] Krisko, A., Leroy, M., Radman, M., and Meselson, M. "Extreme anti-oxidant protection against ionizing radiation in bdelloid rotifers," *PNAS*, 109(7): 2354-2357 (February 2012).

[52] Lohman, G.J.S., Chen, L., and Evans Jr., T.C. "Kinetic Characterization of Single Strand Break Ligation in Duplex DNA by T4 DNA Ligase," *Journal of Biological Chemistry,* 286(51): 44187-44196 (December 2011).

[53] Loshon, C.A., Melly, E., Setlow, B., and Setlow, P. "Analysis of the killing of spores of *Bacillus subtilis* by a new disinfectant, Sterilox ®," *Journal of Applied Microbiology*, 91: 1051-1058 (2001).

[54] Madigan, M.T., Martinko, J.M., and Parker, J. *Brock Biology of Microorganisms, (Tenth Edition.)* Upper Saddle River, N.J.: Pearson Education, Inc., 2003.

[55] Maluf, N.K., Ali, J.A., and Lohman, T.M. "Kinetic Mechanism for Formation of the Active, Dimeric UvrD Helicase-DNA Complex," *The Journal of Biological Chemistry,* 278(34): 31930-31940 (2003).

[56] Mancinelli, R.L. and Klovstad, M. "Martian soil and UV radiation: microbial viability assessment on spacecraft surfaces," *Planetary and Space Science,* 48(11): 1093-1097 (September 2000).

[57] McKenney, P.T., Driks, A., and Eichenberger, P. "The Bacillus subtilis endospore: assembly and functions of the multilayered coat," *Nature Reviews Microbiology,* 11(1): 33-44 (December 2012).

[58] McNaught, A.D. and Wilkinson, A. *International Union of Pure and Applied Chemistry, Compendium of Chemical Terminology, (2nd edition).* Oxford: Blackwell Scientific Publications, 1997.

[59] Melly, E., Genest, P.C., Gilmore, M.E., Little, S., Popham, D.L., Driks, A., and Setlow, P. "Analysis of the properties of spores of *Bacillus subtilis* prepared at different temperatures," *Journal of Applied Microbiology,* 92: 1105-1115 (2000).

[60] Minton, K.W. "Repair of ionizing-radiation damage in the radiation resistant bacterium *Deinococcus radiodurans*," *DNA Repair*, 363: 1-7 (1996).

[61] Moeller, R., Douki, T., Cadet, J., Stackebrandt, E., Nicholson, W.L., Rettberg, P., Reitz, G., and Horneck, G. "UV-radiation-induced formation of DNA bipyrimidine photoproducts in *Bacillus subtilis* endospores and their repair during germination," *International Microbiology,* 10: 39-46 (2007).

[62] Mohr, P.J., Taylor, B.N., and Newell, D.B. "CODATA Recommended Values of the Fundamental Physical Constants: 2006," *Review of Modern Physics,* 80: 633-730 (December 2007).

[63] Moler, C. *Numerical Computing with MATLAB (Second Edition).* Philadelphia, PA: Society for Industrial and Applied Mathematics, 2008.

[64] Moore, W.J. *Physical Chemistry (Third Edition).* Englewood Cliffs, NJ: Prentice-Hall, Inc., 1962.

[65] Mouri, K., Nacher, J.C., and Akutsu T. "A Mathematical Model for the Detection Mechanism of DNA Double-Strand Breaks Depending on Autophosphorylation of ATM," *PLoS ONE,* 4(4): e5131 (2009)

[66] Mozumder, A. *Fundamentals of Radiation Chemistry,* San Diego: Academic Press, 1999.

[67] Murray, J.D. *Mathematical Biology I: An Introduction (3rd Edition).* New York: Springer-Verlag, 2002.

[68] Nicholson, W.L., Munakata, N., Horneck, G., Melosh, H.J., and Setlow, P. "Resitance of *Bacillus* Endospores to Extreme Terrestrial and Extraterrestrial Environments," *Microbiology and Molecular Biology Reviews,* 64(3): 548-572 (September 2000).

[69] Orren, D.K., Selby, C.P., Hearst, J,E., and Sancar, A. "Post-incision Steps of Nucleotide Excision Repair in *Escherichia coli*," *The Journal of Biological Chemistry*, 267(2): 780-788 (1992).

[70] Orren, D.K. and Sancar, A. "Formation and Enzymatic Properties of the UvrB-DNA Complex," *The Journal of Biological Chemistry*, 265(26): 15796-15803 (1990).

[71] Pakotiprapha, D. and Jeruzalmi, D. "Small-angle X-ray scattering reveals architecture and A_2B_2 stoichiometry of the UvrA-UvrB DNA damage sensor," *Proteins,* 81: 132-139 (2013).

[72] Pakotiprapha, D., Samuels, M., Shen, K., Hu, J.H., and Jeruzalmi, D. "Structure and mechanism of the UvrA-UvrB DNA damage sensor," *Nature Structural and Molecular Biology,* 19(3): 291-299 (March 2012).

[73] Palop, A., Rutherford, G.C., and Marquis, R.E. "Inactivation of enzymes within spores of *Bacillus megaterium* ATCC 19213 by hydroperoxides," *Canadian Journal of Microbiology,* 44: 465-470 (1998).

[74] Lamothe, D. "Pentagon: Live anthrax inadvertently distributed by Army laboratory," *The Washington Post,* 27 May 2015. 25 August 2015 https://www.washingtonpost.com/news/checkpoint/wp/2015/05/27/pentagon-army-laboratory-inadvertently-distributed-live-anthrax/.

[75] Petit, C. and Sancar, A. "Nucleotide excision repair: From *E. coli* to man," *Biochimie* 81:15-25 (1999).

[76] Petit, M.-A., Dervyn, E., Rose, M., Entian, K.-D., McGovern, S., Ehrlich, S.D., and Bruand, C., "PcrA is an essential DNA helicase of *Bacillus subtilis* fulfilling functions both in repair and rolling-circle replication," *Molecular Microbiology,* 29(1): 261-273 (1998).

[77] Phillips, R., Kondev, J., and Theriot, J. *Physical Biology of the Cell.* Garland Science, 2009.

[78] Politi, A., Moné, M.J., Houtsmuller, A.B., Hoogstraten, D., Vermeulen, W., Heinrich, R., and van Driel, R. "Mathematical Modeling of Nucleotide Excision Repair Reveals Efficiency of Sequential Assembly Strategies," *Molecular Cell,* 19: 679-690 (September 2005).

[79] Popham, D.L., Sengupta, S., and Setlow, P. "Heat, Hydrogen Peroxide, and UV Resistance of *Bacillus subtilis* Spores with Increased Core Water Content and with or without Major DNA-Binding Proteins," *Applied and Environmental Microbiology,* 61(10): 3633-3638 (October 1995).

[80] Rahmanian, S., Taleei, R., and Nikjoo, H. "Radiation induced base excision repair (BER): A mechanistic mathematical approach," *DNA Repair,* 22: 89-103 (2014).

[81] Ravanat, J.-L., Douki, T., and Cadet, J. "Direct and indirect effects of UV radiation on DNA and its components," *Journal of Photochemistry and Photobiology B: Biology,* 63: 88-102 (2001).

[82] "Ribosome mRNA translation en," Wikipedia, 29 September 2008. 20 June 2014 http://en.wikipedia.org/wiki/Translation (biology).

[83] Richard, M., Fryett, M., Miller, S., Booth, I., Grebogi, C., and Moura, A. "Optimality in DNA repair," *Journal of Theorectical Biology,* 292: 39-43 (2012).

[84] Roszak, D.B. and Colwell, R.R. "Survival Strategies of Bacteria in the Natural Environment," *Microbiological Reviews,* 51(3): 365-379 (September 1987).

[85] Rubinow, S.I. *Introduction to Mathematical Biology.* New York: John Wiley and Sons, 1975.

[86] Seeley, T.W. and Grossman, L. "The role of Escherichia coli UvrB in nucleotide excision repair," *The Journal of Biological Chemistry,* 265: 7158-7165 (1990).

[87] Center for Disease Control. "Select Agents and Toxins List" National Select Agent Registry, 2014. 23 April 2014 http://www.selectagents.gov/Select Agents and Toxins List.htmll.

[88] Setlow, B. and Setlow, P. "Role of DNA repair in *Bacillus subtilis* spore resistance," *Journal of Bacteriology,* 178(12): 3486 (1996).

[89] Setlow, P. "Bacterial Stress Responses," *Bacterial Stress Responses.* Washington DC: American Society for Microbiology, (2000).

[90] Setlow, P. "Resistance of Spores of *Bacillus* Species to Ultraviolet Light," *Environmental and Molecular Mutagenesis,* 38: 97-104 (2001).

[91] Setlow, P. "Spores of *Bacillus subtilis*: their resistance to and killing by radiation, heat and chemicals," *Journal of Applied Microbiology,* 101: 514-525 (2006).

[92] Shiota, M., Saitou, K., Mizumoto, H., Matsusaka, M., Agata, N., Nakayama, M., Kage, M., Tatsumi, S., Okamoto, A., Yamaguchi, S., Ohta, M., and Hata, D. "Rapid Detoxification of Cereulide in *Bacillus cereus* Food Poisoning " *PEDIATRICS* 125(4): e951-e955 (April 2010).

[93] Smelt, J.P.P.M., Hellemons, J.C., Wouters, P.C., and van Gerwen, S.J.C. "Physiological and mathematical aspects in setting criteria for decontamination of foods by physical means," *International Journal of Food Microbiology,* 78: 57-77 (2002).

[94] Sokhansanj, B.A., Rodrigue, G.R., Fitch, J.P., and Willson III, D.M. "A quantitative model of human DNA base excision repair. I. mechanistic insights," *Nucleic Acids Research,* 30(8):1817-1825 (2002).

[95] Stewart, P.S. "Diffusion in Biofilms," *Journal of Bacteriology*, 185(5): 1485-1491, (2003).

[96] Sunde, E.P., Setlow, P., Hederstedt, L., and Halle, B. "The physical state of water in bacterial spores," *Proceedings of the National Academy of Sciences USA* 106(46): 19334-19339.

[97] Sutherland, J.C. "Repair dependent radiation survival: a stochastic model with Euler gamma function solutions," *Physics in Medicine and Biology,* 51: 4883-4901 (2006).

[98] National Institutes of Health."Talking Glossary of Genetic Terms." National Human Genome Research Institute. 24 April 2014 http://www.genome.gov/glossary/

[99] Tortora, G.J., Funke, B.R., and Case, C.L. *Microbiology: An Introduction (7th Edition)*. San Francisco: Benjamin Cummings, 2002.

[100] Truglio, J.J., Croteau, D.L., Van Houten, B., and Kisker, C. "Prokaryotic Nucleotide Excision Repair: The UvrABC System," *Chemical Reviews,* 106: 233-252 (2006)

[101] Uphoff, S., Reyes-Lamothe, R., de Leon, F.G., Sherrat, D.J., and Kapanidis, A.N., "Single-molecule DNA repair in live bacteria," *Proceedings of the National Academy of Sciences USA,* 110(20): 8063-8068 (14 May 2013).

[102] Stewart, P. "U.S. Army chief says no human error seen in anthrax mishap," *Reuters* 28 May 2015, 25 August 2015 http://www.reuters.com/article/2015/05/28/us-usa-miltary-anthrax-idUSKBN0OC2KU20150528.

[103] Van Houten, B. "Nucleotide excision repair in Escherichia coli," *Microbiology and Molecular Biology Reviews*, 54(1):18-51 (1990).

[104] VanHouten, B. and Kad, N. "Investigation of bacterial nucleotide excision repair using single-molecule techniques," *DNA Repair*, 20: 41-48 (2014).

[105] Voet, D. and Voet, J.G. *Biochemistry (Fourth Edition)*. United States of America: John Wiley and Sons, INC., 2011.

[106] Westphal, A.J., Price, P.B., Leighton, T.J., and Wheeler, K.E. "Kinetics of size changes of individual *Bacillus thuringiensis* spores in response to changes in relative humidity," *Proceedings of the National Academy of Sciences of the USA,* 100: 3461-3466 (18 March 2003).

[107] Xu, S., Labuza, T.P., and Diez-Gonzalez, F. "Inactivation of *Bacillus anthracis* Spores by a Combination of Biocides and Heating under High-Temperature Short-Time Pasteurization Conditions," *Applied and Environmental Microbiology*, 74: 3336-3341 (June 2008).

[108] Yoshii, H., Furuta, T., Noma, S., and Noda, T. "Kinetic Analysis of Soy-protein Denaturation by a Temperature-programmed Heat-denaturation Technique," *Agricultural and Biological Chemistry*, 54: 863-869 (1990).

[109] Zou, Y., Walker, R., Bassett, H., Geacintov, N.E., and Van Houten, B., "Formation of DNA Repair Intermediates and Incision by the ATP-dependent UvrB-UvrC Endonuclease," *The Journal of Biological Chemistry*, 272(8): 4820-4827 (1997).

REPORT DOCUMENTATION PAGE

Form Approved
OMB No. 0704–0188

The public reporting burden for this collection of information is estimated to average 1 hour per response, including the time for reviewing instructions, searching existing data sources, gathering and maintaining the data needed, and completing and reviewing the collection of information. Send comments regarding this burden estimate or any other aspect of this collection of information, including suggestions for reducing this burden to Department of Defense, Washington Headquarters Services, Directorate for Information Operations and Reports (0704–0188), 1215 Jefferson Davis Highway, Suite 1204, Arlington, VA 22202–4302. Respondents should be aware that notwithstanding any other provision of law, no person shall be subject to any penalty for failing to comply with a collection of information if it does not display a currently valid OMB control number. **PLEASE DO NOT RETURN YOUR FORM TO THE ABOVE ADDRESS.**

1. REPORT DATE *(DD–MM–YYYY)*	2. REPORT TYPE	3. DATES COVERED *(From — To)*
17–09–2015	Dissertation	October 2012–September 2015

4. TITLE AND SUBTITLE

Modeling Radiation Effectiveness for Inactivation of *Bacillus* Spores

5a. CONTRACT NUMBER

5b. GRANT NUMBER

5c. PROGRAM ELEMENT NUMBER

6. AUTHOR(S)

Knight, Emily A., Major, USAF

5d. PROJECT NUMBER

5e. TASK NUMBER

5f. WORK UNIT NUMBER

7. PERFORMING ORGANIZATION NAME(S) AND ADDRESS(ES)

Air Force Institute of Technology
Graduate School of Engineering and Management (AFIT/EN)
2950 Hobson Way
Wright-Patterson AFB, OH 45433-7765

8. PERFORMING ORGANIZATION REPORT NUMBER

AFIT-ENC-DS-15-S-001

9. SPONSORING / MONITORING AGENCY NAME(S) AND ADDRESS(ES)

Douglas Allen Dalton
Defense Threat Reduction Agency
J9-BAS, Cube 3650D
8725 Kingman Road
Fort Belvoir, VA 22060
Ph: (703) 767-3054 Fx: (703) 767-3335

10. SPONSOR/MONITOR'S ACRONYM(S)

DTRA

11. SPONSOR/MONITOR'S REPORT NUMBER(S)

12. DISTRIBUTION / AVAILABILITY STATEMENT

DISTRIBUTION STATEMENT A. APPROVED FOR PUBLIC RELEASE;
DISTRIBUTION UNLIMITED.

13. SUPPLEMENTARY NOTES

This work is declared a work of the U.S. Government and is not subject to copyright protection in the United States.

14. ABSTRACT

This research models and analyzes the inactivation of *Bacillus* spores following a radiation exposure and the process enacted by the *Bacillus* spore to repair the resulting damage. Irradiation of a spore and the medium surrounding the spore induces chemical reactions that produce reactive oxygen species (ROS). This research will consider the reaction-diffusion of these ROS throughout the spore. These ROS can react with the spore's DNA and enzymes to degrade them to such an extent that the DNA cannot be repaired or replicated, thus causing spore death. In order to survive a dose of radiation, a spore must repair its damaged DNA during germination. The DNA repair process is dependent on reactions catalyzed by enzymes that remain viable after the radiation treatment. Increased damage to the enzymes during radiation exposure effects the rate at which the spore's DNA is repaired. If the enzymes are damaged to such an extent that they cannot complete the DNA repair method, the spore will be unable to reproduce and achieve cellular outgrowth. A probability of survival model is created based on radiation damage due to the reaction of ROS with the spore's DNA and enzymes and the repair process.

15. SUBJECT TERMS

Add four or five key words/phrases for indexing

16. SECURITY CLASSIFICATION OF:

a. REPORT	b. ABSTRACT	c. THIS PAGE
U	U	U

17. LIMITATION OF ABSTRACT

UU

18. NUMBER OF PAGES

130

19a. NAME OF RESPONSIBLE PERSON
Dr. William P. Baker (ENC)

19b. TELEPHONE NUMBER *(include area code)*
(937) 255-3636x4517 William.Baker@afit.edu

Standard Form 298 (Rev. 8–98)
Prescribed by ANSI Std. Z39.18